

# Resonant Leptogenesis, Collider Signals and Neutrinoless Double Beta Decay from Flavor and CP Symmetries

---

Garv Chauhan,<sup>a,b</sup> P. S. Bhupal Dev<sup>b</sup>

<sup>a</sup>*Centre for Cosmology, Particle Physics and Phenomenology (CP3), Université catholique de Louvain, Chemin du Cyclotron 2, B-1348 Louvain-la-Neuve, Belgium*

<sup>b</sup>*Department of Physics and McDonnell Center for the Space Sciences, Washington University, St. Louis, MO 63130, USA*

*E-mail:* [garv.chauhan@uclouvain.be](mailto:garv.chauhan@uclouvain.be), [bdev@wustl.edu](mailto:bdev@wustl.edu)

**ABSTRACT:** We present a low-scale type-I seesaw scenario with discrete flavor and CP symmetries. This scenario not only explains the measured values of the lepton mixing angles, but also makes predictions for leptonic CP violation, and connects the low-energy CP phases relevant for neutrino oscillation and neutrinoless double beta decay experiments with the high-energy CP phases relevant for leptogenesis. We show that the three right-handed Majorana neutrinos in this scenario have (almost) degenerate masses and their decays can explain the observed baryon asymmetry of the universe via resonant leptogenesis. We study the correlation of the predicted baryon asymmetry with lepton-number-violating signals at high-energy colliders, including both prompt and displaced vertex/long-lived signatures, as well as in low-energy neutrinoless double beta decay experiments. We find that the normal ordering of light neutrino masses leads to an enhanced collider signal, whereas the neutrinoless double beta decay provides a promising probe in the inverted ordering case.

**KEYWORDS:** Discrete Symmetries, Beyond Standard Model, Neutrino Physics

---

## Contents

<b>1</b>	<b>Introduction</b>	<b>1</b>
<b>2</b>	<b>Framework</b>	<b>3</b>
2.1	Yukawa Sector	4
2.2	RHN Mass Spectrum	6
2.3	Light Neutrino Masses and Mixing	7
<b>3</b>	<b>Different Cases</b>	<b>8</b>
3.1	Case 1	9
3.1.1	Residual Symmetries	9
3.1.2	Constraints from and on Light Neutrino Sector	10
3.1.3	Enhanced Residual Symmetries	14
3.2	Case 2	14
3.2.1	Residual Symmetries	14
3.2.2	Constraints from and on Light Neutrino Sector	16
3.3	Case 3	17
3.3.1	Residual Symmetries	17
3.3.2	Constraints from and on Light Neutrino Sector	19
<b>4</b>	<b>CP Asymmetries for Resonant Leptogenesis</b>	<b>20</b>
<b>5</b>	<b>Collider Signatures</b>	<b>24</b>
5.1	Production of RHNs	24
5.2	Decay Lengths	27
5.2.1	Case 1	27
5.2.2	Case 2	28
5.2.3	Case 3	29
5.3	Branching Ratios	30
5.4	Same-sign dilepton signals	34
5.5	Correlation with leptogenesis	35
<b>6</b>	<b>Correlation of BAU with <math>0\nu\beta\beta</math></b>	<b>38</b>
6.1	Case 1	40
6.2	Case 2	41
6.3	Case 3	42
<b>7</b>	<b>Conclusion</b>	<b>43</b>
<b>A</b>	<b>Group Theory of <math>\Delta(6n^2)</math> and Representation Matrices</b>	<b>44</b>
<b>B</b>	<b>CP symmetries and form of CP transformations</b>	<b>45</b>

<b>C</b>	<b>Form of the Representation Matrices for Residual Symmetries</b>	<b>46</b>
<b>D</b>	<b>Explicit Form of the Yukawa Couplings</b>	<b>47</b>
D.1	Case 1	47
D.2	Case 2	48
D.3	Case 3a	48
D.4	Case 3b.1	49

---

## 1 Introduction

The origin of the observed baryon asymmetry of the universe (BAU) [1] remains an open question, as it calls for some beyond the Standard Model (BSM) physics. A dynamical generation of the BAU requires fulfilling the three necessary (but not sufficient) Sakharov conditions [2], namely, baryon number (B) violation, charge conjugation (C) and charge conjugation-parity (CP) violation, and departure from thermal equilibrium. There exist several viable baryogenesis mechanisms satisfying these basic Sakharov conditions; see Ref. [3] for a recent review. A particularly attractive mechanism is leptogenesis [4], which can potentially link the BAU to another outstanding puzzle that also necessarily requires BSM physics, namely, the origin of neutrino mass; see Refs. [5–7] for reviews on various aspects of leptogenesis.

The central idea of thermal leptogenesis is the production of a net leptonic asymmetry in the early universe, via the CP-violating out-of-equilibrium decays of heavy right-handed neutrinos (RHNs), which is then converted to a net baryon asymmetry through non-perturbative electroweak sphaleron processes [8]. The same complex Yukawa interactions ( $Y_D$ ) of the RHNs with the SM lepton ( $L$ ) and Higgs ( $H$ ) doublets, in conjunction with the Majorana masses ( $M_R$ ) of the RHNs, are also responsible for the neutrino mass generation via the type-I seesaw mechanism [9–14]:

$$M_\nu \simeq -M_D M_R^{-1} M_D^T, \quad (1.1)$$

where  $M_D = vY_D$  is the Dirac neutrino mass matrix and  $v \simeq 174$  GeV is the electroweak vacuum expectation value (VEV). In the so-called vanilla leptogenesis scenario with hierarchical RHNs, the maximum CP violation from the complex Yukawa interactions can be related to the lightest RHN mass through the seesaw formula, and the requirement of successful leptogenesis imposes a lower limit on  $M_R \gtrsim 10^9$  GeV, known as the Davidson-Ibarra bound [15]. Although this limit can be somewhat relaxed by including flavor effects and with some cancellation between the tree and one-loop level contributions to the light neutrino mass matrix [16], it still remains beyond the reach of any foreseeable laboratory experiment. An appealing alternative is the resonant leptogenesis mechanism [17] (see Ref. [18] for a review) in which the CP asymmetry can be resonantly enhanced [19–21], even up to order one [22, 23], if at least two RHNs are quasi-degenerate, thereby allowing significantly

lower values of  $M_R$  all the way down to the electroweak scale [24, 25],<sup>1</sup> while maintaining agreement with neutrino oscillation data. Moreover, embedding such a resonant leptogenesis mechanism into a gauge theory, in which the RHNs exist naturally for anomaly cancellation, makes it testable at the colliders via searches for RHNs and new gauge/scalar bosons [27–43]; see Ref. [44] for a review on the testable signatures of leptogenesis.

Although the seesaw connection to leptogenesis is qualitatively attractive, it can make quantitative predictions consistent with the low-energy neutrino data only after the flavor structures of  $Y_D$  and  $M_R$  are specified [45]. Without loss of generality, we can always choose the basis in which the charged-lepton mass matrix  $M_\ell$  and the RHN mass matrix  $M_R$  are diagonal. In this case the Dirac Yukawa coupling matrix  $Y_D$  can be conveniently written in the so-called Casas-Ibarra (CI) parametrization [46]:

$$Y_D = \frac{i}{v} U \sqrt{\hat{D}_\nu} O \sqrt{\hat{D}_R}, \quad (1.2)$$

where  $U$  is the Pontecorvo-Maki-Nakagawa-Sakata (PMNS) neutrino mixing matrix used to diagonalize  $M_\nu$  [cf. Eq. (1.1)] in the chosen basis, i.e.  $U^\dagger M_\nu U^* = \hat{D}_\nu = \text{diag}(m_1, m_2, m_3)$ ;  $\hat{D}_R = \text{diag}(M_1, M_2, M_3)$  is the diagonal RHN mass matrix; and  $O$  is an arbitrary complex orthogonal matrix. It is the complex phases hidden in  $Y_D$  that govern the CP asymmetries  $\varepsilon_{i\alpha}$  between the lepton-number-violating (LNV) decays of the RHNs  $N_i \rightarrow L_\alpha + H$  and  $N_i \rightarrow \bar{L}_\alpha + H^c$  (where  $H^c \equiv \epsilon H^*$ ,  $\epsilon$  being the  $SU(2)$  antisymmetric tensor). In particular, the flavored CP asymmetries  $\varepsilon_{i\alpha}$  depend on both  $(Y_D^*)_{\alpha i} (Y_D)_{\alpha j}$  and  $(Y_D^\dagger Y_D)_{ij}$  (for  $j \neq i$ ), whereas the unflavored asymmetries  $\varepsilon_i \equiv \sum_\alpha \varepsilon_{i\alpha}$  only depend on the combination  $(Y_D^\dagger Y_D)_{ij}$  [47]. Given the CI parametrization of  $Y_D$  [cf. Eq. (1.2)], one can immediately see that the CP asymmetries  $\varepsilon_i$  have nothing to do with the PMNS mixing matrix  $U$ . In other words, due to the arbitrariness of the  $O$  matrix in Eq. (1.2), the high-energy CP phases present in the Yukawa couplings  $Y_D$  that are responsible for leptogenesis are in general unrelated to the low-energy CP phases in  $U$  [48–53], i.e. the Dirac phase  $\delta$  that is measurable in neutrino oscillation experiments [54] and a combination of the two Majorana phases  $\alpha_1$  and  $\alpha_2$  that is potentially measurable in neutrinoless double beta decay ( $0\nu\beta\beta$ ) experiments [55]. It is only when we assume  $O$  in Eq. (1.2) to be real, the flavored CP asymmetries  $\varepsilon_{i\alpha}$  will depend directly on the PMNS phases [56–62]; see Ref. [63] for a review on the implications of low-energy leptonic CP violation for leptogenesis.

Since the experiments are only sensitive to the low-energy CP phases, it is desirable to have a theoretical setup where the high- and low-energy CP phases can be related, which can provide a highly predictive leptogenesis scenario. Examples are models with residual flavor and CP symmetries [64–67]. In particular, a non-abelian discrete flavor symmetry  $G_f$  combined with a CP symmetry, both acting non-trivially on flavor space, turns out to be highly constraining for the lepton mixing angles and both low- and high-energy CP phases, because in this case the PMNS mixing matrix depends on a single free parameter [68–70]. In this paper we will adopt this setup with  $G_f$  being a member of the series of groups  $\Delta(3n^2)$  [71] or  $\Delta(6n^2)$  [72] which are known to give several interesting neutrino mixing patterns [73–76]. We will show that this framework provides a complementary probe

<sup>1</sup>The RHNs can be even lighter, as low as GeV-scale, in the parametric regime of ARS leptogenesis [26].

of the resonant leptogenesis mechanism in collider and  $0\nu\beta\beta$  experiments. In particular, the predicted BAU is shown to be correlated with the low-energy  $0\nu\beta\beta$  rate that can in principle be tested in future tonne-scale  $0\nu\beta\beta$  experiments. In addition, we identify points of *enhanced residual symmetry* (ERS), where one of the three RHNs is long-lived and can be detected in dedicated long-lived particle (LLP) searches [77, 78], while at the same time the remaining two RHNs can be searched for via either prompt or displaced vertex signals at the LHC [79, 80], provided the RHNs are charged under a new gauge group, so that their production cross section is not necessarily suppressed by the small light-heavy neutrino mixing. We take this new gauge group to be  $U(1)_{B-L}$  with the associated  $Z'$  boson in the multi-TeV range and scan the parameter space in the  $(M_{Z'}, M_R)$  plane to find regions that lead to successful leptogenesis. The detection prospects of these regions using LNV signals at the high-luminosity LHC [81], as well as at a futuristic 100 TeV hadron collider [82], are also discussed.

The rest of the paper is organized as follows: In Section 2, we discuss the embedding of the charged-lepton sector and light neutrinos (with masses arising from the type-I seesaw mechanism) with three RHNs in the flavor group  $G_f = \Delta(6n^2)$  and a CP symmetry group, with the Yukawa sector presented in Section 2.1, RHN mass spectrum in Section 2.2, and light neutrino masses and mixing in Section 2.3. In Section 3, we discuss the residual symmetries and the form of the corresponding representation matrices for the different cases, along with additional constraints imposed from light neutrino masses. In Section 4, we discuss the CP asymmetries produced in our scenario through out-of-equilibrium decays of the quasi-degenerate RHNs via resonant leptogenesis. In Section 5, we study the collider phenomenology of our scenario, starting with the production of RHNs in Section 5.1, their decay lengths in Section 5.2 and branching ratios (BRs) in Section 5.3, same-sign dilepton signals in Section 5.4, and finally the correlation with leptogenesis in Section 5.5. The correlation of BAU with  $0\nu\beta\beta$  is studied in Section 6. Our conclusions are given in Section 7. Appendix A reviews the group theory of  $\Delta(6n^2)$  and representation matrices. Appendix B discusses the CP symmetries and the form of CP transformations. Appendix C gives the form of the representation matrices for residual symmetries. Appendix D gives the explicit form of the Yukawa couplings in terms of the other model parameters.

## 2 Framework

We focus on the lepton sector and assume that light neutrino masses arise from the type-I seesaw mechanism with three RHNs [cf. Eq. (1.1)]. We consider a scenario with a flavor symmetry  $G_f$  and a CP symmetry which are broken into residual groups  $G_\ell$  and  $G_\nu$  that determine the forms of the charged lepton and neutrino mass matrices, respectively.

For flavor symmetry  $G_f$ , following the approach to lepton mixing presented in Ref. [74], we use a discrete, finite, non-abelian group of the form  $\Delta(6n^2)$  [72] with  $n$  even and not divisible by three.<sup>2</sup> The group theory and relevant representation matrices of  $\Delta(6n^2)$  are given in Appendix A. The groups  $\Delta(6n^2)$  for  $n \geq 2$  are particularly interesting, as they

---

<sup>2</sup>We could also consider a group of the form  $\Delta(3n^2)$  [71], but since this is a subgroup of  $\Delta(6n^2)$ , it is sufficient to focus on the latter group only.

possess at least one irreducible, faithful, complex three-dimensional representation  $\mathbf{3}$ . In the following, we assign the three generations of left-handed (LH) lepton doublets  $L_\alpha$  (with  $\alpha = e, \mu, \tau$ ) to this  $\mathbf{3}$ . The three generations of RHNs  $N_i$  (with  $i = 1, 2, 3$ ) are unified in an irreducible, in general unfaithful, real representation  $\mathbf{3}'$  of  $G_f$  which requires the index  $n$  of the group  $\Delta(6n^2)$  to be even; see Appendix A for details.<sup>3</sup> Assigning LH leptons and RHNs to these in general different three-dimensional representations of  $G_f$  is crucial, as the assignment  $L_\alpha \sim \mathbf{3}$  allows to fully explore the predictive power of  $G_f$  (and not only of one of its subgroups), while  $N_i \sim \mathbf{3}'$  permits the RHNs to have a flavor-universal mass term without breaking  $G_f$  and the CP symmetry. The right-handed charged leptons  $\alpha_R$  are assigned to the trivial one-dimensional representation  $\mathbf{1}$  of  $G_f$ . In order to distinguish them, we assume the existence of a  $Z_3$  symmetry, called  $Z_3^{(\text{aux})}$ , under which  $e_R, \mu_R$  and  $\tau_R$  are assigned charges 1,  $\omega$  and  $\omega^2$  respectively (with  $\omega = e^{2\pi i/3}$  being the third root of unity), whereas LH leptons and RHNs are assumed to be invariant under  $Z_3^{(\text{aux})}$ .

The CP symmetry imposed on the theory corresponds to an automorphism of  $G_f$  [69, 70]. They are represented by the CP transformation  $X(\mathbf{r})$  in the different (irreducible) representations  $\mathbf{r}$  of  $G_f$  and depend on the parameters determining the automorphism. For completeness, we show the form of the automorphisms and of  $X(\mathbf{r})$  for the relevant representations in Appendix B.

The residual symmetry in the charged lepton sector is chosen as  $G_\ell = Z_3^{(\text{D})}$  which is the diagonal abelian subgroup of the  $Z_3$  group contained in  $G_f$  and the additional auxiliary group  $Z_3^{(\text{aux})}$  (see Appendix A). In the neutrino sector, we use the residual symmetry  $G_\nu = Z_2 \times \text{CP}$ , where the  $Z_2$  symmetry is a subgroup of  $G_f$  and the CP symmetry the one of the underlying theory (see Appendix B). In the following, the generator  $Z$  of the residual  $Z_2$  symmetry in the different representations  $\mathbf{r}$  is denoted as  $Z(\mathbf{r})$ . The  $Z_2$  symmetry and CP commute, i.e. they fulfill

$$X(\mathbf{r}) Z(\mathbf{r}) - Z(\mathbf{r})^* X(\mathbf{r}) = 0 \quad (2.1)$$

for all representations  $\mathbf{r}$  of  $G_f$ . The mismatch of the residual symmetries  $G_\ell$  and  $G_\nu$  determines the form of lepton mixing [65, 74]. Specifically, it has been found that lepton mixing patterns can be classified into four distinct types, called Case 1, Case 2, Case 3a and Case 3b.1 in Ref. [65], depending on the choices of  $Z(\mathbf{r})$  and  $X(\mathbf{r})$ . The form of the lepton mixing matrices for these four different types are shown in Section 3; see also Appendix C. The aim of this paper is to study resonant leptogenesis and its correlation with  $0\nu\beta\beta$  and collider signals for these four representative cases, which have different mixing patterns.

## 2.1 Yukawa Sector

The forms of the charged lepton mass matrix  $M_\ell$ , the neutrino Yukawa coupling matrix  $Y_D$  and the RHN Majorana mass matrix  $M_R$  are determined by  $G_\ell$  and  $G_\nu$ . The form of the relevant Lagrangian is

$$-\mathcal{L} \supset (Y_\ell)_{\alpha\beta} \bar{L}_\alpha H \beta_R + (Y_D)_{\alpha i} \bar{L} H^c N_i + \frac{1}{2} (M_R)_{ij} \bar{N}_i^c N_j + \text{H.c.}, \quad (2.2)$$

---

<sup>3</sup>Only for  $n = 2$  this representation is faithful. This, however, does not affect our discussion.

where the superscript  $c$  denotes charge conjugation. In our chosen basis (see Appendix A), the charged lepton mass matrix  $M_\ell = vY_\ell$  is diagonal and contains three independent parameters corresponding to the three charged lepton masses, i.e.  $M_\ell = \text{diag}(m_e, m_\mu, m_\tau)$ . As  $M_\ell$  is diagonal, there is no contribution to lepton mixing from the charged lepton sector. As for the neutrino sector, we take the neutrino Yukawa coupling matrix  $Y_D$  to be invariant under  $G_\nu$ , whereas the matrix  $M_R$  does neither break  $G_f$  nor CP. Being invariant under  $Z_2 \times \text{CP}$ , the matrix  $Y_D$ , in the basis in which LH fields are on the left and RH ones on the right [cf. Eq. (2.2)], fulfills the following relations

$$Z(\mathbf{3})^\dagger Y_D Z(\mathbf{3}') = Y_D \quad \text{and} \quad X(\mathbf{3})^* Y_D X(\mathbf{3}') = Y_D^*. \quad (2.3)$$

We can rewrite the conditions in Eq. (2.3) using the unitary matrices  $\Omega(\mathbf{3})$  and  $\Omega(\mathbf{3}')$ , which are determined by the form of the CP transformations  $X(\mathbf{3})$  and  $X(\mathbf{3}')$  in the representations of LH leptons and RHNs, i.e. they fulfil

$$X(\mathbf{3}) = \Omega(\mathbf{3}) \Omega(\mathbf{3})^T \quad \text{and} \quad X(\mathbf{3}') = \Omega(\mathbf{3}') \Omega(\mathbf{3}')^T. \quad (2.4)$$

We find that  $\Omega(\mathbf{3})^\dagger Y_D \Omega(\mathbf{3}')$  is real and can be diagonalized by two rotation matrices from the left and right, respectively:

$$\Omega(\mathbf{3})^\dagger Y_D \Omega(\mathbf{3}') = R_{ij}(\theta_L) \begin{pmatrix} y_1 & 0 & 0 \\ 0 & y_2 & 0 \\ 0 & 0 & y_3 \end{pmatrix} R_{kl}(-\theta_R), \quad (2.5)$$

and the form of  $Y_D$  is thus given by

$$Y_D = \Omega(\mathbf{3}) R_{ij}(\theta_L) \begin{pmatrix} y_1 & 0 & 0 \\ 0 & y_2 & 0 \\ 0 & 0 & y_3 \end{pmatrix} R_{kl}(-\theta_R) \Omega(\mathbf{3}')^\dagger. \quad (2.6)$$

The matrices  $R_{ij}(\theta_L)$  and  $R_{kl}(\theta_R)$  denote rotations in the  $(ij)$  and  $(kl)$  planes (where  $i, j, k, l = 1, 2, 3$  with  $i < j$  and  $k < l$ ) through the angles  $\theta_L$  and  $\theta_R$ , respectively. Explicitly,

$$R_{12}(\theta) = \begin{pmatrix} \cos \theta & \sin \theta & 0 \\ -\sin \theta & \cos \theta & 0 \\ 0 & 0 & 1 \end{pmatrix}, \quad R_{13}(\theta) = \begin{pmatrix} \cos \theta & 0 & \sin \theta \\ 0 & 1 & 0 \\ -\sin \theta & 0 & \cos \theta \end{pmatrix}, \quad R_{23}(\theta) = \begin{pmatrix} 1 & 0 & 0 \\ 0 & \cos \theta & \sin \theta \\ 0 & -\sin \theta & \cos \theta \end{pmatrix}. \quad (2.7)$$

The angles  $\theta_L$  and  $\theta_R$  in Eq. (2.6) are free parameters, i.e. not fixed by the residual symmetry  $G_\nu$ , and can take values in the range  $[0, \pi)$ . The planes, in which the rotations  $R_{ij}(\theta_L)$  and  $R_{kl}(\theta_R)$  act, are determined by the  $(ij)$ - and  $(kl)$ -subspaces of degenerate eigenvalues of the generator  $Z$  in the representation  $\mathbf{3}$  and  $\mathbf{3}'$ , when transformed with the matrix  $\Omega(\mathbf{3})$  and  $\Omega(\mathbf{3}')$ , respectively.<sup>4</sup> In addition to these two angles,  $Y_D$  contains three more real parameters, namely, the Yukawa couplings  $y_f$  (with  $f = 1, 2, 3$ ). As the choice of CP symmetry and thus the corresponding CP transformations  $X(\mathbf{3})$  is in general indicated by natural numbers [see e.g. the parameter  $s$  in Eq. (3.2)], also the matrices  $\Omega(\mathbf{3})$  and  $\Omega(\mathbf{3}')$  (potentially) depend on these parameters; see Section 3 for more details.

<sup>4</sup>Examples can be found in the discussion of the different cases (Case 1 through Case 3b.1) in Section 3.

## 2.2 RHN Mass Spectrum

As the RHN Majorana mass matrix  $M_R$  leaves  $G_f$  and CP invariant, its form is simply

$$M_R = M_N \begin{pmatrix} 1 & 0 & 0 \\ 0 & 0 & 1 \\ 0 & 1 & 0 \end{pmatrix}, \quad (2.8)$$

with  $M_N > 0$ , setting the overall mass scale of the RHNs. From Eq. (2.8), it is clear that the three RHNs are exactly degenerate in the flavor symmetry limit. However, in order to successfully generate the BAU via resonant leptogenesis, the masses of at least two of the RHNs have to be slightly different, such that when the mass difference is of the order of their decay width, we can get the resonant enhancement in the self-energy contribution to the CP asymmetry [18]. This can be achieved by small corrections  $\delta M_R$  to the RHN Majorana mass matrix in Eq. (2.8). These corrections are expected to arise by (higher order) residual symmetry breaking effects which are generically present in model realizations. In the following, without specifying any particular breaking mechanism, we consider general corrections to  $M_R$  which are invariant under the residual symmetry  $G_\ell$ . The generator of  $G_\ell$  is represented in the representation of the RHNs  $N_i$  as

$$a(\mathbf{3}') = \begin{pmatrix} 1 & 0 & 0 \\ 0 & \omega & 0 \\ 0 & 0 & \omega^2 \end{pmatrix}, \quad (2.9)$$

since  $N_i$ 's are not charged under the auxiliary symmetry  $Z_3^{(\text{aux})}$ . The correction  $\delta M_R$  must thus fulfil

$$a(\mathbf{3}')^T \delta M_R a(\mathbf{3}') = \delta M_R, \quad (2.10)$$

meaning that it is of the form

$$\delta M_R = \kappa M_N \begin{pmatrix} 2 & 0 & 0 \\ 0 & 0 & -1 \\ 0 & -1 & 0 \end{pmatrix}, \quad (2.11)$$

with  $\kappa \ll 1$  being a small dimensionless symmetry breaking parameter. The RHN masses  $M_i$  (with  $i = 1, 2, 3$ ) then acquire a small correction, as follows:

$$M_1 = M_N (1 + 2\kappa) \text{ and } M_2 = M_3 = M_N (1 - \kappa). \quad (2.12)$$

It is the mass splitting between  $N_1$  and  $N_{2,3}$  that turns out to be relevant for resonant leptogenesis in our model. In the following numerical analysis, we will treat  $\kappa$  as a free parameter and choose its value suitably in order to maximize the CP asymmetry for each case.

We emphasize here that the higher-dimensional operators connecting different sectors of the theory are responsible for the eventual breaking of the residual symmetries  $G_\nu$  and  $G_\ell$  and thus affect the given forms of  $M_D$ ,  $M_\ell$  and  $M_R$ . In particular, they are the source

of corrections leading to the small splitting in the RHN masses which is crucial for resonant leptogenesis. As we will see in Section 3, the same higher-dimensional operators also source corrections to the tribimaximal (TB) form of the PMNS mixing matrix which is needed to explain the nonzero reactor mixing angle. Therefore, this provides a natural setup for motivating the quasi-degeneracy of the RHNs for resonant leptogenesis. This is reminiscent of radiative resonant leptogenesis models [83–89] where the RHN mass matrix is  $O(N)$ -symmetric at high scale, and small  $O(N)$ -breaking effects are induced naturally at low scale due to renormalization group evolution effects.

### 2.3 Light Neutrino Masses and Mixing

The light neutrino mass matrix  $M_\nu$  follows from the type-I seesaw formula, cf. Eq. (1.1). As the charged lepton mass matrix  $M_\ell$  is diagonal, lepton mixing arises from the diagonalization of  $M_\nu$  only. In general, the resulting lepton mixing angles involve a combination of all parameters appearing in  $Y_D$ . However, if

$$[\Omega(\mathbf{3}')^T M_R^{-1} \Omega(\mathbf{3}')^\star, R_{kl}(\theta_R)] = 0 \quad (2.13)$$

(see Section 3 for such cases), the lepton mixing angles only depend on the free parameter  $\theta_L$  and the parameters describing the flavor and CP symmetry as well as the residual symmetry  $G_\nu$ . In these cases, we find that the PMNS mixing matrix is given by

$$U = \Omega(\mathbf{3}) R_{ij}(\theta_L) K_\nu, \quad (2.14)$$

where  $K_\nu$  is a diagonal matrix with entries equal to  $\pm 1$  and  $\pm i$ , and is necessary to make neutrino masses positive. This matrix is generally parametrized in the following form:

$$K_\nu = \begin{pmatrix} 1 & 0 & 0 \\ 0 & i^{k_1} & 0 \\ 0 & 0 & i^{k_2} \end{pmatrix} \quad \text{with } k_{1,2} = 0, 1, 2, 3. \quad (2.15)$$

We can easily verify that  $U$  fulfills

$$U^\dagger M_\nu U^\star = \text{diag}(m_1, m_2, m_3), \quad (2.16)$$

with the mass spectrum of the light neutrinos being determined by the Yukawa couplings  $y_f$  in Eq. (2.6), i.e.

$$m_f = \frac{y_f^2 v^2}{M_N} \quad \text{for } f = 1, 2, 3. \quad (2.17)$$

As the Yukawa couplings are not constrained other than being real, the light neutrino mass spectrum is not predicted in our scenario. It can thus accommodate both normal ordering (NO) and inverted ordering (IO), depending in general on the parameters encoded in  $Y_D$ . In turn, we can constrain these parameters by the experimental information available on neutrino masses, i.e. the measurement of the two mass squared differences [90] and the upper bound on the sum of the neutrino masses [1].

For NO, the three light neutrino masses  $m_i$  are parametrized as

$$m_1 = m_0, \quad m_2 = \sqrt{m_0^2 + \Delta m_{\text{sol}}^2}, \quad m_3 = \sqrt{m_0^2 + \Delta m_{\text{atm}}^2}, \quad (2.18)$$

with  $m_0$  denoting the lightest neutrino mass. For IO, the masses  $m_i$  are written as

$$m_1 = \sqrt{m_0^2 + |\Delta m_{\text{atm}}^2| - \Delta m_{\text{sol}}^2}, \quad m_2 = \sqrt{m_0^2 + |\Delta m_{\text{atm}}^2|}, \quad m_3 = m_0, \quad (2.19)$$

where  $m_0$  is the lightest neutrino mass. In each case, we use the  $3\sigma$  allowed range of the solar and atmospheric mass-squared differences  $\Delta m_{\text{sol}}^2$  and  $\Delta m_{\text{atm}}^2$  respectively from a recent global fit result [91]. Note that the current oscillation data has a slight preference for NO over IO at about  $2\sigma$  level [90].

Similarly, the 95% CL Planck (TT,TE,EE,lowE+lensing+BAO) upper limit on the sum of neutrino masses  $\sum_i m_i < 0.12$  eV [1] translates into an upper bound on the lightest neutrino mass

$$m_0 \lesssim 0.05 \text{ eV}. \quad (2.20)$$

In our numerical analysis, we will fix  $m_0$  for both NO and IO which then determines  $m_f$  from Eqs. (2.18) and (2.19) respectively. Furthermore, for a given value of  $M_N$ , the Yukawa coupling parameters  $y_f$  are calculated using Eq. (2.17), which are used to get the form of  $Y_D$  in Eq. (2.6) that goes as an input into the leptogenesis calculation.

Note that the resulting PMNS mixing matrix in Eq. (2.14) is fixed by the symmetries  $G_f$ , CP,  $G_\ell$  and  $G_\nu$  up to the free real parameter  $\theta_L$ . Consequently, all mixing angles and CP phases are strongly correlated, because they all only depend on  $\theta_L$ . Since all lepton mixing angles  $\theta_{ij}$  (with  $i, j = 1, 2, 3$  and  $i < j$ ) have been measured with some accuracy [90], the admitted values of  $\theta_L$  are usually constrained to a rather narrow range [65].

As for the parametrization of the PMNS mixing matrix in terms of the low-energy lepton mixing angles, we take [74]

$$U = \tilde{U} \text{diag} \left( 1, e^{i\alpha_1/2}, e^{i(\alpha_2/2+\delta)} \right), \quad (2.21)$$

with  $\tilde{U}$  being of the form of the Cabibbo-Kobayashi-Maskawa (CKM) matrix  $V_{\text{CKM}}$  [90]

$$\tilde{U} = \begin{pmatrix} c_{12}c_{13} & s_{12}c_{13} & s_{13}e^{-i\delta} \\ -s_{12}c_{23} - c_{12}s_{23}s_{13}e^{i\delta} & c_{12}c_{23} - s_{12}s_{23}s_{13}e^{i\delta} & s_{23}c_{13} \\ s_{12}s_{23} - c_{12}c_{23}s_{13}e^{i\delta} & -c_{12}s_{23} - s_{12}c_{23}s_{13}e^{i\delta} & c_{23}c_{13} \end{pmatrix}, \quad (2.22)$$

and  $s_{ij} \equiv \sin \theta_{ij}$  and  $c_{ij} \equiv \cos \theta_{ij}$ . The mixing angles  $\theta_{ij}$  range from 0 to  $\pi/2$ , while the Majorana phases  $\alpha_1, \alpha_2$  as well as the Dirac phase  $\delta$  take values between 0 and  $2\pi$ . Note that one of the Majorana phases becomes unphysical, if the lightest neutrino mass  $m_0$  vanishes.

### 3 Different Cases

In this Section, we discuss the residual symmetries and the form of the corresponding representation matrices for four different cases, namely, Case 1, Case 2, Case 3a and Case

3b.1, as singled out in Ref. [74]. We discuss additional constraints imposed from light neutrino masses and the constraints on the neutrino mass spectrum arising from imposing the condition in Eq. (2.3). Furthermore, we briefly review the results for lepton mixing, as found in [65]. We also comment on the special points corresponding to specific choices of the parameters  $\theta_L$  and  $\theta_R$ , that lead to ERS of the Dirac neutrino Yukawa couplings.

### 3.1 Case 1

#### 3.1.1 Residual Symmetries

In this case, the residual  $Z_2$  symmetry in the neutrino sector is generated by

$$Z = c^{n/2}, \quad (3.1)$$

where  $c$  is one of the group generators (cf. Appendix A) and  $n$  is the index of the flavor group  $\Delta(6n^2)$ . Eq. (3.1) requires  $n$  to be even. The explicit form of  $Z$  in the irreducible, faithful, complex three-dimensional representation  $\mathbf{3}$  and in the irreducible, unfaithful, (in general) real three-dimensional representation  $\mathbf{3}'$  can be found in Appendix A. As we will see in Section 3.1.2, due to the form of the generator  $Z$  in  $\mathbf{3}'$  for  $n$  divisible by four the Dirac neutrino Yukawa coupling matrix  $Y_D$  becomes singular and the light neutrino mass is not viable. For this reason, we will only focus on  $4 \nmid n$  (in addition to  $3 \nmid n$ ) for Case 1.

The CP symmetry corresponds to the automorphism, given in Eq. (B.1), conjugated with the inner automorphism associated with the group transformation  $abc^s d^{2s}$  with  $s = 0, 1, \dots, n-1$ . The corresponding CP transformations  $X(s)$  read

$$X(s)(\mathbf{3}) = a(\mathbf{3})b(\mathbf{3})c(\mathbf{3})^s d(\mathbf{3})^{2s} X_0(\mathbf{3}), \quad (3.2a)$$

$$X(s)(\mathbf{3}') = a(\mathbf{3}')b(\mathbf{3}')c(\mathbf{3}')^s d(\mathbf{3}')^{2s} X_0(\mathbf{3}'), \quad (3.2b)$$

in  $\mathbf{3}$  and  $\mathbf{3}'$  respectively. The explicit forms of  $X(s)(\mathbf{3})$  and  $X(s)(\mathbf{3}')$  can be obtained using the group generators  $a, b, c, d$  given in Appendix A.

The unitary matrix  $\Omega(s)(\mathbf{3})$ , derived from  $X(\mathbf{3})(s)$ , can be chosen as

$$\Omega(s)(\mathbf{3}) = e^{i\phi_s} U_{\text{TB}} \begin{pmatrix} 1 & 0 & 0 \\ 0 & e^{-3i\phi_s} & 0 \\ 0 & 0 & -1 \end{pmatrix}, \quad (3.3)$$

with  $\phi_s = \pi s/n$  and the TB form for [92]

$$U_{\text{TB}} = \begin{pmatrix} \sqrt{2/3} & \sqrt{1/3} & 0 \\ -\sqrt{1/6} & \sqrt{1/3} & \sqrt{1/2} \\ -\sqrt{1/6} & \sqrt{1/3} & -\sqrt{1/2} \end{pmatrix}. \quad (3.4)$$

Based only on theoretical requirements, the form of the matrix  $\Omega(s)(\mathbf{3}')$  depends on whether  $s$  is even or odd, i. e.

$$\Omega(s \text{ even})(\mathbf{3}') = U_{\text{TB}}, \quad \Omega(s \text{ odd})(\mathbf{3}') = U_{\text{TB}} \begin{pmatrix} i & 0 & 0 \\ 0 & 1 & 0 \\ 0 & 0 & i \end{pmatrix}. \quad (3.5)$$

Comparing these forms to the form of  $\Omega(s)(\mathbf{3})$  in Eq. (3.3), we observe that they have the same structure, but the crucial difference lies in the phase matrix multiplied from the right (overall phases are clearly irrelevant).

In order to determine the plane in which the rotation  $R_{ij}(\theta_L)$  acts, we look at

$$\Omega(s)(\mathbf{3})^\dagger Z(\mathbf{3}) \Omega(s)(\mathbf{3}) = \begin{pmatrix} -1 & 0 & 0 \\ 0 & 1 & 0 \\ 0 & 0 & -1 \end{pmatrix}, \quad (3.6)$$

implying that the rotation through  $\theta_L$  will be in the (13)-plane [74]. Therefore, the PMNS mixing matrix is given by

$$U = \Omega(s)(\mathbf{3}) R_{13}(\theta) K_\nu, \quad (3.7)$$

where the rotation angle  $\theta$  is a free real parameter (related to  $\theta_L$ ) which is to be adjusted to its best-fit value  $\theta_{\text{bf}}$  in order to reproduce the best-fit with the measured lepton mixing angles.

Similarly, we can find the plane in which the rotation  $R_{kl}(\theta_R)$  acts. The representation matrix  $Z(\mathbf{3}')$  for  $4 \nmid n$  reads, after the transformation with  $\Omega(s)(\mathbf{3}')$  for both  $s$  even and  $s$  odd,

$$\Omega(s)(\mathbf{3}')^\dagger Z(\mathbf{3}') \Omega(s)(\mathbf{3}') = \begin{pmatrix} -1 & 0 & 0 \\ 0 & 1 & 0 \\ 0 & 0 & -1 \end{pmatrix}, \quad (3.8)$$

meaning that  $R_{kl}(\theta_R)$  also acts in the (13)-plane.

### 3.1.2 Constraints from and on Light Neutrino Sector

First, we discuss constraints on the possible choices of the residual symmetry  $G_\nu$  arising from the light neutrino mass spectrum. In order to find these we consider the form of the Dirac neutrino Yukawa coupling matrix  $Y_D$  fulfilling the conditions in Eq. (2.3). For  $n$  divisible by four,  $Z(\mathbf{3}')$  is nothing but the identity matrix [cf. Eq. (C.2)] and we find that the form of  $Y_D$  needs to be

$$Y_D = \begin{pmatrix} y_{11} & y_{12} & y_{13} \\ y_{11} & y_{12} & y_{13} \\ y_{11} & y_{12} & y_{13} \end{pmatrix}, \quad (3.9)$$

with  $y_{1i}$  complex,  $i = 1, 2, 3$ . It is clear from the form of  $Y_D$  in Eq. (3.9) that the determinant vanishes and that  $Y_D$  has two zero eigenvalues. As a consequence, the light neutrino mass matrix arising from the type-I seesaw mechanism [cf. Eq. (2.17)] also has two zero eigenvalues. Furthermore, we can check that the non-zero eigenvalue has to correspond to the second light neutrino mass, since it is always associated with the eigenvector proportional to  $(1, 1, 1)^T$  which can only be identified with the second column of the PMNS mixing matrix. It is, however, experimentally highly disfavored that such a form can be the dominant contribution to light neutrino masses. Indeed, we can show that, if  $Z(\mathbf{3}')$  is

the identity matrix and  $Z(\mathbf{3})$  is any generator of a  $Z_2$  symmetry, i.e. it can be represented by a matrix  $Z(\mathbf{3})$  that fulfills

$$V^\dagger Z(\mathbf{3}) V = \text{diag}(1, -1, -1), \quad (3.10)$$

with  $V$  being a unitary matrix, then

$$Z(\mathbf{3})^\dagger Y_D = V \text{diag}(1, -1, -1) V^\dagger Y_D = Y_D, \quad (3.11)$$

or we can rewrite this condition as

$$\text{diag}(1, -1, -1) \left[ V^\dagger Y_D \right] = \left[ V^\dagger Y_D \right]. \quad (3.12)$$

Consequently, the combination  $V^\dagger Y_D$  must have two vanishing rows, namely the second and the third ones. In particular, the determinant of  $V^\dagger Y_D$  vanishes. From the latter, we can conclude for  $Y_D$  itself that its determinant must vanish, since the determinant of  $V$  cannot be zero. In addition, we can also know that  $Y_D$  must have two vanishing eigenvalues. So, in general knowing that  $Z(\mathbf{3}')$  is given by the identity matrix is sufficient in order to discard this case as realistic without corrections which can induce, at least, one further non-vanishing neutrino mass. We thus do not discuss further the case where  $n$  is divisible by four.

For  $n$  not divisible by four, the form of the matrix  $Z(\mathbf{3}')$  is shown in Eq. (C.3). Again, we can compute the constraints on  $Y_D$ , arising from imposing the conditions in Eq. (2.3). In particular, we see that the first condition in Eq. (2.3) reduces the number of free (complex) parameters in  $Y_D$  from nine to five, meaning the other four can be expressed in terms of these, e.g.

$$\begin{aligned} y_{23} &= y_{11} + y_{12} + y_{13} - y_{21} - y_{22}, & y_{31} &= y_{12} + y_{13} - y_{21}, \\ y_{32} &= y_{11} + y_{13} - y_{22}, & y_{33} &= -y_{13} + y_{21} + y_{22}. \end{aligned} \quad (3.13)$$

The five free complex parameters in  $Y_D$  are further constrained by requiring that also the second condition in Eq. (2.3) is fulfilled. As a consequence, these parameters have to be real. This is consistent with the findings in the general case where  $Y_D$  contains three real Yukawa couplings  $y_f$ ,  $f = 1, 2, 3$  and two angles  $\theta_L$  and  $\theta_R$ . In general, such a matrix  $Y_D$  has a non-vanishing determinant and three different eigenvalues, namely (proportional to)  $y_f$ .

We know from the type-I seesaw formula [cf. Eq. (1.1)] that for eventually relating the parameters of  $Y_D$  to the light neutrino masses, we have to look at the following expression

$$\Omega(s)(\mathbf{3}')^\dagger M_R^{-1} \Omega(s)(\mathbf{3}')^*, \quad (3.14)$$

with  $M_R$  as in Eq. (2.8). For  $\Omega(s)(\mathbf{3}')$  in (3.5) we find

$$\Omega(s \text{ even})(\mathbf{3}')^\dagger M_R^{-1} \Omega(s \text{ even})(\mathbf{3}')^* = \frac{1}{M_N} \begin{pmatrix} 1 & 0 & 0 \\ 0 & 1 & 0 \\ 0 & 0 & -1 \end{pmatrix}, \quad (3.15a)$$

$$\Omega(s \text{ odd})(\mathbf{3}')^\dagger M_R^{-1} \Omega(s \text{ odd})(\mathbf{3}')^* = \frac{1}{M_N} \begin{pmatrix} -1 & 0 & 0 \\ 0 & 1 & 0 \\ 0 & 0 & 1 \end{pmatrix}. \quad (3.15b)$$

Note that in both cases the resulting structure is simple but does not commute with the arbitrary rotations  $R_{13}(\theta_{L,R})$ . Hence, this has to be taken into account when computing the light neutrino masses from the type-I seesaw formula [cf. Eq. (1.1)]. Indeed only the light neutrino mass  $m_2$  is related to  $y_2$  and  $M_N$  in a trivial way [cf. Eq. (D.1b)], while for the full matrix part, we calculate

$$M_\nu = v^2 \begin{pmatrix} y_1 & 0 & 0 \\ 0 & y_2 & 0 \\ 0 & 0 & y_3 \end{pmatrix} R_{13}(-\theta_R) \Omega(s)(\mathbf{3}')^\dagger M_R^{-1} \Omega(s)(\mathbf{3}')^* R_{13}(\theta_R) \begin{pmatrix} y_1 & 0 & 0 \\ 0 & y_2 & 0 \\ 0 & 0 & y_3 \end{pmatrix} \quad (3.16)$$

which yields

$$M_\nu (s \text{ even}) = \frac{v^2}{M_N} \begin{pmatrix} y_1^2 \cos 2\theta_R & 0 & y_1 y_3 \sin 2\theta_R \\ 0 & y_2^2 & 0 \\ y_1 y_3 \sin 2\theta_R & 0 & -y_3^2 \cos 2\theta_R \end{pmatrix}, \quad (3.17a)$$

$$M_\nu (s \text{ odd}) = \frac{v^2}{M_N} \begin{pmatrix} -y_1^2 \cos 2\theta_R & 0 & -y_1 y_3 \sin 2\theta_R \\ 0 & y_2^2 & 0 \\ -y_1 y_3 \sin 2\theta_R & 0 & y_3^2 \cos 2\theta_R \end{pmatrix}. \quad (3.17b)$$

The difference is just the overall sign so we can nicely treat both cases of  $s$  even and  $s$  odd at once, as shown in Appendix D.1.

We note a few things regarding the matrices in Eq. (3.17): if we set  $y_1 = 0$ , then  $m_1$  vanishes and we obtain NO with the matrix being automatically diagonal and does not need a further rotation; on the other hand, if we set  $y_3 = 0$ ,  $m_3 = 0$  follows, and we obtain IO and again the matrix is automatically diagonal with no further rotation required. We can also set  $\sin 2\theta_R = 0$  leading to no further rotation needed as well, but in this case there are also no constraints on the neutrino masses. Some values of  $\theta_R$  are not admitted, e.g.  $\cos 2\theta_R = 0$  and consequently,  $\sin 2\theta_R = \pm 1$  (meaning  $\theta_R = \pi/4, 3\pi/4$ , etc.), since then two of the neutrino masses are degenerate.<sup>5</sup> Similar statements hold in the other cases that have matrices like in Eq. (3.17) as part of the light neutrino mass matrix, because the combination in (3.14) is not trivial in flavor space.

The general solution for both cases goes as follows: For  $s$  even, the PMNS lepton mixing matrix [cf. Eq. (3.7)] is given by

$$U = \Omega(s)(\mathbf{3}) R_{13}(\theta_L - \psi) \text{diag}(1, 1, \pm i), \quad (3.18)$$

with

$$\tan^2 \psi \equiv \frac{m_1 + m_3 - \sqrt{m_1^2 + m_3^2 + 2m_1 m_3 \cos(4\theta_R)}}{m_1 + m_3 + \sqrt{m_1^2 + m_3^2 + 2m_1 m_3 \cos(4\theta_R)}}. \quad (3.19)$$

---

<sup>5</sup>For the matrices in Eq. (3.17), these two are the first and the third neutrino masses, and thus, the spectrum becomes completely unrealistic.

The Yukawa matrix  $Y_D$  is constructed from Eq. (2.6), using the expressions of  $\Omega(s)(\mathbf{3})$  and  $\Omega(s)(\mathbf{3}')$  corresponding to  $s$ -even, as given in Eqs. (3.3) and (3.5) respectively. The Yukawa parameters  $y_f$  in this case are explicitly given in Appendix D.1. For  $s$  odd, the PMNS lepton mixing matrix is

$$U = \Omega(s)(\mathbf{3}) R_{13}(\theta_L - \psi) \text{diag}(\pm i, 1, 1), \quad (3.20)$$

with  $\psi$  introduced in Eq. (3.19). The Yukawa matrix  $Y_D$  is constructed using the expressions of  $\Omega(s)(\mathbf{3})$  and  $\Omega(s)(\mathbf{3}')$  corresponding to  $s$ -odd. The parameters  $y_f$  are same as in the  $s$  even case, cf. Appendix D.1. Notice that  $y_f$  are real quantities, provided  $-\pi/4 < \theta_R < \pi/4$ .

For our numerical study of Case 1 in this paper, we will choose  $n = 26$  as an example which fulfills all the constraints on  $n$ , i.e.  $n$  even and not divisible by three or four. The corresponding form of  $Y_D$  can be easily computed from Eq. (2.6), but we can also explicitly check by applying the conditions in Eq. (2.3) to a general complex  $3 \times 3$  matrix  $Y_D$  that this is the correct form of the Dirac mass matrix of the neutrinos. The actual expressions are quite lengthy and not very illuminating, thus we do not display them explicitly here, but they can be easily derived with the information given above.

We notice that only five real parameters  $y_f$  (with  $f = 1, 2, 3$ ),  $\theta_L$  and  $\theta_R$  appear in  $Y_D$  and that lepton mixing depends effectively only on one free parameter  $\theta = \theta_L - \psi$ , which has to be adjusted to  $\theta_{\text{bf}}$  in order to obtain the best-fit with the measured mixing angles [91]. If the expression in Eq. (3.14) is proportional to the identity matrix,  $\theta$  is simply given by  $\theta_L$  (since  $\psi = 0$  in this case) and  $y_f$  can be directly matched to the light neutrino masses  $m_f$ . If this is not true and we find a situation like in Eq. (3.15), there is only one coupling  $y_{f'}$  directly proportional to one light neutrino mass  $m_{f'}$ , whereas the other two together with  $\theta_R$  determine the remaining two light neutrino masses, as shown in Appendix D.1. In addition, these three parameters determine another mixing angle  $\psi$  given by Eq. (3.19), that together with  $\theta_L$  gives  $\theta_{\text{bf}} \equiv \theta_L - \psi$ . Hence, in both cases there are four experimentally constrained quantities (three neutrino masses and  $\theta_{\text{bf}}$ ) which determine five free parameters, namely,  $y_f$ ,  $\theta_L$  and  $\theta_R$ . Thus, only one of them (usually  $\theta_R$ ) can be chosen freely.

We give here an example from Ref. [74] which leads to the mixing pattern of Case 1. The characteristics of this mixing pattern are the following: the mixing angles can always be fitted well, independent of the choice of the group  $\Delta(6n^2)$  as well as the CP symmetry  $X(s)$ , if we choose the free parameter  $\theta_{\text{bf}}$  correctly. In the limit of residual symmetries  $G_\nu$  and  $G_\ell$ , we obtain that the lepton mixing angles can be accommodated well for  $\theta_L \approx 0.18$  (2.96), for which we get  $\sin^2 \theta_{13} \approx 0.0219$ ,  $\sin^2 \theta_{12} \approx 0.341$  and  $\sin^2 \theta_{23} \approx 0.605$  (0.395). The results of the CP phases are simple: the Dirac phase  $\delta$  as well as one of the Majorana phases  $\alpha_2$  are trivial, i.e.  $\sin \delta = 0$ <sup>6</sup> and  $\sin \alpha_2 = 0$ , while the other Majorana phase  $\alpha_1$  depends on the chosen CP symmetry  $X(s)$ . For strong NO (IO), we get

$$\sin \alpha_1 = (-1)^{k+r+s} \sin(6\phi_s), \quad \text{and} \quad \cos \alpha_1 = (-1)^{k+r+s+1} \cos(6\phi_s), \quad (3.21)$$

where  $k = 0$  ( $k = 1$ ) for  $\cos 2\theta_R > 0$  ( $\cos 2\theta_R < 0$ ) and  $r = 0$  ( $r = 1$ ).

---

<sup>6</sup>Although there is a mild preference for a nonzero  $\delta$  in the global fit of neutrino oscillation data [91],  $\delta = 0$  is still allowed at 1-2 $\sigma$  confidence level [90]; therefore our Case 1 is not excluded yet.

### 3.1.3 Enhanced Residual Symmetries

For particular values of  $\theta_L$  and  $\theta_R$ , the residual symmetry  $G_\nu = Z_2 \times \text{CP}$  can be enhanced. If  $\theta_L = 0$  or  $\pi$ , the combination  $M_D M_D^\dagger$  becomes invariant under a further  $Z_2$  subgroup of  $G_f$ . Similarly, for the choices  $\theta_R = 0, \pi/2, \pi$  and  $3\pi/2$ , the combination  $M_D^\dagger M_D$  preserves a symmetry larger than  $G_\nu$ . This symmetry is also larger than the one of  $M_D M_D^\dagger$  for  $\theta_L = 0, \pi$  since RHNs transform as the real representation  $\mathbf{3}'$  of  $G_f$  that is unfaithful for  $n > 2$ .

These points of ERS are of particular relevance for phenomenology, since  $\theta_L$  deviating from  $\theta_{L,0} = 0$  or  $\pi$  leads to a non-zero value of the reactor mixing angle  $\theta_{13}$ , as confirmed experimentally [90]. Similarly,  $\theta_R$  close to  $\theta_{R,0} = 0, \pi/2, \pi$  or  $3\pi/2$  makes it possible for the RHN  $N_3$  to be long-lived enough for being detected with the LLP searches (see Section 5.2), while simultaneously maximizing the CP asymmetries  $\varepsilon_{i\alpha}$  relevant for leptogenesis (see Section 4). One can argue that the larger the ERS is, the smaller the deviation from points of ERS will be, i.e.  $\theta_R$  is expected to deviate from  $\theta_{R,0}$  by  $\delta\theta_R = |\theta_R - \theta_{R,0}| \lesssim 0.01$ , while  $\theta_L$  can deviate from  $\theta_{L,0}$  up to  $\delta\theta_L = |\theta_L - \theta_{L,0}| \sim 0.2$ .

In one type of explicit models [93], the flavor and CP symmetry are spontaneously broken to the residual symmetries  $G_\nu$  and  $G_\ell$  with the help of flavor symmetry breaking fields and a peculiar alignment of their VEVs, achieved with a particular form of the potential. Depending on the fields and the form of the potential, an ERS larger than  $G_\nu$  and  $G_\ell$  can be preserved at leading order. Higher-dimensional operators then induce small deviations from these points of ERS, thus explaining the particular sizes of  $\theta_L$  and  $\theta_R$ . An example can be found in Ref. [94], where the correct size of  $\theta_L$  and thus the observed reactor mixing angle  $\theta_{13}$  are generated in this way.

## 3.2 Case 2

### 3.2.1 Residual Symmetries

The residual  $Z_2$  symmetry in the neutrino sector is generated by the same element  $Z = c^{n/2}$  as in Case 1 [cf. Eq. (3.1)]; therefore,  $n$  must be even. Thus, all comments made in the context of Case 1, and in particular, the forms of  $Z(\mathbf{3})$  and  $Z(\mathbf{3}')$  in Eqs. (C.1) and (C.2), (C.3), apply respectively.

The CP symmetry is given by the automorphism in Eq. (B.1) and the inner automorphism  $h = c^s d^t$  with  $0 \leq s, t \leq n-1$  and thus depends on two parameters:  $X(s, t)$ . In the three-dimensional representations  $\mathbf{3}$  and  $\mathbf{3}'$ ,  $X(s, t)$  is respectively given by

$$X(s, t)(\mathbf{3}) = c(\mathbf{3})^s d(\mathbf{3})^t X_0(\mathbf{3}) \quad \text{and} \quad X(s, t)(\mathbf{3}') = c(\mathbf{3}')^s d(\mathbf{3}')^t X_0(\mathbf{3}'). \quad (3.22)$$

The explicit forms can be found in Appendix B.

In the analysis of lepton mixing patterns for Case 2 in Ref. [74], it turned out to be more convenient to use the parameters  $u$  and  $v$  that are linearly related to  $s$  and  $t$  as follows:

$$u = 2s - t \quad \text{and} \quad v = 3t. \quad (3.23)$$

Since  $0 \leq s, t \leq n-1$ , the admitted intervals for  $u$  and  $v$  are  $-(n-1) \leq u \leq 2(n-1)$  and  $0 \leq v \leq 3(n-1)$ . Here we use  $(s, t)$  and  $(u, v)$  interchangeably as needed. A suitable

choice of the matrix  $\Omega(s, t)(\mathbf{3})$  is given by

$$\Omega(s, t)(\mathbf{3}) = e^{i\phi_v/6} U_{\text{TB}} R_{13} \left( -\frac{\phi_u}{2} \right) \begin{pmatrix} 1 & 0 & 0 \\ 0 & e^{-i\phi_v/2} & 0 \\ 0 & 0 & -i \end{pmatrix}, \quad (3.24)$$

with  $\phi_u = \pi u/n$  and  $\phi_v = \pi v/n$ .

The form of the matrix  $\Omega(s, t)(\mathbf{3}')$ , derived from  $X(\mathbf{3})(s, t)$ , depends like the latter on whether  $s$  and  $t$  are even or odd. The explicit form of  $\Omega(s, t)(\mathbf{3}')$ , however, does neither contain  $s$  nor  $t$  as parameters, and is given by

$$\Omega(s \text{ even}, t \text{ even})(\mathbf{3}') = U_{\text{TB}} \begin{pmatrix} 1 & 0 & 0 \\ 0 & 1 & 0 \\ 0 & 0 & i \end{pmatrix}, \quad (3.25a)$$

$$\Omega(s \text{ odd}, t \text{ even})(\mathbf{3}') = U_{\text{TB}} \begin{pmatrix} i & 0 & 0 \\ 0 & 1 & 0 \\ 0 & 0 & 1 \end{pmatrix}, \quad (3.25b)$$

$$\Omega(s \text{ even}, t \text{ odd})(\mathbf{3}') = e^{-i\pi/4} U_{\text{TB}} R_{13} \left( \frac{\pi}{4} \right) \begin{pmatrix} e^{-i\pi/2} & 0 & 0 \\ 0 & e^{-i\pi/4} & 0 \\ 0 & 0 & 1 \end{pmatrix}, \quad (3.25c)$$

$$\Omega(s \text{ odd}, t \text{ odd})(\mathbf{3}') = e^{-3i\pi/4} U_{\text{TB}} R_{13} \left( \frac{\pi}{4} \right) \begin{pmatrix} e^{-i\pi/2} & 0 & 0 \\ 0 & e^{i\pi/4} & 0 \\ 0 & 0 & 1 \end{pmatrix}. \quad (3.25d)$$

Similar as in Case 1, the rotation associated with the representation  $\mathbf{3}$  and thus with LH leptons is always  $R_{13}(\theta_L)$ . Therefore, the PMNS mixing matrix is given by a form similar to Eq. (3.7), i.e.

$$U = \Omega(s, t)(\mathbf{3}) R_{13}(\theta) K_\nu. \quad (3.26)$$

For all choices of  $(s, t)$  above,  $\Omega(s, t)(\mathbf{3}')$  fulfills the two equations, i.e.  $Z(\mathbf{3}')$  always like in Eq. (C.3) and

$$\Omega(s, t)(\mathbf{3}')^\dagger Z(\mathbf{3}') \Omega(s, t)(\mathbf{3}') = \begin{pmatrix} -1 & 0 & 0 \\ 0 & 1 & 0 \\ 0 & 0 & -1 \end{pmatrix} \quad (3.27)$$

and hence, also for the representation  $\mathbf{3}'$  for RHNs, the relevant rotation is in the (13)-plane, namely  $R_{13}(\theta_R)$ . We observe that for none of the above combinations of  $X$  and  $Z$  in  $\mathbf{3}$  and  $\mathbf{3}'$ , we find zero eigenvalues for  $Y_D$  as long as we only consider cases in which  $n$  is not divisible by four so that  $Z(\mathbf{3}')$  is not the identity matrix; see discussion in Section 3.1.1.

### 3.2.2 Constraints from and on Light Neutrino Sector

As a further step, we present the form of the relevant matrix combination appearing in the type-I seesaw formula, involving  $\Omega(s, t)(\mathbf{3}')$  and  $M_R$  [cf. (3.14)]. We find that

$$\Omega(s \text{ even}, t \text{ even})(\mathbf{3}')^\dagger M_R^{-1} \Omega(s \text{ even}, t \text{ even})(\mathbf{3}')^\star = \frac{1}{M_N} \begin{pmatrix} 1 & 0 & 0 \\ 0 & 1 & 0 \\ 0 & 0 & 1 \end{pmatrix} \quad (3.28a)$$

$$\Omega(s \text{ odd}, t \text{ even})(\mathbf{3}')^\dagger M_R^{-1} \Omega(s \text{ odd}, t \text{ even})(\mathbf{3}')^\star = \frac{1}{M_N} \begin{pmatrix} -1 & 0 & 0 \\ 0 & 1 & 0 \\ 0 & 0 & -1 \end{pmatrix} \quad (3.28b)$$

$$\Omega(s \text{ even}, t \text{ odd})(\mathbf{3}')^\dagger M_R^{-1} \Omega(s \text{ even}, t \text{ odd})(\mathbf{3}')^\star = \frac{1}{M_N} \begin{pmatrix} 0 & 0 & -1 \\ 0 & -1 & 0 \\ -1 & 0 & 0 \end{pmatrix} \quad (3.28c)$$

$$\Omega(s \text{ odd}, t \text{ odd})(\mathbf{3}')^\dagger M_R^{-1} \Omega(s \text{ odd}, t \text{ odd})(\mathbf{3}')^\star = \frac{1}{M_N} \begin{pmatrix} 0 & 0 & 1 \\ 0 & -1 & 0 \\ 1 & 0 & 0 \end{pmatrix}. \quad (3.28d)$$

Using this, we thus obtain the form of the light neutrino mass matrix for the different choices of  $s$  and  $t$ :

$$M_\nu(s \text{ even}, t \text{ even}) = \frac{v^2}{M_N} \begin{pmatrix} y_1^2 & 0 & 0 \\ 0 & y_2^2 & 0 \\ 0 & 0 & y_3^2 \end{pmatrix} \quad (3.29a)$$

$$M_\nu(s \text{ odd}, t \text{ even}) = \frac{v^2}{M_N} \begin{pmatrix} -y_1^2 & 0 & 0 \\ 0 & y_2^2 & 0 \\ 0 & 0 & -y_3^2 \end{pmatrix} \quad (3.29b)$$

$$M_\nu(s \text{ even}, t \text{ odd}) = \frac{v^2}{M_N} \begin{pmatrix} y_1^2 \sin 2\theta_R & 0 & -y_1 y_3 \cos 2\theta_R \\ 0 & -y_2^2 & 0 \\ -y_1 y_3 \cos 2\theta_R & 0 & -y_3^2 \sin 2\theta_R \end{pmatrix} \quad (3.29c)$$

$$M_\nu(s \text{ odd}, t \text{ odd}) = \frac{v^2}{M_N} \begin{pmatrix} -y_1^2 \sin 2\theta_R & 0 & y_1 y_3 \cos 2\theta_R \\ 0 & -y_2^2 & 0 \\ y_1 y_3 \cos 2\theta_R & 0 & y_3^2 \sin 2\theta_R \end{pmatrix}. \quad (3.29d)$$

These forms are very similar to those encountered before in Case 1 [cf. Eq. (3.17)] and thus can be treated in the same way to obtain PMNS lepton mixing matrix. It turns out that the expressions for the  $y_f$ 's only depend on whether  $t$  is even or odd, irrespective of the choice of  $s$ . For  $t$  even, the  $y_f$ 's are trivially related to the  $m_f$ 's; see Eq. (D.2). For  $t$ -odd,  $s$ -even case, the PMNS lepton mixing matrix (3.26) is

$$U = \Omega(s, t)(\mathbf{3}) R_{13}(\theta_L - \eta) \text{diag}(\pm i, \pm i, 1), \quad (3.30)$$

with

$$\tan^2 \eta \equiv \frac{m_1 + m_3 + \sqrt{m_1^2 + m_3^2 - 2m_1 m_3 \cos(4\theta_R)}}{m_1 + m_3 - \sqrt{m_1^2 + m_3^2 - 2m_1 m_3 \cos(4\theta_R)}}. \quad (3.31)$$

The Yukawa matrix  $Y_D$  is constructed from Eq. (2.6), using the expressions of  $\Omega(s, t)(\mathbf{3})$  and  $\Omega(s, t)(\mathbf{3}')$  corresponding to  $s$ -even and  $t$ -odd. The parameters  $y_f$  in this case are given in Eq. (D.3). We get the same  $y_f$  expressions for the  $t$ -odd,  $s$ -odd case. Note that these Yukawa parameters are real for  $0 < \theta_R < \pi/2$ .

The results for lepton mixing in Case 2 are much richer than in Case 1, and indeed, in general all CP phases are non-trivial. We can observe the following approximate dependence of the different CP phases on the parameters  $u$  and  $v$  (for  $k_{1,2} = 0$  in Eq. (2.15) and no shift in  $u$ ):

$$\sin \delta \approx \pm 1 \mp 3.3 \phi_u^2, \quad \sin \alpha_1 \approx -\sin \phi_v, \quad \sin \alpha_2 \approx \mp 5.6 \phi_u \pm 23 \phi_u^3. \quad (3.32)$$

Detailed numerical results, including tables with examples of  $n$ ,  $u$ ,  $v$  and  $\theta_{\text{bf}}$  that permit agreement of the three lepton mixing angles with experimental observations at the  $3\sigma$  level or better can be found in Ref. [74]. In our numerical analysis, we will use  $n = 14$  and  $u = 0$  as the representative example for Case 2. In this case, we get  $\theta_{\text{bf}} \approx 2.96$ , and  $\sin^2 \theta_{12} \approx 0.341$ ,  $\sin^2 \theta_{13} \approx 0.0218$ ,  $\sin^2 \theta_{23} \approx 0.5$ . As for the CP phases, we find  $\sin \delta = 1$  and  $\sin \alpha_2 = 0$ , whereas  $\alpha_1$  is non-trivial and depends on the choice of  $v$  [cf. Eq. (3.32)].

As for the ERS points, we will see in Section 5.2 that the ERS points only occur for  $t$  even (irrespective of whether  $s$  is even or odd) and at the same  $\theta_R$  values as in Case 1.

### 3.3 Case 3

#### 3.3.1 Residual Symmetries

In this case the  $Z_2$  symmetry in the neutrino sector is generated by

$$Z = bc^m d^m \quad \text{with } 0 \leq m \leq n-1. \quad (3.33)$$

Since  $Z$  involves the generator  $b$ , this case can only be realized for the flavor group  $\Delta(6n^2)$ . We have in general  $n$  different choices for the generator  $Z$ . However, as discussed in Ref. [74], preferred values of  $m$  are either around  $m \approx 0$  and  $m \approx n$  for Case 3a, or  $m \approx n/2$  for Case 3b.1, as long as the charged lepton masses are ordered canonically. The form of  $Z$  in the representations  $\mathbf{3}$  and  $\mathbf{3}'$  can be found in Appendix A.

The CP symmetry is induced by the automorphism, shown in Eq. (B.1), conjugated with the inner one, represented by the group transformation  $h = b c^s d^{n-s}$  with  $0 \leq s \leq n-1$ . The corresponding CP transformations  $X(s)$  in  $\mathbf{3}$  and  $\mathbf{3}'$  are respectively given by

$$X(s)(\mathbf{3}) = b(\mathbf{3})^s c(\mathbf{3})^s d(\mathbf{3})^{n-s} X_0(\mathbf{3}), \quad X(s)(\mathbf{3}') = b(\mathbf{3}')^s c(\mathbf{3}')^s d(\mathbf{3}')^{n-s} X_0(\mathbf{3}'). \quad (3.34)$$

The explicit forms of  $X(s)(\mathbf{3})$  and  $X(s)(\mathbf{3}')$  can be found in Appendix B.

The form of the matrix  $\Omega(s, m)(\mathbf{3})$ , derived from  $X(s, m)(\mathbf{3})$  in Eq. (B.5), is given by

$$\Omega(s, m)(\mathbf{3}) = e^{i\phi_s} \begin{pmatrix} 1 & 0 & 0 \\ 0 & \omega & 0 \\ 0 & 0 & \omega^2 \end{pmatrix} U_{\text{TB}} \begin{pmatrix} 1 & 0 & 0 \\ 0 & e^{-3i\phi_s} & 0 \\ 0 & 0 & -1 \end{pmatrix} R_{13}(\phi_m), \quad (3.35)$$

with  $\phi_s = \pi s/n$  and  $\phi_m = \pi m/s$ . The form of the matrix  $\Omega(s)(\mathbf{3}')$  only depends on whether  $s$  is even or odd and is independent of the choice of the parameter  $m$ . We use

$$\Omega(s \text{ even})(\mathbf{3}') = \begin{pmatrix} 1 & 0 & 0 \\ 0 & \omega & 0 \\ 0 & 0 & \omega^2 \end{pmatrix} U_{\text{TB}} \begin{pmatrix} 1 & 0 & 0 \\ 0 & 1 & 0 \\ 0 & 0 & -1 \end{pmatrix}, \quad (3.36a)$$

$$\Omega(s \text{ odd})(\mathbf{3}') = \begin{pmatrix} 1 & 0 & 0 \\ 0 & \omega & 0 \\ 0 & 0 & \omega^2 \end{pmatrix} U_{\text{TB}} \begin{pmatrix} i & 0 & 0 \\ 0 & -1 & 0 \\ 0 & 0 & -i \end{pmatrix}. \quad (3.36b)$$

We note that the form of  $\Omega(s \text{ even})(\mathbf{3}')$  coincides with  $\Omega(s, m)(\mathbf{3})$  for the special choices  $s = 0$  and  $m = 0$ . Similarly,  $\Omega(s \text{ odd})(\mathbf{3}')$  coincides with  $\Omega(s, m)(\mathbf{3})$  for  $s = n/2$  and  $m = 0$ .

We have to compute the form of the matrix  $Z(m)(\mathbf{3})$  in the basis rotated via  $\Omega(s, m)(\mathbf{3})$  for the representation  $\mathbf{3}$  which means

$$\Omega(s, m)(\mathbf{3})^\dagger Z(m)(\mathbf{3}) \Omega(s, m)(\mathbf{3}) = \begin{pmatrix} 1 & 0 & 0 \\ 0 & 1 & 0 \\ 0 & 0 & -1 \end{pmatrix}. \quad (3.37)$$

Note that this holds for all choices of  $s$ ,  $m$  and  $n$ . So, we know that LH leptons, being in the representation  $\mathbf{3}$ , are always accompanied with a rotation  $R_{12}(\theta_L)$  with the rotation angle  $\theta_L$  related to the fitting of the lepton mixing angles. Therefore, the PMNS mixing matrix in this case is

$$U = \Omega(s, m)(\mathbf{3}) R_{12}(\theta) K_\nu. \quad (3.38)$$

In the next step we consider the form of  $Z(\mathbf{3}')$  [cf. Eq. (C.6)] in the basis rotated by  $\Omega(s \text{ even})(\mathbf{3}')$  and  $\Omega(s \text{ odd})(\mathbf{3}')$ , respectively. The matrix  $Z(m \text{ even})(\mathbf{3}')$  reads as follows in the basis rotated by  $\Omega(s \text{ even})(\mathbf{3}')$ :

$$\Omega(s \text{ even})(\mathbf{3}')^\dagger Z(m \text{ even})(\mathbf{3}') \Omega(s \text{ even})(\mathbf{3}') = \begin{pmatrix} 1 & 0 & 0 \\ 0 & 1 & 0 \\ 0 & 0 & -1 \end{pmatrix} \quad (3.39)$$

and in the basis rotated by  $\Omega(s \text{ odd})(\mathbf{3}')$  it reads the same:

$$\Omega(s \text{ odd})(\mathbf{3}')^\dagger Z(m \text{ even})(\mathbf{3}') \Omega(s \text{ odd})(\mathbf{3}') = \begin{pmatrix} 1 & 0 & 0 \\ 0 & 1 & 0 \\ 0 & 0 & -1 \end{pmatrix}. \quad (3.40)$$

Hence, in both cases we need a rotation  $R_{12}(\theta_R)$  for the RHN fields in the representation  $\mathbf{3}'$ . Doing the same for the matrix  $Z(m \text{ odd})(\mathbf{3}')$  in the basis rotated with  $\Omega(s \text{ even})(\mathbf{3}')$ , we get

$$\Omega(s \text{ even})(\mathbf{3}')^\dagger Z(m \text{ odd})(\mathbf{3}') \Omega(s \text{ even})(\mathbf{3}') = \begin{pmatrix} -1 & 0 & 0 \\ 0 & 1 & 0 \\ 0 & 0 & 1 \end{pmatrix}, \quad (3.41)$$

and in the basis rotated by  $\Omega(s \text{ odd})(\mathbf{3}')$ , we find as well

$$\Omega(s \text{ odd})(\mathbf{3}')^\dagger Z(m \text{ odd})(\mathbf{3}') \Omega(s \text{ odd})(\mathbf{3}') = \begin{pmatrix} -1 & 0 & 0 \\ 0 & 1 & 0 \\ 0 & 0 & 1 \end{pmatrix}. \quad (3.42)$$

Thus, in both bases the free rotation due to  $Z(m \text{ odd})(\mathbf{3}')$  is given by  $R_{23}(\theta_R)$  among the RHNs.

### 3.3.2 Constraints from and on Light Neutrino Sector

A further step is to check the relevant combination in (3.14) for which we find

$$\Omega(s \text{ even})(\mathbf{3}')^\dagger M_R^{-1} \Omega(s \text{ even})(\mathbf{3}')^\star = \frac{1}{M_N} \begin{pmatrix} 1 & 0 & 0 \\ 0 & 1 & 0 \\ 0 & 0 & -1 \end{pmatrix}, \quad (3.43a)$$

$$\Omega(s \text{ odd})(\mathbf{3}')^\dagger M_R^{-1} \Omega(s \text{ odd})(\mathbf{3}')^\star = \frac{1}{M_N} \begin{pmatrix} -1 & 0 & 0 \\ 0 & 1 & 0 \\ 0 & 0 & 1 \end{pmatrix}. \quad (3.43b)$$

Using these results, we see that for  $m$  even,  $s$  even, and for  $m$  odd,  $s$  odd, the structure of the light neutrino mass matrix is trivial, i.e. diagonal, and we obtain a direct relation between the Yukawa couplings and the light neutrino masses, cf. Eq. (D.4). The same is true in Case 3b.1, except for an additional permutation of the rows of the PMNS mixing matrix, cf. Eq. (D.7). For the other two combinations of  $m$  and  $s$ , the structure is analogous to the ones shown in Eq. (3.17), although we have to change the rotation plane for  $R_{ij}(\theta_R)$ . For  $m$  even,  $s$  odd, we get

$$\begin{aligned} M_\nu &= v^2 \begin{pmatrix} y_1 & 0 & 0 \\ 0 & y_2 & 0 \\ 0 & 0 & y_3 \end{pmatrix} R_{12}(-\theta_R) \Omega(s \text{ odd})(\mathbf{3}')^\dagger M_R^{-1} \Omega(s \text{ odd})(\mathbf{3}')^\star R_{12}(\theta_R) \begin{pmatrix} y_1 & 0 & 0 \\ 0 & y_2 & 0 \\ 0 & 0 & y_3 \end{pmatrix} \\ &= \frac{v^2}{M_N} \begin{pmatrix} -y_1^2 \cos 2\theta_R & -y_1 y_2 \sin 2\theta_R & 0 \\ -y_1 y_2 \sin 2\theta_R & y_2^2 \cos 2\theta_R & 0 \\ 0 & 0 & y_3^2 \end{pmatrix}, \end{aligned} \quad (3.44)$$

and for  $m$  odd,  $s$  even, we get

$$\begin{aligned} M_\nu &= v^2 \begin{pmatrix} y_1 & 0 & 0 \\ 0 & y_2 & 0 \\ 0 & 0 & y_3 \end{pmatrix} R_{23}(-\theta_R) \Omega(s \text{ even})(\mathbf{3}')^\dagger M_R^{-1} \Omega(s \text{ even})(\mathbf{3}')^\star R_{23}(\theta_R) \begin{pmatrix} y_1 & 0 & 0 \\ 0 & y_2 & 0 \\ 0 & 0 & y_3 \end{pmatrix} \\ &= \frac{v^2}{M_N} \begin{pmatrix} y_1^2 & 0 & 0 \\ 0 & y_2^2 \cos 2\theta_R & y_2 y_3 \sin 2\theta_R \\ 0 & y_2 y_3 \sin 2\theta_R & -y_3^2 \cos 2\theta_R \end{pmatrix}. \end{aligned} \quad (3.45)$$

In these latter two cases, the relation (2.17) holds for only one of the three neutrino generations, whereas the other two belong to a sub-sector that requires further diagonalization,

in a way discussed already for Case 1. As an example, we present the general result for one of the cases ( $m$  even and  $s$  odd) in which the lepton mixing matrix is

$$U = \Omega(m, s)(\mathbf{3}) R_{12}(\theta_L - \zeta) \text{diag}(\pm i, 1, 1), \quad (3.46)$$

with

$$\tan^2 \zeta \equiv \frac{m_1 + m_2 - \sqrt{m_1^2 + m_2^2 + 2m_1 m_2 \cos(4\theta_R)}}{m_1 + m_3 + \sqrt{m_1^2 + m_3^2 + 2m_1 m_2 \cos(4\theta_R)}}. \quad (3.47)$$

The Yukawa matrix  $Y_D$  is constructed from (2.6), using the expressions of  $\Omega(m, s)(\mathbf{3})$  and  $\Omega(m, s)(\mathbf{3}')$  corresponding to  $m$ -even and  $s$ -odd. The parameters  $y_f$  in this case are given in Eq. (D.5) which are real for  $-\pi/4 < \theta_R < \pi/4$ . The remaining case with  $m$ -odd and  $s$ -even, as well as those in Case 3b.1 can be similarly analyzed and the results are given in Eqs. (D.6), (D.8) and (D.9) respectively.

As for the lepton mixing results, note that this time there is no additional constraint on the choice of the index  $n$ , i.e. both  $n$  even and odd are allowed. As for the choice of  $m$ , in Case 3a effectively a small ratio  $m/n$  (or close to one) is needed for achieving small  $\theta_{13}$ . Regarding the choice of the CP transformation  $X(s)$  there are, indeed, in total 16 choices [74] and all of them lead to a reasonable agreement of the lepton mixing angles with experimental data. Some of them like  $s = 0$  and  $s = 8$  lead to CP conservation (either due to symmetry or rather accidentally) and values  $s > n/2$  usually reproduce results like the corresponding value  $s' = n - s < n/2$ . For our numerical analysis of Case 3a, we will use the example of  $n = 16$ . In this case, the ERS points can only be achieved for NO and for  $m$  even,  $s$  even. As we will see later, leptogenesis in this scenario cannot be done at the ERS points, because  $N_1$  becomes long-lived. Therefore, we will use an  $m$ -odd,  $s$ -odd example for leptogenesis with  $m = s = 1$ . In this case, we have  $\theta_{\text{bf}} \approx 2.00$ , which gives  $\sin^2 \theta_{12} \approx 0.304$ ,  $\sin^2 \theta_{13} \approx 0.0254$  and  $\sin^2 \theta_{23} \approx 0.613$ . As for the CP phases, we get  $\sin \delta \approx 0.458$ ,  $\sin \alpha_1 \approx 0.939$  and  $\sin \alpha_2 \approx 0.662$ .

For the mixing pattern of Case 3b.1, with the particular choice  $m/n = 1/2$ , the sines of the two Majorana phases  $\alpha_1$  and  $\alpha_2$  have the same magnitude [74]. The particular choice  $s = n/2$  gives trivial Majorana phases and maximal Dirac phase, as well as maximal atmospheric mixing. Again, some values of  $s$  like  $s = 0$  lead to no CP violation at all and other values of  $s$  like  $s' = n - s > n/2$  only produce results equivalent to those of  $s < n/2$ . For our numerical analysis of Case 3b.1, we will use the example of  $n = 10$ . In this case, the ERS points can only be achieved for IO and for  $m$  even,  $s$  even. Like in Case 3a, leptogenesis cannot be done at the ERS points in this case, because  $N_1$  is long-lived. Therefore, we will choose an example from  $m$ -odd,  $s$ -odd with  $m = s = 5$ . In this case, we have  $\theta_{\text{bf}} \approx 1.31$ , which gives  $\sin^2 \theta_{23} \approx 0.5$ ,  $\sin^2 \theta_{12} \approx 0.318$ ,  $\sin^2 \theta_{13} \approx 0.0220$ . As for the CP phases, we get  $\sin \delta = -1$ , whereas the Majorana phases are trivial, i.e.  $\sin \alpha_1 = \sin \alpha_2 = 0$ .

## 4 CP Asymmetries for Resonant Leptogenesis

In the minimal framework of resonant leptogenesis, the lepton asymmetry is generated from the CP-violating on-shell decays of the RHNs  $N_i \rightarrow L_\alpha H$  and  $N_i \rightarrow \bar{L}_\alpha H^c$  via the Yukawa

couplings  $(Y_D)_{\alpha i}$ . The lepton asymmetry is obtained from the interference of tree- and self-energy diagrams for  $N_i$  decay, which is resonantly enhanced if the intermediate state  $N_j$  ( $j \neq i$ ) in the self-energy diagram is quasi-degenerate with  $N_i$  [22]. In the semi-analytic Boltzmann approach, the flavored lepton asymmetry (or lepton-to-photon ratio) can be approximated as [25, 95, 96]

$$\eta_{L_\alpha} \simeq \frac{3}{2z_c K_\alpha^{\text{eff}}} \sum_i \varepsilon_{i\alpha} d_i, \quad (4.1)$$

where  $z_c = M_N/T_c$  ( $T_c$  being the critical temperature below which the electroweak sphalerons freeze-out and  $M_N$  being the average mass of  $N_i$  and  $N_j$ ),  $K_\alpha^{\text{eff}}$  are the effective washout factors in presence of Yukawa and any additional interactions present in the model, and  $d_i$  are the corresponding dilution factors given in terms of ratios of thermally-averaged rates for decays and scatterings involving  $N_i$  (see Ref. [96] for details). This final lepton asymmetry at temperature  $T_c$  is then converted to a baryon asymmetry via (B+L)-violating electroweak sphaleron processes [8]. The conversion of the total lepton-to-photon ratio  $\sum_\alpha \eta_{L_\alpha}$  to the current baryon-to-photon ratio  $\eta_B$  is given by the relation

$$\eta_B \simeq -0.02 \sum_\alpha \eta_{L_\alpha}, \quad (4.2)$$

where the prefactor contains the product of the sphaleron conversion rate of 28/51 and the entropy dilution factor of 1/27.3. The theoretical prediction for  $\eta_B$  in Eq. (4.2) is to be compared (in both magnitude and sign) with the observed baryon-to-photon ratio [1]

$$\eta_B^{\text{obs}} = (6.12 \pm 0.08) \times 10^{-10}. \quad (4.3)$$

Using the analytic forms of the  $Y_D$  matrix given in Section 3, we can calculate the flavored CP asymmetries analytically. The general formula for the flavored CP asymmetry reads

$$\varepsilon_{i\alpha} = \frac{\Gamma(N_i \rightarrow L_\alpha H) - \Gamma(N_i \rightarrow \bar{L}_\alpha H^c)}{\Gamma(N_i \rightarrow L_\alpha H) + \Gamma(N_i \rightarrow \bar{L}_\alpha H^c)}, \quad (4.4)$$

where  $\Gamma$  stands for the RHN decay rate. In the resonant regime, Eq. (4.4) can be written in a compact form [18]

$$\varepsilon_{i\alpha} \simeq \frac{1}{8\pi (Y_D^\dagger Y_D)_{ii}} \sum_{j \neq i} \text{Im} \left[ (Y_D^*)_{\alpha i} (Y_D)_{\alpha j} \right] \text{Re} \left[ (Y_D^\dagger Y_D)_{ij} \right] \frac{M_i M_j (M_i^2 - M_j^2)}{(M_i^2 - M_j^2)^2 + A_{ij}^2}, \quad (4.5)$$

where the  $Y_D$  matrices are evaluated in the RHN mass basis,<sup>7</sup> and  $A_{ij}$  is a regulator that controls the behavior of the CP asymmetry in the limit  $\Delta M \equiv |M_1 - M_2| \rightarrow 0$ . Moreover, as pointed out in Refs. [96, 97], in the resonant regime there are two distinct contributions to the lepton asymmetry from RHN mixing and oscillation effects, which can be effectively

<sup>7</sup>Normally this is denoted by  $\hat{Y}_D$ , but we drop the hat for brevity.

captured by the same form of  $\varepsilon_{i\alpha}$  as in Eq. (4.5) but with different regulators:

$$A_{ij}^{\text{mix}} = M_i \Gamma_j, \quad \text{and} \quad A_{ij}^{\text{osc}} = (M_1 \Gamma_1 + M_2 \Gamma_2) \left[ \frac{\det \left( \text{Re} \left( Y_D^\dagger Y_D \right) \right)}{\left( Y_D^\dagger Y_D \right)_{ii} \left( Y_D^\dagger Y_D \right)_{jj}} \right]^{1/2}. \quad (4.6)$$

The net CP asymmetry that goes into Eq. (4.1) is then the sum of the mixing and oscillation contributions. This analytic approximation tends to agree well with the full quantum kinetic treatment [97–99] in the strong washout regime.

From Eq. (4.5), we observe the following important features:

- If  $\text{Re} \left[ \left( Y_D^\dagger Y_D \right)_{ij} \right] = 0$  for some  $i$  and all  $j \neq i$ , then  $\varepsilon_{i\alpha} = 0$ , i.e. that particular RHN flavor does not contribute to the CP asymmetry.
- If  $\text{Re} \left[ \left( Y_D^\dagger Y_D \right)_{ij} \right] = 0$  for some  $i$  and one  $j$ , then  $\varepsilon_{i\alpha}$  has only one contribution.
- Since the regulator part is independent of the lepton flavor  $\alpha$ , we can sum over  $\alpha$  to obtain the total CP asymmetry for a given RHN  $N_i$ :

$$\varepsilon_i \equiv \sum_{\alpha} \varepsilon_{i\alpha} = \frac{1}{8\pi \left( Y_D^\dagger Y_D \right)_{ii}} \sum_{j \neq i} \text{Im} \left[ \left( Y_D^\dagger Y_D \right)_{ij} \right] \text{Re} \left[ \left( Y_D^\dagger Y_D \right)_{ij} \right] \mathcal{F}_{ij}, \quad (4.7)$$

where we have defined the dimensionless quantity

$$\mathcal{F}_{ij} = \frac{M_i M_j (M_i^2 - M_j^2)}{(M_i^2 - M_j^2)^2 + A_{ij}^2}. \quad (4.8)$$

Eq. (4.7) implies that if  $\text{Im} \left[ \left( Y_D^\dagger Y_D \right)_{ij} \right] = 0$  for some  $i$  and all  $j \neq i$ , then  $\varepsilon_i = 0$ . This is reflected in the vanishing weak-basis CP-odd invariants [100–102].

We can exemplify the usefulness of these results by applying them to Case 1 with  $s$  even. We find that  $\text{Re} \left[ \left( Y_D^\dagger Y_D \right)_{ij} \right] = 0$  for either  $i$  or  $j$  being 3, but not both. This implies that  $\varepsilon_{3\alpha} = 0$ , i.e. the RHN mass eigenstate  $N_3$  does not contribute to the CP asymmetry. We also have  $\text{Im} \left[ \left( Y_D^\dagger Y_D \right)_{ij} \right] = 0$  if either  $i = j$  or  $i, j$  are both 1, 2. This implies that  $\varepsilon_{1\alpha}$  and  $\varepsilon_{2\alpha}$  both depend on one term only, e.g.

$$\varepsilon_{1\alpha} \simeq \frac{1}{8\pi \left( Y_D^\dagger Y_D \right)_{11}} \text{Im} \left[ (Y_D^*)_{\alpha 1} (Y_D)_{\alpha 2} \right] \text{Re} \left[ \left( Y_D^\dagger Y_D \right)_{12} \right] \mathcal{F}_{12}, \quad (4.9)$$

with  $\text{Im} \left[ (Y_D^*)_{\alpha 1} (Y_D)_{\alpha 2} \right] \propto \sin(3\phi_s)$  for all  $\alpha$ . By evaluating Eq. (4.9) in the strong NO and IO limits, we obtain the following compact analytical expressions for  $\varepsilon_{1\alpha}$ : for strong NO, we get

$$\varepsilon_{1\alpha} \approx \frac{y_2 y_3}{9} \left[ -2y_2^2 + y_3^2 (1 - \cos 2\theta_R) \right] \sin 3\phi_s \sin \theta_R \sin \theta_{L,\alpha} \mathcal{F}_{12}, \quad (4.10)$$

and for strong IO, we get

$$\varepsilon_{1\alpha} \approx \frac{y_1 y_2}{9} [-2y_2^2 + y_1^2(1 + \cos 2\theta_R)] \sin 3\phi_s \cos \theta_R \cos \theta_{L,\alpha} \mathcal{F}_{12}, \quad (4.11)$$

with  $\theta_{L,\alpha} = \theta_L + \rho_\alpha 4\pi/3$  and  $\rho_e = 0$ ,  $\rho_\mu = 1$ ,  $\rho_\tau = -1$ . For strong NO (IO)  $\varepsilon_{i\alpha}$  becomes very small, if  $\theta_R \approx 0$ ,  $\pi$  ( $\theta_R \approx \pi/2, 3\pi/2$ ). In addition,  $\mathcal{F}_{ij}$  vanishes for  $\cos 2\theta_R = 0$ . The CP asymmetries  $\varepsilon_{2\alpha}$  are the negatives of  $\varepsilon_{1\alpha}$  with  $\mathcal{F}_{12}$  being replaced by  $\mathcal{F}_{21}$ . For  $s$  odd, similar expressions are obtained with  $\sin(3\phi_s)$  being replaced by  $-\cos(3\phi_s)$ . All these analytic results have been verified numerically.

We note that different values of  $s$  can lead to the same value of  $\varepsilon_{i\alpha}$ . In particular,

$$\varepsilon_{i\alpha}(s) = (-1)^s \varepsilon_{i\alpha}(n-s) = \varepsilon_{i\alpha}(n/2-s) = (-1)^{s+1} \varepsilon_{i\alpha}(n/2+s) \text{ for } s \leq n/2. \quad (4.12)$$

Eqs. (3.21), (4.10) and (4.11) show the close correlation between CP violation at low and high energies due to the flavor and CP symmetries chosen here.

The analytic expressions for  $\varepsilon_{i\alpha}$  in Cases 2 and 3 are more involved and not very illuminating. We can simplify them somewhat by taking  $\mathcal{F}_{23} = \mathcal{F}_{32} = 0$  because  $M_2 = M_3$  in our scenario [cf. Eq. (2.12)]. As a consequence,  $\varepsilon_{i\alpha}$  for  $i = 2$  and  $i = 3$  (and all  $\alpha$ ) only have one contribution. However, the expressions for  $\varepsilon_{i\alpha}$  turn out to be different for different charged lepton flavors. Just as an example, we present below the Case 2 result for  $s$  even,  $t$  even, and assuming that both  $\mathcal{F}_{12}$  and  $\mathcal{F}_{13}$  are of similar size, which we commonly write as  $\mathcal{F}$ :

$$\begin{aligned} \varepsilon_{1e} = & \frac{4\mathcal{F}}{9} \left( -y_1 y_3 (y_1^2 - y_3^2) \sin \phi_u \cos \theta_R \sin \theta_R \right. \\ & + \cos \left( \frac{\phi_v}{2} \right) \sin \left( \frac{\phi_u}{2} \right) [-y_1 y_2 (y_1^2 - y_2^2) \cos \theta_R \sin \theta_L - y_2 y_3 (y_2^2 - y_3^2) \cos \theta_L \sin \theta_R] \\ & \left. + \cos \left( \frac{\phi_u}{2} \right) \sin \left( \frac{\phi_v}{2} \right) [y_1 y_2 (y_1^2 - y_2^2) \cos \theta_R \cos \theta_L - y_2 y_3 (y_2^2 - y_3^2) \sin \theta_L \sin \theta_R] \right), \end{aligned} \quad (4.13a)$$

$$\begin{aligned} \varepsilon_{1\mu} = & \frac{4\mathcal{F}}{9} \left( y_1 y_3 (y_1^2 - y_3^2) \sin \phi_{u,-} \cos \theta_R \sin \theta_R \right. \\ & + \cos \left( \frac{\phi_v}{2} \right) \cos \left( \frac{\phi_{u,-}}{2} \right) [y_1 y_2 (y_1^2 - y_2^2) \cos \theta_R \sin \theta_L + y_2 y_3 (y_2^2 - y_3^2) \cos \theta_L \sin \theta_R] \\ & \left. + \sin \left( \frac{\phi_{u,-}}{2} \right) \sin \left( \frac{\phi_v}{2} \right) [y_1 y_2 (y_1^2 - y_2^2) \cos \theta_R \cos \theta_L - y_2 y_3 (y_2^2 - y_3^2) \sin \theta_L \sin \theta_R] \right), \end{aligned} \quad (4.13b)$$

$$\begin{aligned} \varepsilon_{1\tau} = & \frac{4\mathcal{F}}{9} \left( y_1 y_3 (y_1^2 - y_3^2) \sin \phi_{u,+} \cos \theta_R \sin \theta_R \right. \\ & + \cos \left( \frac{\phi_v}{2} \right) \cos \left( \frac{\phi_{u,+}}{2} \right) [-y_1 y_2 (y_1^2 - y_2^2) \cos \theta_R \sin \theta_L - y_2 y_3 (y_2^2 - y_3^2) \cos \theta_L \sin \theta_R] \\ & \left. + \sin \left( \frac{\phi_{u,+}}{2} \right) \sin \left( \frac{\phi_v}{2} \right) [-y_1 y_2 (y_1^2 - y_2^2) \cos \theta_R \cos \theta_L + y_2 y_3 (y_2^2 - y_3^2) \sin \theta_L \sin \theta_R] \right), \end{aligned} \quad (4.13c)$$

where  $\phi_{u,\pm} = \phi_u \pm \pi/3$ . Similar expressions for  $\varepsilon_{i\alpha}$  (with  $\alpha = 2, 3$ ), as well as for other choices of  $s$  and  $t$  can be obtained, but we do not show them here.

Similarly for Case 3, we only show one subcase with  $m$  and  $s$  even just for illustration, again assuming that both  $\mathcal{F}_{12}$  and  $\mathcal{F}_{13}$  are of similar size:

$$\varepsilon_{1e} = \frac{2\mathcal{F}}{9} y_1 y_2 (y_1^2 - y_2^2) \cos \phi_m \sin 3\phi_s \left( 4 \cos 2\theta_R + \sqrt{2} \sin 2\theta_R \right), \quad (4.14a)$$

$$\varepsilon_{1\mu} = -\frac{2\mathcal{F}}{9} y_1 y_2 (y_1^2 - y_2^2) \cos \phi_{m,+} \sin 3\phi_s \left( 4 \cos 2\theta_R + \sqrt{2} \sin 2\theta_R \right), \quad (4.14b)$$

$$\varepsilon_{1\tau} = -\frac{2\mathcal{F}}{9} y_1 y_2 (y_1^2 - y_2^2) \cos \phi_{m,-} \sin 3\phi_s \left( 4 \cos 2\theta_R + \sqrt{2} \sin 2\theta_R \right), \quad (4.14c)$$

where  $\phi_{m,\pm} = \phi_m \pm \pi/3$ .

Plugging in these CP asymmetries into Eq. (4.1) which feeds into Eq. (4.2), we will calculate the BAU predictions in all the four cases considered here, and compare those with the observed value in Eq. (4.3) to identify the parameter space for successful leptogenesis (see Section 5.5) and to correlate the high- and low-energy CP phases (see Section 6). We will choose a value for the mass splitting between the RHNs  $N_1$  and  $N_{2,3}$ , i.e.  $\Delta M_N = 3\kappa M_N$  [cf. Eq. (2.12)], which maximizes the CP asymmetry in Eq. (4.7). We find it to happen at

$$\frac{\Delta M_N}{M_N} = 3\kappa_{\max} \sim 1.23 \frac{\Gamma_N}{M_N}, \quad (4.15)$$

where  $\Gamma_N$  stands for the average decay width of the  $N_i$ -pair participating in resonant leptogenesis, and the factor 1.23 is obtained numerically by maximizing the sum of the regulator parts for the mixing and oscillation contributions. Since  $\Gamma_N$  scales as  $M_N^2$ ,  $\kappa_{\max}$  increases linearly with  $M_N$ . We will use this fact to choose the appropriate  $\kappa_{\max}$  for our leptogenesis scans presented in Section 5.5.

## 5 Collider Signatures

In this section, we discuss the collider signatures of the RHNs in our scenario and show how they can be used to test resonant leptogenesis in our model. Firstly, we will discuss in Section 5.1 the production of heavy RHNs at hadron colliders and our use of a simple gauge extension of the SM for enhancing the production cross section. Next, in Section 5.2 we discuss the RHN decay lengths and identify the ERS points where one of the RHNs becomes long-lived. In Section 5.3, we analyze how the RHN decay BRs into charged leptons of different flavors vary in different cases. Using these BRs, we study the smoking-gun same-sign dilepton signal of RHNs in Section 5.4. Finally, in Section 5.5 we show the correlation between the collider signal and leptogenesis, and study the detection prospects of the parameter space for successful leptogenesis at the HL-LHC, as well as at a future 100-TeV collider.

### 5.1 Production of RHNs

As already mentioned in Section 1, a nice feature of the resonant leptogenesis mechanism is that it allows the RHNs to be as light as the electroweak scale [24, 25, 96], thus making it *testable* in laboratory experiments [44].<sup>8</sup> However, in the minimal type-I seesaw within the

<sup>8</sup>In contrast, the high-scale leptogenesis mechanism can only be *falsified* [103–105].

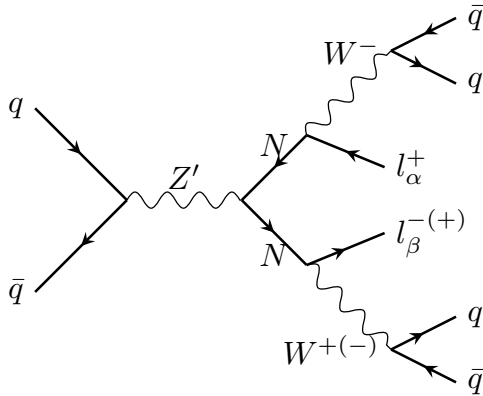


**Figure 1.** Smoking-gun (LNV) signature of RHNs at hadron colliders in the  $U(1)_{B-L}$  model. The final-state lepton flavors are dictated by the same Yukawa coupling structure  $Y_D$  that governs leptogenesis.

SM gauge group, the constraints from light neutrino masses and mixing usually restrict the Yukawa couplings  $y_f \lesssim 10^{-7}$  for TeV-scale RHNs.<sup>9</sup> This makes the RHN production cross section for the smoking-gun collider signature of same-sign dilepton plus two jets without missing transverse energy [124–131] too small to be accessible at the LHC [132, 133].

Therefore, for the collider tests of the RHNs to be feasible, one needs to find a more efficient production mechanism that is not suppressed by the neutrino Yukawa couplings. One way is to extend the SM gauge group and make the RHNs as well as the SM quarks (and leptons) charged under this new group, so that the RHN production can occur via mediation of the new gauge bosons [79]. Here we will consider one such simple  $U(1)_{B-L}$  extension of the SM [134, 135]. In this model, the RHNs can be pair-produced via the  $U(1)_{B-L}$  gauge-boson mediation:  $pp \rightarrow Z' \rightarrow N_i N_i$  [136–141] (see Figure 1). This production channel is only kinematically suppressed by the mass of the new gauge boson,  $M_{Z'}$ . If  $M_i < M_{Z'}/2$ , the two RHNs are produced on-shell. Very similar production cross sections are expected for all  $N_i$  in our scenario, since their masses are (almost) degenerate, see Eq. (2.12).

There exist stringent limits on the  $Z'$  mass and the corresponding gauge coupling  $g_{B-L}$  from existing collider data. The contact interaction bound from  $e^+e^- \rightarrow f\bar{f}$  data at LEP-II requires  $M_{Z'}/g_{B-L} \gtrsim 7.0$  TeV [142]. For  $Z'$  masses kinematically accessible at the LHC, more stringent bounds are obtained from high-mass dilepton resonance searches [143, 144]. The LHC limits are usually derived in the so-called sequential SM where the  $Z'$  couplings are the same as those of the SM  $Z$  boson. In the  $U(1)_{B-L}$  model with RHNs, these limits are slightly modified [145]. In fact, in a general  $U(1)_X$  gauge group which is a linear combination of the  $U(1)_Y$  and  $U(1)_{B-L}$  [146], the  $Z'$  limits depend on the choice of two scalars charges  $x_H$  and  $x_\Phi$ . In fact, the RHN collider signal can be enhanced for special

<sup>9</sup>Exceptions can be made by choosing specific textures of  $M_D$  and/or  $M_R$ , thereby allowing some of the Yukawa entries to be large [106–118], but at the expense of making the relevant RHNs quasi-Dirac and thus suppressing the corresponding LNV signal [79, 119–123].

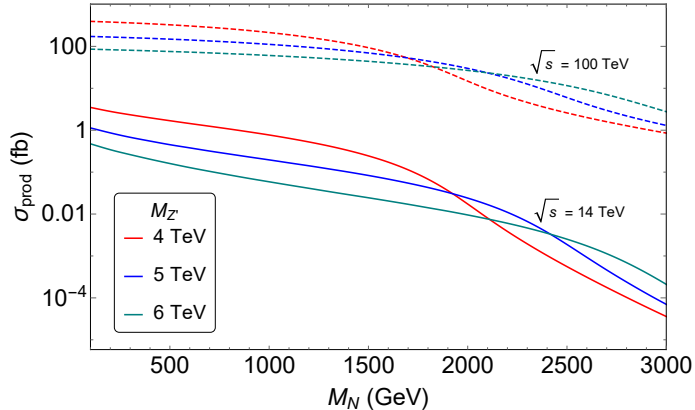


**Figure 2.** RHN pair production ( $pp \rightarrow Z' \rightarrow N_i N_i$ ) cross section as a function of the RHN mass  $M_N$  at  $\sqrt{s} = 14$  TeV LHC (solid lines) and  $\sqrt{s} = 100$  TeV future collider (dotted lines) for  $M_{Z'} = 4$  TeV (red), 5 TeV (blue) and 6 TeV (green). Here we have normalized the cross-section for  $g_{B-L} = 1$ .

values of  $(x_H, x_\Phi)$  due to an enhancement in the  $\text{BR}(Z' \rightarrow N_i N_i)$  [147]. There also exist other  $U(1)_X$  models where the  $Z'$  is leptophobic [148–152], thus avoiding the LHC dilepton bounds, and can be lighter, as long as it satisfies the weaker dijet bounds [153, 154]. In this work, we only consider the simplest case with  $(x_H, x_\Phi) = (0, 2)$ , which corresponds to the minimal  $B-L$  model with flavor-diagonal and flavor-universal  $Z'$  couplings to leptons. Furthermore, we will use a benchmark value of  $g_{B-L} = 0.1$  for which the current LHC limit is  $M_{Z'} \gtrsim 4.1$  TeV.

To calculate the hadron collider production cross sections

$$\sigma_{\text{prod}} \equiv \sigma(pp \rightarrow Z' \rightarrow N_i N_i), \quad (5.1)$$

we implement the model Lagrangian into `FeynRules` [155] and generate the Universal Feyn-Rules Output (UFO) file for the  $B-L$  embedding [137, 156]. This is then imported to the `MadGraph_aMC@NLO-v2.8.3` event generator [157] with the default PDF set to calculate  $\sigma_{\text{prod}}$  at parton level. Our results for the gauge coupling  $g_{B-L} = 1$  are shown in Figure 2 for three different values of  $M_{Z'} = 4, 5, 6$  TeV (red, blue and green, respectively). The solid lines are for the LHC center-of-energy  $\sqrt{s} = 14$  TeV, whereas the dotted lines are for a future 100 TeV collider. The change in the slope of the curves occurs near the kinematic threshold for on-shell pair-production, i.e.  $M_N = M_{Z'}/2$ . For  $M_N < M_{Z'}/2$ , the cross-section scales as  $g_{B-L}^2$ , whereas above the  $M_{Z'}/2$  threshold, the cross-section scales as  $g_{B-L}^4$ . From Figure 2, we find that the cross section is below fb-level at the LHC for realistic values of the  $Z'$  mass and coupling consistent with the dilepton bound mentioned above, which makes it challenging to find sizable number of events even at the HL-LHC, as we will see explicitly in Section 5.5. Therefore, we have included the 100 TeV option which has far better sensitivity to the leptogenesis parameter space discussed in Section 5.5.

## 5.2 Decay Lengths

After being produced, the RHNs decay into SM final states through their Yukawa couplings  $Y_D$ . The total decay width  $\Gamma_i$  of the RHN  $N_i$  at tree-level is given by

$$\Gamma_i = \frac{(Y_D^\dagger Y_D)_{ii}}{8\pi} M_i, \quad (5.2)$$

where the form of  $Y_D$  in our model is determined by the choice for generator  $Z$  of the  $Z_2$  symmetry and the choice of the CP transformation  $X$ , as discussed in Section 3. Despite this dependence on the generators of  $Z_2$  symmetry and CP transformation, we will see that  $\Gamma_i$  is independent of the value of  $n$  and depends only on odd/even behavior of the parameters  $s, t, m$  and on the rotation angle  $\theta_R$ . Even in some cases,  $\Gamma_i$  is completely independent of all these parameters, as shown below.

### 5.2.1 Case 1

The expressions for the decay widths of the three heavy RHNs in this case do not depend on the values of  $s$ , and only depend on the Yukawa couplings  $y_f$  and the angle  $\theta_R$ :

$$\Gamma_1 = \frac{M_N}{24\pi} (2y_1^2 \cos^2 \theta_R + y_2^2 + 2y_3^2 \sin^2 \theta_R), \quad (5.3a)$$

$$\Gamma_2 = \frac{M_N}{24\pi} (y_1^2 \cos^2 \theta_R + 2y_2^2 + y_3^2 \sin^2 \theta_R), \quad (5.3b)$$

$$\Gamma_3 = \frac{M_N}{8\pi} (y_1^2 \sin^2 \theta_R + y_3^2 \cos^2 \theta_R). \quad (5.3c)$$

We calculate the corresponding decay lengths in the laboratory frame and plot them as a function of  $\theta_R$  in Figure 3 for two different values of  $M_N$  (upper panels, with  $m_0 = 0$ ) and three different values of the lightest neutrino mass  $m_0$  (lower panels, with  $M_N = 250$  GeV) for both NO (left panels) and IO (right panels). In doing so, we have assumed that  $N_i$  are produced via  $Z'$  with mass  $M_{Z'} = 4$  TeV, meaning the Lorentz boost factor is given by  $\gamma = M_{Z'}/2M_N = 8$  (13.3) for  $M_N = 250$  (150) GeV.

The Yukawa couplings are fixed by the light neutrino mass spectrum [cf. Eq. (D.1)]. Therefore, we show the decay lengths for NO and IO in the left and right panels of Figure 3, respectively. In Case 1, strong NO and strong IO correspond to  $y_1 = 0$  and  $y_3 = 0$  respectively, when the lightest neutrino becomes massless, i.e.  $m_0 = 0$ . For the ERS points  $\theta_R \rightarrow \pi/2, 3\pi/2$  (NO) or  $\theta_R \rightarrow 0, \pi$  (IO), we see from Eq. (5.3) that  $\Gamma_3 \rightarrow 0$ , or  $N_3$  becomes long-lived, as shown by the shaded region corresponding to  $L > 1$  cm. Thus, for sufficiently large production cross section,  $N_3$  can be searched for either with displaced vertex searches at the LHC or with dedicated LLP detectors like FASER [158] and MATHUSLA [159], depending on the amount of deviation from the ERS point which can be parametrized by  $\delta\theta_R = |\theta - \theta_{\text{ERS}}|$ . For  $M_N$  in the few hundred GeV range and  $10^{-4} \lesssim \delta\theta_R \lesssim 10^{-2}$ ,  $N_3$  can have decay lengths of a few hundred m which is in the range of the LLP detectors like MATHUSLA. If  $10^{-3} \lesssim \delta\theta_R \lesssim 10^{-1}$ ,  $N_3$  can be detected either with the LLP searches or can be probed at the LHC via displaced vertex signatures, similar to the scenarios studied in Refs. [160, 161]. There are also accompanying signals from  $N_{1,2}$  decays, which are mostly

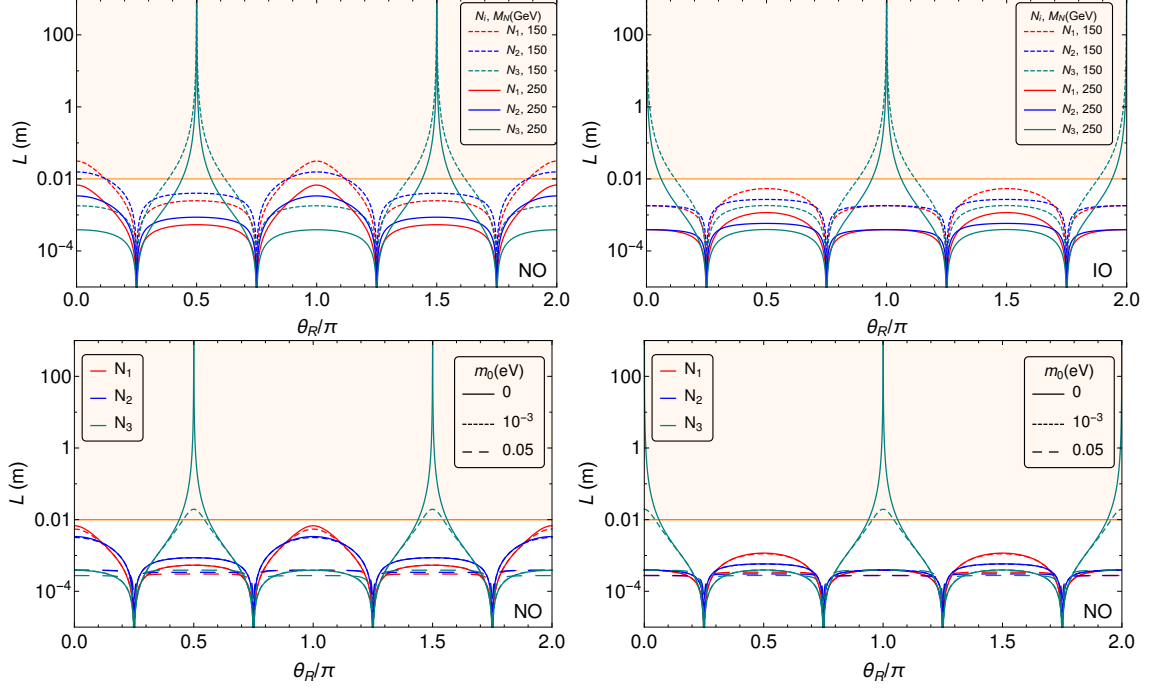


**Figure 3.** *Case 1.*  $N_{1,2,3}$  decay lengths are plotted against  $\theta_R$  for different values of the RHN mass scale  $M_N$  (upper panels, with  $m_0 = 0$ ) and light neutrino mass  $m_0$  (lower panels, with  $M_N = 250$  GeV). The left (right) panels are for NO (IO). The unshaded (shaded) region indicates the prompt (displaced/long-lived) signal regime.

prompt (but can also be displaced, depending on the choice of  $\theta_R$ ), as shown in the upper panels of Figure 3. For  $m_0 \neq 0$ , the ERS becomes less pronounced, as shown by the flattening of the  $N_3$  peaks in the lower panels of Figure 3. For  $m_0$  close to its maximum allowed value [cf. Eq. (2.20)], the three RHN decay widths become almost indistinguishable.

### 5.2.2 Case 2

The decay widths of the RHNs in this case just depend on whether  $t$  is even/odd and are independent of  $s$ .

For  $t$ -even,

$$\Gamma_1 = \frac{M_N}{24\pi} (2y_1^2 \cos^2 \theta_R + y_2^2 + 2y_3^2 \sin^2 \theta_R), \quad (5.4a)$$

$$\Gamma_2 = \frac{M_N}{24\pi} (y_1^2 \cos^2 \theta_R + 2y_2^2 + y_3^2 \sin^2 \theta_R), \quad (5.4b)$$

$$\Gamma_3 = \frac{M_N}{8\pi} (y_1^2 \sin^2 \theta_R + y_3^2 \cos^2 \theta_R). \quad (5.4c)$$

For  $t$ -odd,

$$\Gamma_1 = \frac{M_N}{24\pi} (y_1^2 + y_2^2 + y_3^2), \quad (5.5a)$$

$$\Gamma_2 = \frac{M_N}{24\pi} (y_1^2 + 4y_2^2 + y_3^2), \quad (5.5b)$$

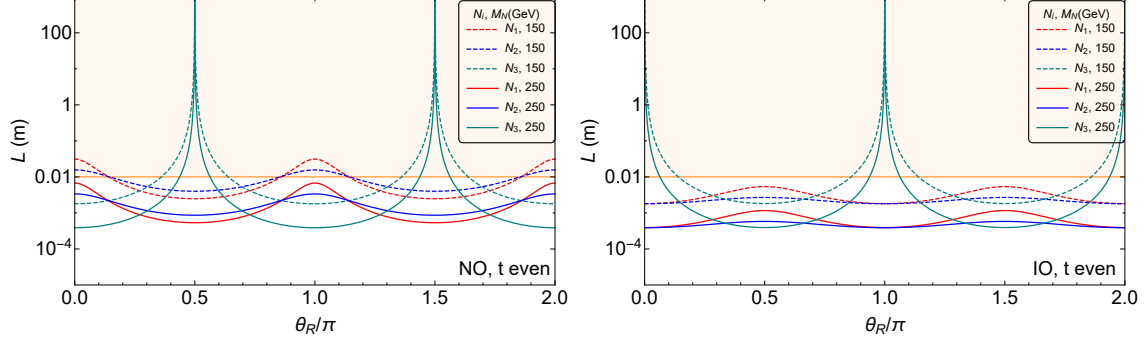


**Figure 4.** *Case 2* with  $t$  even.  $N_{1,2,3}$  decay lengths are plotted against  $\theta_R$  for different values of the RHN mass scale  $M_N$  with  $m_0 = 0$ . The left (right) panels are for NO (IO). The unshaded (shaded) region indicates the prompt (displaced/long-lived) signal regime.

$$\Gamma_3 = \frac{M_N}{24\pi} (y_1^2 + y_3^2). \quad (5.5c)$$

As can be seen above, the decay lengths are independent of  $\theta_R$  for odd values of  $t$  and non-zero in all cases including strong NO and strong IO. Thus in Case 2, the ERS points are present only for even values of  $t$  and lie at the same values of  $\theta_R$  as in Case 1 for both mass orderings, irrespective of the  $s$  values as shown in Figure 4. Note that similar to Case 1, strong NO and strong IO in this case correspond to  $y_1 = 0$  and  $y_3 = 0$  respectively. We do not show the variation with respect to  $m_0$  in this case because it follows the same trend as in Case 1. In what follows, we will set  $m_0 = 0$  for concreteness, unless otherwise specified.

### 5.2.3 Case 3

The decay widths of the RHNs in Case 3a and 3b.1 depend on the combination of  $(m, s)$  being even/odd. There is an important distinction to be noted that unlike other cases where  $N_3$  becomes long-lived, in Case 3a and 3b.1, it is  $N_1$  for which the decay length is the longest near the ERS points. The decay widths are explicitly given as follows:

For  $m$ -even,  $s$ -even,

$$\Gamma_1 = \frac{M_N}{48\pi} \left( 3(y_1^2 + y_2^2) + (y_1^2 - y_2^2)(\cos 2\theta_R - 2\sqrt{2} \sin 2\theta_R) \right), \quad (5.6a)$$

$$\Gamma_2 = \frac{M_N}{192\pi} \left( 3(y_1^2 + y_2^2 + 6y_3^2) - (y_1^2 - y_2^2)(\cos 2\theta_R - 2\sqrt{2} \sin 2\theta_R) \right), \quad (5.6b)$$

$$\Gamma_3 = \frac{M_N}{64\pi} \left( 3(y_1^2 + y_2^2) + 2y_3^2 - (y_1^2 - y_2^2)(\cos 2\theta_R - 2\sqrt{2} \sin 2\theta_R) \right). \quad (5.6c)$$

For  $m$ -even,  $s$ -odd,

$$\Gamma_1 = \frac{M_N}{48\pi} \left( 3(y_1^2 + y_2^2) + (y_1^2 - y_2^2) \cos 2\theta_R \right), \quad (5.7a)$$

$$\Gamma_2 = \frac{M_N}{192\pi} \left( 3(y_1^2 + y_2^2 + 6y_3^2) - (y_1^2 - y_2^2) \cos 2\theta_R \right), \quad (5.7b)$$

$$\Gamma_3 = \frac{M_N}{64\pi} \left( 3(y_1^2 + y_2^2) + 2y_3^2 - (y_1^2 - y_2^2) \cos 2\theta_R \right). \quad (5.7c)$$

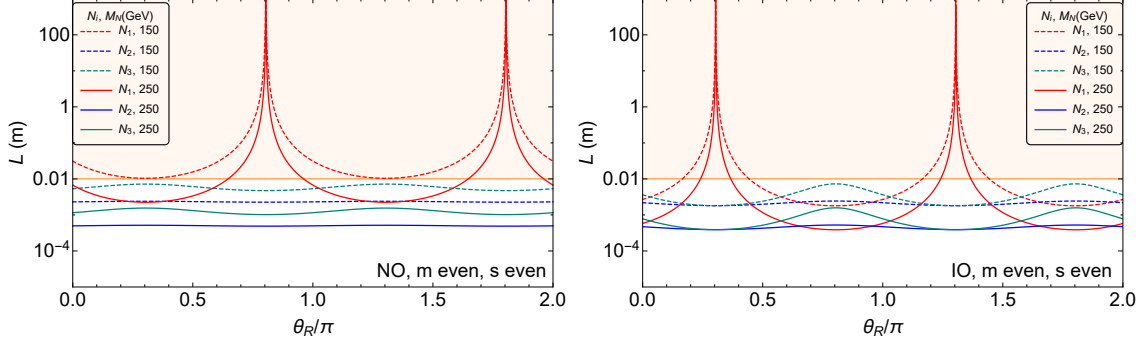


**Figure 5.** *Case 3a* with NO (left panel) and *Case 3b.1* with IO (right panel), both with  $m$  even,  $s$  even.  $N_{1,2,3}$  decay lengths are plotted against  $\theta_R$  for two different values of the RHN mass scale  $M_N$ , assuming  $m_0 = 0$ . The unshaded (shaded) region indicates the prompt (displaced/long-lived) signal regime.

For  $m$ -odd,  $s$ -even,

$$\Gamma_1 = \frac{M_N}{48\pi} (4y_1^2 + y_2^2 + y_3^2 + (y_2^2 - y_3^2) \cos 2\theta_R) , \quad (5.8a)$$

$$\Gamma_2 = \frac{M_N}{192\pi} (2y_1^2 + 11(y_2^2 + y_3^2) - 7(y_2^2 - y_3^2) \cos 2\theta_R) , \quad (5.8b)$$

$$\Gamma_3 = \frac{M_N}{64\pi} (2y_1^2 + 3(y_2^2 + y_3^2) + (y_2^2 - y_3^2) \cos 2\theta_R) . \quad (5.8c)$$

For  $m$ -odd,  $s$ -odd,

$$\Gamma_1 = \frac{M_N}{48\pi} (4y_1^2 + y_2^2 + y_3^2 + (y_2^2 - y_3^2) \cos 2\theta_R) , \quad (5.9a)$$

$$\Gamma_2 = \frac{M_N}{192\pi} (2y_1^2 + 11(y_2^2 + y_3^2) - (y_2^2 - y_3^2)(7 \cos 2\theta_R + 6\sqrt{2} \sin 2\theta_R)) , \quad (5.9b)$$

$$\Gamma_3 = \frac{M_N}{64\pi} (2y_1^2 + 3(y_2^2 + y_3^2) + (y_2^2 - y_3^2)(\cos 2\theta_R + 2\sqrt{2} \sin 2\theta_R)) . \quad (5.9c)$$

In Case 3a, strong NO and strong IO correspond to  $y_1 = 0$  and  $y_3 = 0$  respectively. As can be verified, ERS points are exhibited only for even values of  $(m, s)$  with NO mass ordering, as shown in the left panel of Figure 5. These points correspond to values of  $\theta_R \approx 0.8\pi, 1.8\pi$ .

In Case 3b.1, strong NO and strong IO corresponds to  $y_3 = 0$  and  $y_2 = 0$  respectively. In this case, ERS points are also exhibited only for even values of  $(m, s)$  but with IO mass ordering, as shown in the right panel of Figure 5. These points correspond to values of  $\theta_R \approx 0.3\pi, 1.3\pi$ .

### 5.3 Branching Ratios

Assuming  $M_N > \{m_H, m_W, m_Z\}$ , the heavy RHN  $N_i$  can decay into  $\ell_\alpha W$ ,  $\nu_\alpha Z$  and  $\nu_\alpha H$ , through its mixing with the SM neutrinos, given by  $V_{\alpha i} \simeq (M_D M_R^{-1})_{\alpha i}$ . The corresponding partial decay widths for these channels are [128]

$$\Gamma(N_i \rightarrow \ell_\alpha W) = \frac{g^2 v^2 (M_i^2 - m_W^2)^2 (M_i^2 + 2m_W^2)}{64\pi M_i^5 m_W^2} |(Y_D)_{\alpha i}|^2 , \quad (5.10a)$$

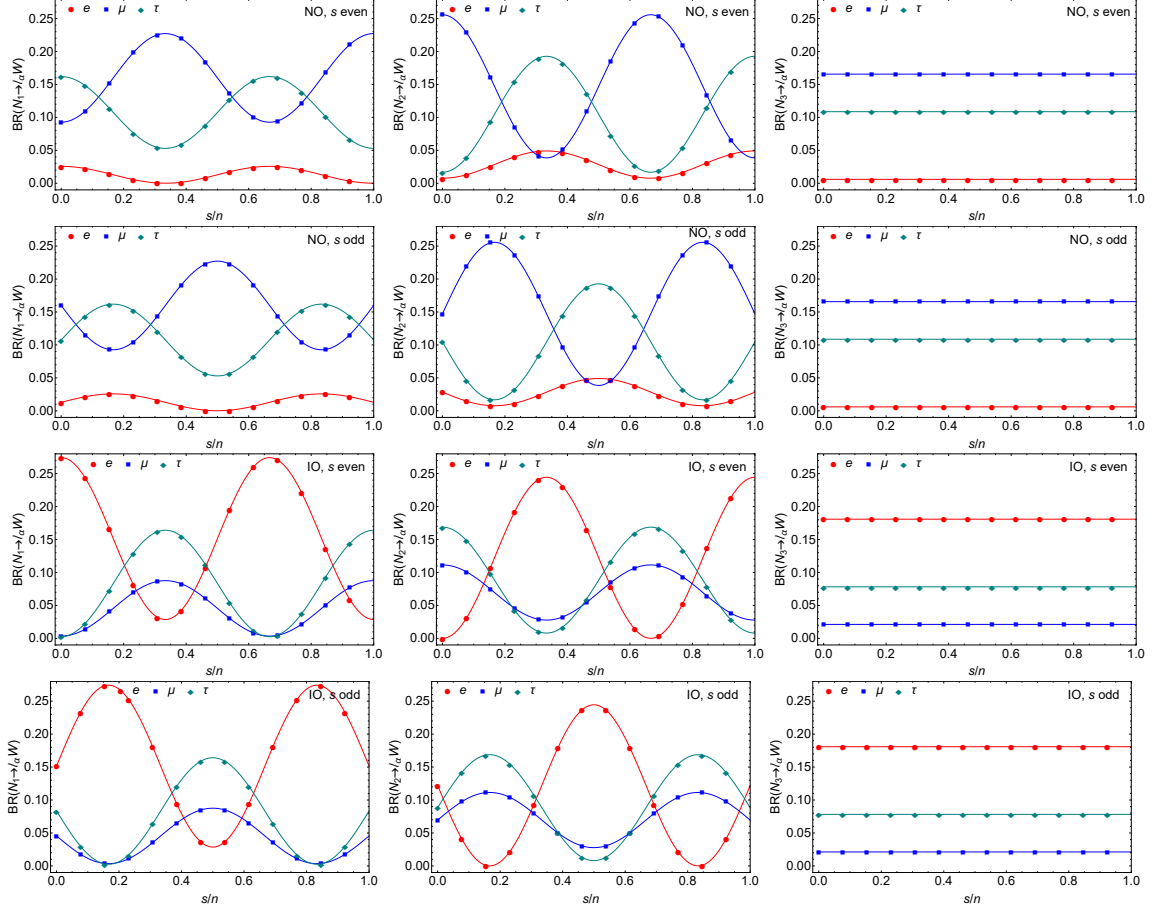


**Figure 6.** For *Case 1*.  $BR(N_i \rightarrow \ell_\alpha W)$  for  $\alpha = e, \mu, \tau$  are shown as a function of  $s/n$ . The left, middle and right columns are for  $N_1$ ,  $N_2$  and  $N_3$  respectively. The top (bottom) two rows are for strong NO (IO) with  $s$  even and  $s$  odd respectively. These results do not depend on the specific choice of  $n$ , but for illustration, we show the results for  $n = 26$  by the discrete points (13 in total, corresponding to  $0 \leq s \leq n - 1$ , either even or odd). We have fixed  $M_N = 250$  GeV and  $\theta_R$  at its ERS value in each case.

$$\Gamma(N_i \rightarrow \nu_\alpha Z) = \frac{g^2 v^2}{128 \pi \cos^2 \theta_w} \frac{(M_i^2 - m_Z^2)^2 (M_i^2 + 2m_Z^2)}{M_i^5 m_Z^2} |(Y_D)_{\alpha i}|^2, \quad (5.10b)$$

$$\Gamma(N_i \rightarrow \nu_\alpha H) = \frac{g^2 v^2}{128 \pi} \frac{(M_i^2 - m_H^2)^2}{M_i^3 m_W^2} |(Y_D)_{\alpha i}|^2, \quad (5.10c)$$

where  $\theta_w$  is the weak mixing angle. Note that for Majorana RHNs, the charge-conjugated final states have the same decay rate; e.g.  $\Gamma(N_i \rightarrow \ell_\alpha^+ W^-) = \Gamma(N_i \rightarrow \ell_\alpha^- W^+)$ . The BR into the charged-lepton final states  $N_i \rightarrow \ell_\alpha^\pm W^\mp$  is given by

$$BR(N_i \rightarrow \ell_\alpha W) = \frac{\Gamma(N_i \rightarrow \ell_\alpha W)}{2 [\Gamma(N_i \rightarrow \ell_\alpha W) + \Gamma(N_i \rightarrow \nu_\alpha Z) + \Gamma(N_i \rightarrow \nu_\alpha H)]}. \quad (5.11)$$

Thus after the RHNs are produced on-shell, their decay BRs are predicted in terms of the underlying Yukawa structure, as shown in Figures 6, 7 and 8 for Case 1, Case 2 and Case

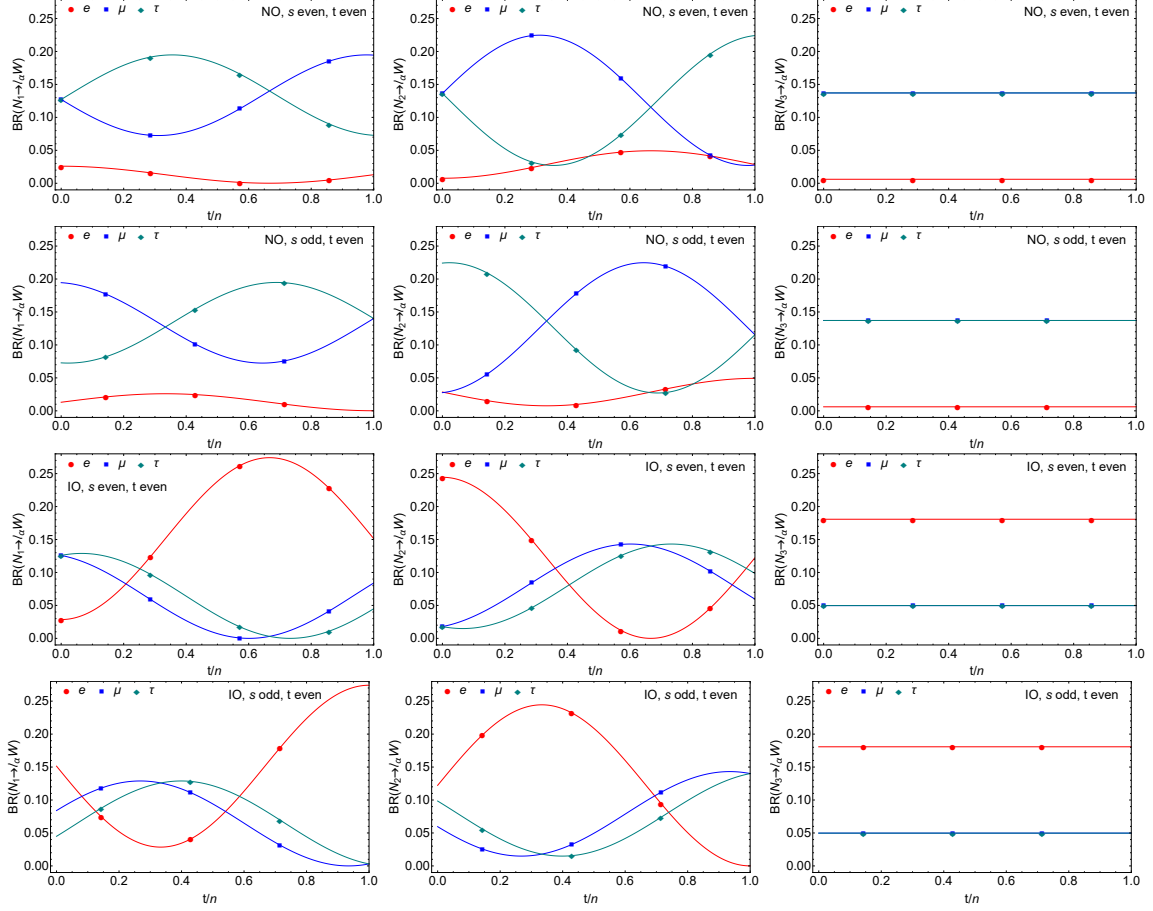


**Figure 7.** For *Case 2*.  $\text{BR}(N_i \rightarrow \ell_\alpha W)$  for  $\alpha = e, \mu, \tau$  as a function of  $t/n$  with  $t$  even. The top (bottom) two rows are for strong NO (IO) with  $s$  even and  $s$  odd, respectively. These results do not depend on the specific choice of  $n$ , but for illustration, we show the results for  $u = 2s - t = 0, n = 14$  by the discrete points (4(3) in total, corresponding to  $s$  ( $0 \leq s \leq n - 1$ ) being even (odd) and  $t$  even). We have fixed  $M_N = 250$  GeV and  $\theta_R$  at its ERS value in each case.

3, respectively. We only show those cases having ERS points (see Section 5.2) and tune the  $\theta_R$  value to one of the ERS points in each case. We also set  $m_0 = 0$  so that we have either strong NO or strong IO. The RHN mass scale is fixed at a representative value of  $M_N = 250$  GeV. The behavior of the BRs is independent of the choice of the index  $n$ ; however, for illustration, we choose  $n = 26$  for which  $s/n$  can only take a finite number of values, which are shown by the points for any given flavor.

Considering the  $N_3$  decay at LLP detector, for *Case 1* we find

$$\text{BR}(N_3 \rightarrow e^\pm W^\mp) : \text{BR}(N_3 \rightarrow \mu^\pm W^\mp) : \text{BR}(N_3 \rightarrow \tau^\pm W^\mp) = \begin{cases} 1 : 27.7 : 18.1 & (\text{NO}) \\ 8.5 : 1 : 3.7 & (\text{IO}) \end{cases}, \quad (5.12)$$

independent of  $\theta_R$  and  $s$ , and almost independent of  $M_N$ , if  $M_N \gg m_W$ . This can be seen from the right column of Figure 6, where  $\text{BR}(N_3 \rightarrow \ell_\alpha W)$  remains constant for all values of  $s/n$ . Thus, measuring these BRs at an LLP detector like MATHUSLA for at least two

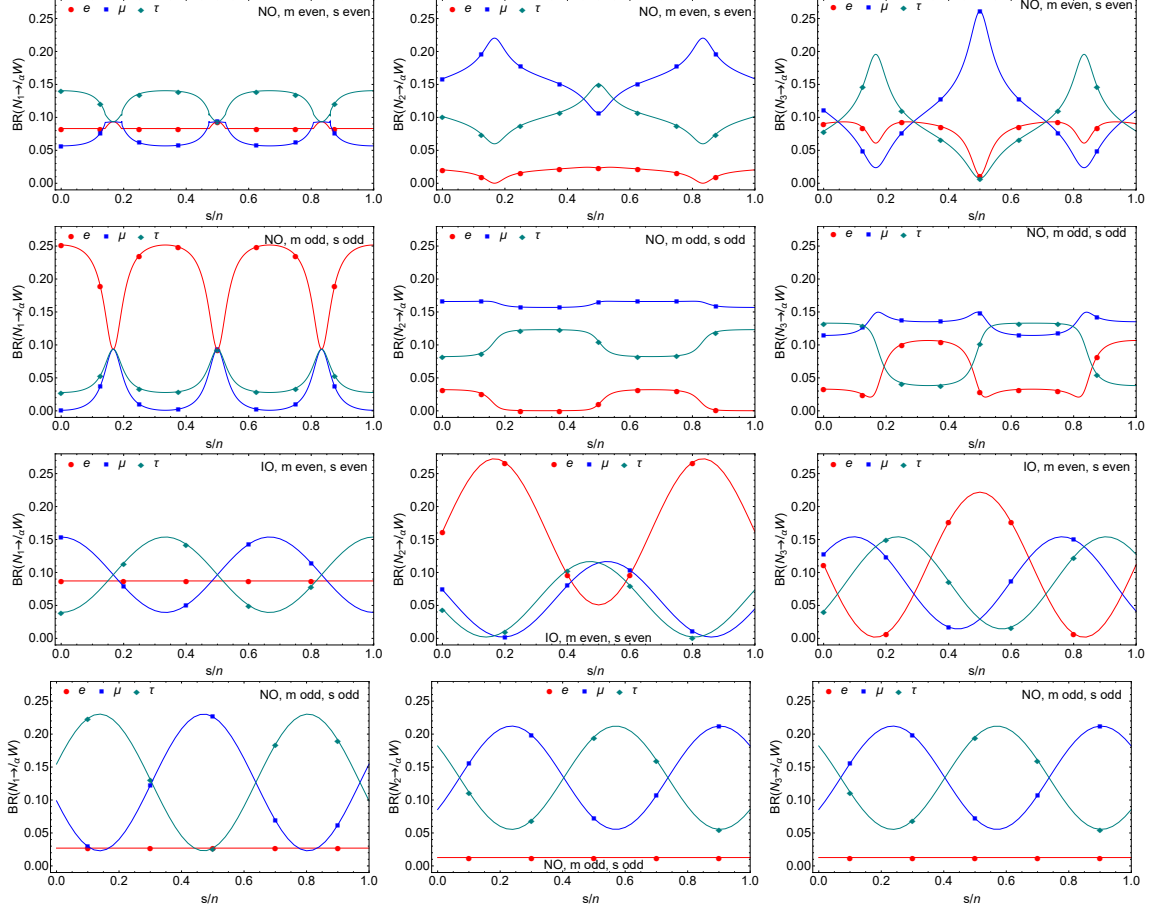


**Figure 8.** For *Case 3a* (top two rows, NO only) and *Case 3b.1* (bottom two rows, IO and NO).  $\text{BR}(N_i \rightarrow \ell_\alpha W)$  for  $\alpha = e, \mu, \tau$  as a function of  $s/n$ . The top two rows are for strong NO with ( $m$  even and  $s$  even) and ( $m$  odd and  $s$  odd), respectively. The bottom two rows are for strong IO and strong NO with ( $m$  even and  $s$  even) and ( $m$  odd and  $s$  odd), respectively. These results do not depend on the specific choice of  $n$ , but for illustration, we show the results for  $n = 16(10)$  for Case 3a(3b.1) by the discrete points (corresponding to  $0 \leq s \leq n - 1$ , either even or odd). We have fixed  $M_N = 250$  GeV and  $\theta_R$  at its ERS value for first and third row, while fixed to  $\theta_R = 0$  for rest, since ERS is absent in these cases.

charged lepton flavors  $\alpha$  allows a test of the neutrino mass hierarchy at the high-energy frontier.

Case 1 can also be tested with prompt or displaced vertex signals at the LHC from the decays of  $N_{1,2}$ . However, their BRs depend on the chosen CP symmetry  $X(s)$  as well as on  $\theta_R$ . For instance, for  $M_N = 250$  GeV,  $s = 2$ ,  $n = 26$  and  $\theta_R$  at an ERS point, we get

$$\text{BR}(N_1 \rightarrow e^\pm W^\mp) : \text{BR}(N_1 \rightarrow \mu^\pm W^\mp) : \text{BR}(N_1 \rightarrow \tau^\pm W^\mp) = \begin{cases} 1 : 4.9 : 6.6 & (\text{NO}) \\ 17.3 : 1 : 1.6 & (\text{IO}) \end{cases}, \quad (5.13)$$

$$\text{BR}(N_2 \rightarrow e^\pm W^\mp) : \text{BR}(N_2 \rightarrow \mu^\pm W^\mp) : \text{BR}(N_2 \rightarrow \tau^\pm W^\mp) = \begin{cases} 1 : 17.6 : 3.0 & (\text{NO}) \\ 1 : 3.3 : 4.8 & (\text{IO}) \end{cases}. \quad (5.14)$$

These ratios of BRs are independent of  $M_N$  for  $M_N \gg m_W$ .

For Case 2, similar to Case 1, the BR for  $N_3$  is independent of  $\theta_R$  and  $s$ , and almost independent of  $M_N$ , if  $M_N \gg M_W$ . Moreover, the BRs for  $(N_3 \rightarrow \mu W)$  and  $(N_3 \rightarrow \tau W)$  are equal for both NO and IO, as can be seen in the right column of Figure 7. The BRs of  $N_1$  and  $N_2$  however depend on the choice of  $s$  and  $t$ , apart from the mass ordering, as shown by the first two columns in Figure 7.

For Case 3a and 3b.1, the BRs are shown in Figure 8 top two and bottom two panels respectively. Unlike the previous two cases, none of the BRs is constant and all of them depend on the chosen CP symmetry  $X(s, m)$  as well as on  $\theta_R$ , apart from the mass ordering. Furthermore, we notice that the BRs in Case 3a do not have a simple sinusoidal dependence on  $s/n$ , unlike all other cases. This is because of the strong dependence of the Yukawa parameters on  $\theta_{\text{bf}}$  which changes with  $s$ .

#### 5.4 Same-sign dilepton signals

As shown in Figure 1, once the Majorana  $N_i$ 's are produced in pairs via the  $Z'$  mediation process in  $pp$  collision, their decay into charged leptons leads to the striking LNV signal

$$pp \rightarrow Z' \rightarrow N_i N_i \rightarrow \ell_\alpha^\pm \ell_\beta^\pm + 2W^\mp \rightarrow \ell_\alpha^\pm \ell_\beta^\pm + 4j. \quad (5.15)$$

Note that for  $\alpha \neq \beta$  this process also violates lepton flavor [152]. The process (5.15) has a much smaller SM background than its lepton number conserving counterpart, namely,  $N_i N_i \rightarrow \ell_\alpha^\pm \ell_\beta^\mp + W^+ W^- \rightarrow \ell_\alpha^\pm \ell_\beta^\mp + 4j$ . In the narrow-width approximation, the cross section for the LNV process can be written as

$$\begin{aligned} \sigma_{\text{LNV}}^{\alpha\beta} &= c_{\alpha\beta} \sum_i \sigma_{\text{prod}}(pp \rightarrow Z' \rightarrow N_i N_i) \\ &\times \text{BR}(N_i \rightarrow \ell_\alpha^\pm W^\mp) \text{BR}(N_i \rightarrow \ell_\beta^\pm W^\mp) [\text{BR}(W^\mp \rightarrow jj)]^2, \end{aligned} \quad (5.16)$$

where  $c_{\alpha\beta} = 1(2)$  for  $\alpha = \beta$  ( $\alpha \neq \beta$ ). The production cross sections [cf. Eq. (5.1) and Figure 2] only depend on the  $Z'$  and RHN masses, and are independent of the Yukawa couplings. On the other hand, the BRs for  $N_i \rightarrow \ell_\alpha W$  encode the Yukawa structure and will be different for the different cases studied above, as discussed in Section 5.3. Finally, the BR for  $W^\mp \rightarrow jj$  is known to be 67.4% in the SM [90], which does not change in our setup. For illustration, the results for  $\sigma_{\text{LNV}}$  for  $N_1$ , normalized to the coupling strength  $g_{B-L} = 1$ , with the Yukawa structure from Case 1 as a function of the RHN mass scale  $M_N$  for fixed  $M_{Z'} = 4$  TeV,  $s = 2$ ,  $n = 26$  is shown in Figure 9 for all possible final-state lepton flavor combinations. The results for other  $g_{B-L}$  values can be obtained by simply scaling the cross-sections as  $g_{B-L}^2$ . We find that for NO, the  $\tau\tau$  ( $ee$ )-channel has the highest (lowest) signal cross section, whereas for IO, the  $ee$  ( $\mu\mu$ )-channel has the highest (lowest) signal cross section. These results can be understood by analyzing the  $N_1$  BRs appearing in Eq. (5.16) from Figure 6. For points corresponding to  $s = 2$ ,  $n = 26$  in Figure 6 top left panel (NO,  $s$  even), the BR for  $N_1 \rightarrow \ell_\alpha W$  is highest (lowest) for the  $\tau$  ( $e$ )-channel. Similarly, in Figure 6 third row left panel (IO,  $s$  even), the BR for  $N_1 \rightarrow \ell_\alpha W$  is highest (lowest) for the  $e$  ( $\mu$ )-channel. From Figure 9, we see that comparing the LNV final states with different charged-lepton flavor combinations can provide an independent,

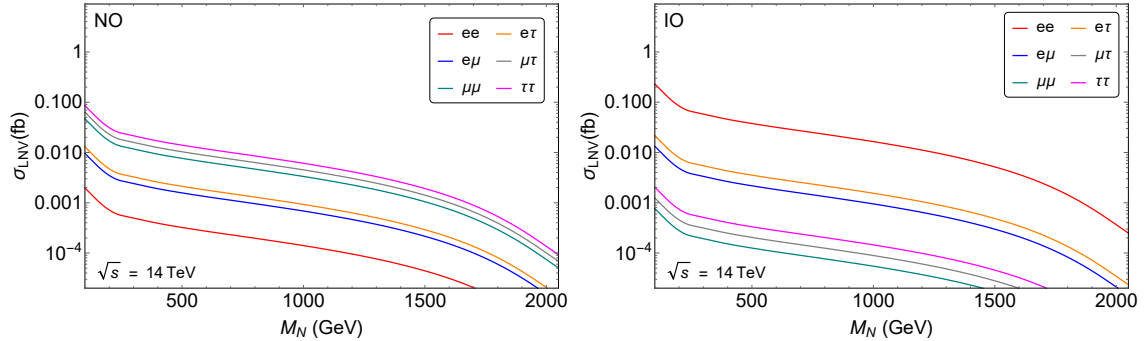


**Figure 9.** LNV signal (5.16) normalized to the  $g_{B-L} = 1$  case as a function of the RHN mass scale  $M_N$  at  $\sqrt{s} = 14$  TeV LHC for all possible lepton flavor combinations in the strong NO (left) and strong IO (right) limit. Here  $M_{Z'} = 4$  TeV.

complementary test of the neutrino mass ordering at the high-energy frontier in our setup. Similar conclusions can be drawn in Cases 2 and 3.

It is also possible to probe the high-energy CP phases in the Yukawa coupling matrix at colliders using simple observables constructed out of the same-sign dilepton charge asymmetry. In particular, the difference  $\sigma_{\text{LNV}}^{\alpha,-}$  between and the sum  $\sigma_{\text{LNV}}^{\alpha,+}$  of the same-sign charged-lepton final states of a given flavor  $\alpha$  can be defined as

$$\sigma_{\text{LNV}}^{\alpha,\pm} = \sum_i \sigma_{\text{prod}}(pp \rightarrow N_i N_i) \left( [\text{BR}(N_i \rightarrow \ell_\alpha^- W^+)]^2 \pm [\text{BR}(N_i \rightarrow \ell_\alpha^+ W^-)]^2 \right) \times [\text{BR}(W \rightarrow jj)]^2. \quad (5.17)$$

Then the ratio  $\sigma_{\text{LNV}}^{\alpha,-}/\sigma_{\text{LNV}}^{\alpha,+}$  is related to the flavored CP asymmetries  $\varepsilon_{i\alpha}$ , as pointed out in Refs. [28, 41, 162]. Therefore, a measurement of  $\sigma_{\text{LNV}}^{\alpha,-}/\sigma_{\text{LNV}}^{\alpha,+}$  also measures the CP asymmetry in our case for a given set of RHN BRs fixed by the group theory parameters.

## 5.5 Correlation with leptogenesis

Following the formalism developed in Ref. [96], we compute the baryon asymmetry  $\eta_B$  in our scenario [cf. Eq. (4.2)]. For the  $U(1)_{B-L}$  case, there are additional washout processes, like  $N_i N_i \rightarrow Z' \rightarrow f \bar{f}$  (where  $f$  stands for any SM fermion), mediated by  $Z'$  [28, 29]. These processes affect both washout and dilution factors in the Boltzmann equations for the RHN and lepton asymmetry number densities, but do not contribute to the CP asymmetry. Therefore, a *lower* limit on  $M_{Z'}$  follows for a given value of  $g_{B-L}$ , if successful leptogenesis is demanded. This is illustrated in Figures 10, 11 and 12 for Case 1, 2 and 3 respectively. Keeping the collider signals discussed earlier in mind, we particularly focus on the ERS points by suitably choosing  $\theta_R$ , which leads to one RHN being long-lived. We also fix the gauge coupling  $g_{B-L} = 0.1$  which corresponds to a dilepton bound of  $M_{Z'} \gtrsim 4.1$  TeV [145] as shown by the vertical shaded region in these plots. Since we are interested in the on-shell production of  $N$  via the decay of  $Z'$ , we do not consider the mass range  $M_N > M_{Z'}/2$  as indicated by the white region.

For Case 1, we take  $n = 26$  and  $\theta_R$  being a point of ERS for strong NO (IO) in the left (right) panel of Figure 10. In addition, we choose  $s = 2$  in order to maximize the Majorana

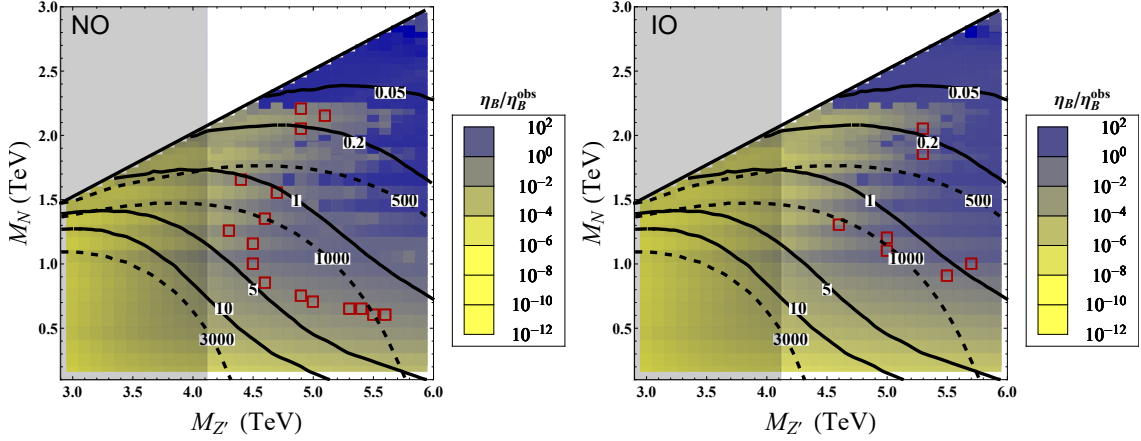


**Figure 10.** For *Case 1* prediction of the baryon asymmetry  $\eta_B$  relative to the observed value  $\eta_B^{\text{obs}}$  in the  $(M_{Z'}, M_N)$  plane for a fixed  $g_{B-L} = 0.1$ . We have fixed  $n = 26$  and set  $s$  to 2 (17) for strong NO (IO) in the left (right) panel, with the corresponding ERS value of  $\theta_R$ . The red points correspond to  $\eta_B$  within 10% of  $\eta_B^{\text{obs}}$ . The contours show  $\sigma_{\text{prod}}$  (in ab) at the  $\sqrt{s} = 14$  TeV LHC (solid) and at  $\sqrt{s} = 100$  TeV future collider (dashed).

phase (see Eq. (3.21)) and generate higher  $\eta_B$  (as well as  $m_{\beta\beta}$ , as discussed in Section 6). The mass splitting  $\Delta M_N$ , or equivalently, the  $\kappa$  value is chosen according to Eq. (4.15) which maximizes the CP asymmetry for each point in the  $(M_{Z'}, M_N)$  plane, meaning this gives the best-case scenario, since we are interested in the lower bound on  $M_{Z'}$ . As one can see in Figure 10, successful leptogenesis requires  $M_{Z'} \gtrsim 4.3$  (5) TeV for strong NO (IO) in Case 1. The red points in the plot give BAU within 10% of the observed value, which we consider as the allowed range, taking into account the theoretical uncertainties in the calculation. In general, all the points with  $\eta_B \gtrsim \eta_B^{\text{obs}}$  are allowed in our scenario, because we have maximized the predicted value of  $\eta_B$  and it can be easily brought down to match the observed value by moving away from the resonance condition. Another important feature to be noted in Figure 10 is that for a given point in the  $(M_{Z'}, M_N)$  plane,  $\eta_B^{\text{NO}} > \eta_B^{\text{IO}}$ . This can be qualitatively understood using Eqs. (4.10) and (4.11):<sup>10</sup>

$$\frac{\eta_B^{\text{NO}}}{\eta_B^{\text{IO}}} \sim \frac{\varepsilon_{\text{NO}}}{\varepsilon_{\text{IO}}} \approx \frac{(y_2 y_3 (-y_2^2 + y_3^2) \sin \theta_{L,\alpha})_{\text{NO}}}{(y_1 y_2 (-y_2^2 + y_1^2) \cos \theta_{L,\alpha})_{\text{IO}}} \approx \frac{2\Delta m_{\text{atm}}^2}{\Delta m_{\text{sol}}^2} \tan \theta_{L,\alpha} \gg 1. \quad (5.18)$$

Furthermore, we compare the results for  $\eta_B$  from resonant leptogenesis with the collider sensitivity in the same  $(M_{Z'}, M_N)$  plane. Figure 10 shows the contours of  $\sigma(pp \rightarrow Z' \rightarrow N_i N_i)$  in ab for both  $\sqrt{s} = 14$  TeV LHC (solid lines) and  $\sqrt{s} = 100$  TeV collider (dashed lines); see also Figure 2. It turns out that the region of parameter space in Case 1 for strong NO allowing successful leptogenesis yields  $\sigma_{\text{prod}} \lesssim 5$  ab at  $\sqrt{s} = 14$  TeV LHC. After taking into account the decay BRs in Eq. (5.16), and even assuming a fairly low SM background, the number of events is still  $< \mathcal{O}(1)$  with the final target luminosity of  $3 \text{ ab}^{-1}$ . For strong IO, the cross sections are smaller than strong NO case by at least an order of magnitude.

<sup>10</sup>For a comprehensive quantitative comparison of  $\eta_B$  in both cases, the efficiency factor for asymmetry production needs to be taken into account, which has been done in our numerical scans.

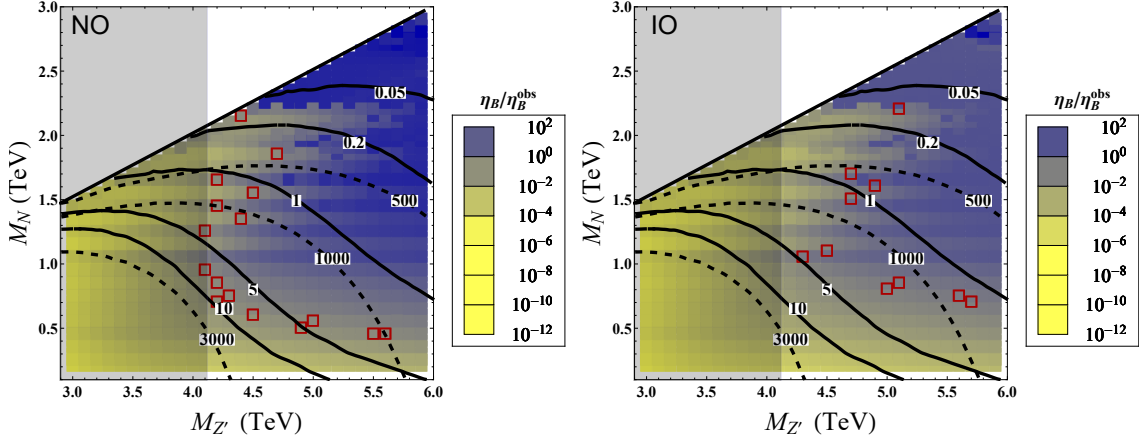


**Figure 11.** For *Case 2* prediction of the baryon asymmetry  $\eta_B$  relative to the observed value  $\eta_B^{\text{obs}}$  in the  $(M_{Z'}, M_N)$  plane for a fixed  $g_{B-L} = 0.1$ . We have fixed  $n = 14$ ,  $s = 1$ ,  $t = 2$  (i.e.  $u = 2s - t = 0$ ) with  $\theta_R$  being a point of ERS for strong NO (IO) in the left (right) panel. The red points correspond to  $\eta_B$  within 10% of  $\eta_B^{\text{obs}}$ . The contours show  $\sigma_{\text{prod}}$  (in ab) at the  $\sqrt{s} = 14$  TeV LHC (solid) and at  $\sqrt{s} = 100$  TeV future collider (dashed).

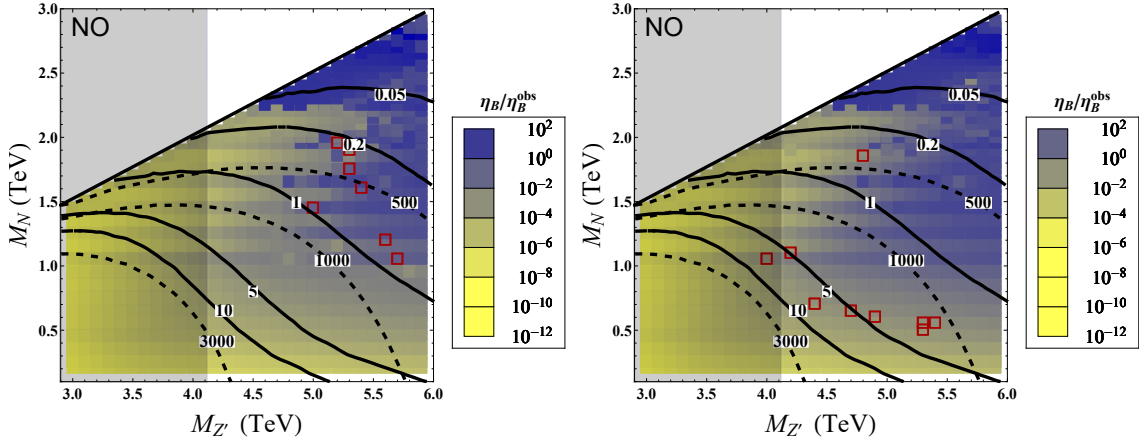


**Figure 12.** *Case 3a* (left panel) and *Case 3b.1* (right panel) predictions of the baryon asymmetry  $\eta_B$  relative to the observed value  $\eta_B^{\text{obs}}$  in the  $(M_{Z'}, M_N)$  plane for a fixed  $g_{B-L} = 0.1$ . We have fixed  $n = 16$ ,  $m = 1$ ,  $s = 1$  for *Case 3a*, and  $n = 10$ ,  $m = 5$ ,  $s = 5$  for *Case 3b.1*. In both cases, we take NO with  $\theta$  set to zero (not an ERS point). The red points correspond to  $\eta_B$  within 10% of  $\eta_B^{\text{obs}}$ . The contours show  $\sigma_{\text{prod}}$  (in ab) at the  $\sqrt{s} = 14$  TeV LHC (solid) and at  $\sqrt{s} = 100$  TeV future collider (dashed).

Therefore, a simultaneous explanation of  $\eta_B$  via resonant leptogenesis and an LNV signal at the LHC in our *Case 1* is precluded. The same conclusion holds for the *Case 2* and *Case 3* benchmark points analyzed in Figures 11 and 12 respectively.

At a future 100 TeV collider,  $\sigma_{\text{prod}}$  can reach up to 2000 ab for the region of successful leptogenesis; taking into account the decay BRs in Eq. (5.16), and assuming a fairly low SM background, we can expect up to about a thousand LNV events with  $30 \text{ ab}^{-1}$  integrated luminosity. The detection prospects at 100 TeV collider might significantly improve by

going to higher  $Z'$  masses than those shown in Figure 10. This is because the experimental limits on  $g_{B-L}$  are relaxed for  $M_{Z'} \gtrsim 6$  TeV [145]. For instance, at  $M_{Z'} = 7$  TeV, only the LEP-II constraint applies and  $g_{B-L}$  is allowed to be as large as one. Since  $\sigma_{\text{prod}}$  scales as  $g_{B-L}^2$  for  $M_N < M_{Z'}/2$ , we gain a factor of 100 in the cross-section, at the expense of a mild suppression due to the  $Z'$  mass change. Another way to improve the sensitivity would be by considering other  $Z'$  variants, such as the leptophobic case; this will be pursued elsewhere.

For Case 2, we choose  $n = 14$ ,  $t = 2$ ,  $s = 1$  (or  $u = 2s - t = 0$ ), which gives a good fit to the neutrino oscillation data [74]. Here successful leptogenesis at the ERS points requires  $M_{Z'} \gtrsim 4.2$  (4.3) TeV for strong NO (IO), with the results for  $\sigma_{\text{prod}}$  remaining the same as in Case 1. The comparison between the leptogenesis and collider accessible regions is shown in Figure 11 both both NO (left panel) and IO (right panel). Again, the LHC will not be able to probe the successful leptogenesis region in this case, but a future 100 TeV collider can do.

For Cases 3a and 3b.1, as mentioned in Section 5.2.3, leptogenesis is not viable at the ERS points, because  $N_1$  becomes long-lived. Since ERS only occurs for  $m$  even and  $s$  even case [cf. Figure 5], we choose a different case with  $m$  odd and  $s$  odd for leptogenesis. In particular, for Case 3a, we fix  $n = 16$ ,  $m = 1$ ,  $s = 1$  which gives a good fit to the neutrino data with NO [74], and furthermore, choose  $\theta_R = 0$  for simplicity. Our results for leptogenesis in the  $(M_{Z'}, M_N)$  plane is shown in Figure 12 left panel. We find that successful leptogenesis requires  $M_{Z'} \gtrsim 5.0$  TeV. Similarly, for Case 3b.1, we fix  $n = 10$ ,  $m = 5$ ,  $s = 5$  which gives a good fit to the neutrino data with NO [74], and furthermore, choose  $\theta_R = 0$  for simplicity. Our results for leptogenesis in the  $(M_{Z'}, M_N)$  plane is shown in Figure 12 right panel. We find that successful leptogenesis requires  $M_{Z'} \gtrsim 4.2$  TeV. The LHC and 100 TeV collider contours for the LNV signal are the same as in Cases 1 and 2. Again, the LHC will not be able to probe the successful leptogenesis region in these cases, but a future 100 TeV collider can do.

## 6 Correlation of BAU with $0\nu\beta\beta$

In this section, we discuss the connection between the high- and low-energy CP phases in our flavor model. To this effect, we consider the classic low-energy LNV process of  $0\nu\beta\beta$  which can unambiguously discern the Majorana nature of the neutrinos [55, 163]. The theory predictions for this yet unobserved process depends explicitly on the low-energy Majorana phases  $\alpha_1$  and  $\alpha_2$ . Therefore, we expect the rate of  $0\nu\beta\beta$  process to be correlated with the baryon asymmetry predictions, which depend on the high-energy CP phases that are related to the low-energy CP phases in our model. We will study this correlation for various scenarios of lepton mixing for which leptogenesis has been studied in Section 4.

A nuclear isotope decaying through  $0\nu\beta\beta$  process

$$(A, Z) \rightarrow (A, Z + 2) + 2e^- \quad (6.1)$$

would exhibit an half-life of

$$T_{1/2}^{0\nu} = \left[ G^{0\nu} |M^{0\nu}|^2 \left( \frac{m_{\beta\beta}}{m_e} \right)^2 \right]^{-1}, \quad (6.2)$$

where  $G^{0\nu}$  is the phase-space factor [164, 165],  $|M^{0\nu}|$  is the nuclear matrix element (NME) for this LNV transition [166, 167],  $m_{\beta\beta}$  is the effective Majorana neutrino mass and  $m_e$  is the electron mass. The values of  $G^{0\nu}$  and  $|M^{0\nu}|^2$  cannot be measured independently but can be computed based on the nuclear isotope, whereas  $m_{\beta\beta}$  is expressed only in terms of the light neutrino masses and lepton mixing parameters, i.e.<sup>11</sup>

$$m_{\beta\beta} = \sum_i |U_{ei}^2 m_i| = |U_{e1}^2 m_1 + U_{e2}^2 m_2 + U_{e3}^2 m_3|. \quad (6.3)$$

With the form of  $U$  given by Eq. (2.21), the effective neutrino mass in Eq. (6.3) reads

$$m_{\beta\beta} = |\cos^2 \theta_{12} \cos^2 \theta_{13} m_1 + \sin^2 \theta_{12} \cos^2 \theta_{13} e^{i\alpha_1} m_2 + \sin^2 \theta_{13} e^{i\alpha_2} m_3|. \quad (6.4)$$

For a strongly hierarchical light neutrino mass spectrum with  $m_0 \rightarrow 0$ , the value of  $m_{\beta\beta}$  depends on the mass ordering. From Eq. (6.4), we get the following in the strong NO ( $m_1 = 0$ ) and strong IO ( $m_3 = 0$ ) limits respectively:

$$m_{\beta\beta}^{\text{NO}} \approx \left| \sin^2 \theta_{12} \cos^2 \theta_{13} e^{i\alpha_1} \sqrt{\Delta m_{\text{sol}}^2} + \sin^2 \theta_{13} e^{i\alpha_2} \sqrt{\Delta m_{\text{atm}}^2} \right|, \quad (6.5a)$$

$$m_{\beta\beta}^{\text{IO}} \approx |\cos^2 \theta_{12} + \sin^2 \theta_{12} e^{i\alpha_1}| \cos^2 \theta_{13} \sqrt{|\Delta m_{\text{atm}}^2|}. \quad (6.5b)$$

An upper bound on the effective Majorana neutrino mass has been set by several experiments, using different nuclear isotopes, such as KamLAND-Zen ( $^{136}\text{Xe}$ ) [170], EXO-200 ( $^{136}\text{Xe}$ ) [171], GERDA ( $^{76}\text{Ge}$ ) [172], CUORE-0 ( $^{130}\text{Te}$ ) [173], and NEMO 3 ( $^{100}\text{Mo}$  among others) [174]. The strongest bound on  $m_{\beta\beta}$  is currently given by the KamLAND-Zen experiment using  $^{136}\text{Xe}$  isotope [170]:

$$m_{\beta\beta} < (61 - 165) \text{ meV} \quad \text{at 90\% C.L.} \quad (6.6)$$

with the spread coming from different NME calculations. Future tonne-scale experiments like nEXO [175] and LEGEND [176] can extend this down to

$$m_{\beta\beta} < \begin{cases} (4.7 - 20.3) \text{ meV} & (\text{nEXO}) \\ (34 - 78) \text{ meV} & (\text{LEGEND-200}) \\ (9 - 21) \text{ meV} & (\text{LEGEND-1000}) \end{cases}. \quad (6.7)$$

As we will see below, our  $m_{\beta\beta}$  predictions for the IO case are within reach of nEXO and LEGEND sensitivities. However, the corresponding predictions for the NO case are at the level of 1-4 meV, which are out of reach of tonne-scale detectors, but the kilotonne-scale detectors might be able to probe this region [177].

---

<sup>11</sup>Here we only consider the canonical light neutrino exchange for the  $0\nu\beta\beta$  process [168, 169]. The heavy RHNs in the model could also mediate the  $0\nu\beta\beta$  process via their mixing  $V_{\ell N}$  with the light neutrinos [114, 116]; however, for the Yukawa couplings being considered here, these RHN contributions are negligible.

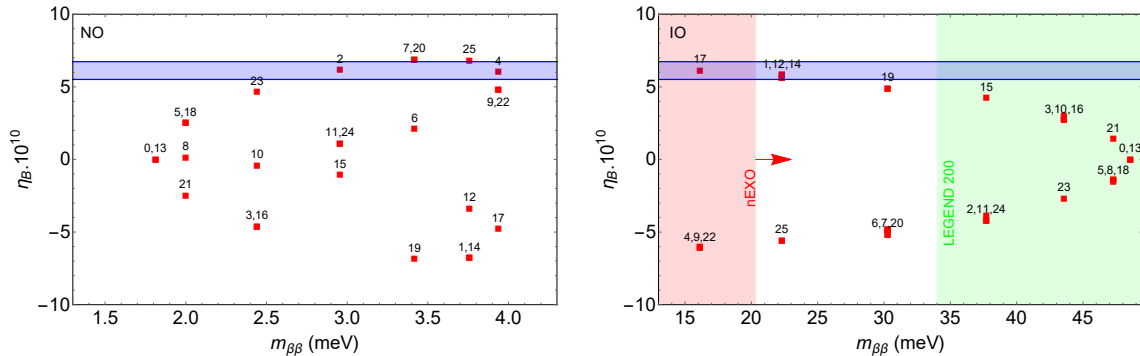


**Figure 13.** Correlation between the predicted BAU  $\eta_B$  and the effective neutrino mass  $m_{\beta\beta}$  for *Case 1* with  $n = 26$ ,  $k_1 = k_2 = 0$  and  $0 \leq s \leq n - 1$  (as shown by the numbered points). We have chosen the benchmark values  $M_N = 0.8$  (1.1) TeV and  $M_{Z'} = 4.9$  (5.0) TeV for strong NO (IO) in the left (right) panel, which according to Figure 10 produce the BAU of the correct magnitude. The blue-shaded horizontal bar corresponds to  $\eta_B$  within 10% of  $\eta_B^{\text{obs}}$ . The vertical shaded bands for the IO case indicate the smallest  $m_{\beta\beta}$  value (including the NME uncertainties) accessible to future  $0\nu\beta\beta$  experiments LEGEND-200 (green) and nEXO (red), as given in Eq. (6.7).

### 6.1 Case 1

In this case the Majorana phase  $\alpha_2$  is always trivial, for any choice of  $\theta$  and the group parameters  $n$  and  $s$ , while the second Majorana phase  $\alpha_1$  can take non-trivial values [cf. Eq. (3.21)]. Using the form of the PMNS mixing matrix given in terms of the model parameters in Eq. (3.7), we get from Eq. (6.3) the effective neutrino mass in strong NO and IO limits respectively as

$$m_{\beta\beta}^{\text{NO}} \approx \frac{1}{3} \left| \sqrt{\Delta m_{\text{sol}}^2} + 2(-1)^{k_1+k_2} \sin^2 \theta e^{6i\phi_s} \sqrt{\Delta m_{\text{atm}}^2} \right|, \quad (6.8a)$$

$$m_{\beta\beta}^{\text{IO}} \approx \frac{1}{3} \left| 1 + 2(-1)^{k_1} \cos^2 \theta e^{6i\phi_s} \right| \sqrt{|\Delta m_{\text{atm}}^2|}. \quad (6.8b)$$

Thus we see that the value of the effective Majorana neutrino mass  $m_{\beta\beta}$ , accessible in  $0\nu\beta\beta$  experiments, crucially depends on the choice of the CP symmetry and is in this scenario considerably restricted [65]. For our choice of  $n = 26$ ,  $k_1 = k_2 = 0$  and for  $\theta = \theta_{\text{bf}} \approx 0.18$ , using the best fit values for  $\Delta m_{\text{sol}}^2$  and  $\Delta m_{\text{atm}}^2$  [91], we get

$$1.8 \text{ meV} \lesssim m_{\beta\beta} \lesssim 4.0 \text{ meV (NO)}, \quad 16 \text{ meV} \lesssim m_{\beta\beta} \lesssim 49 \text{ meV (IO)}. \quad (6.9)$$

This is shown in Figure 13 by the red points, which correspond to different values of  $s$  ranging from 0 to  $n - 1$ . The left (right) panel is for NO (IO). For strong IO, most of the admitted values of  $m_{\beta\beta}$  can be tested with the proposed experiment LEGEND [176] and all of them can be explored with nEXO [175].

To illustrate the correlation between the high- and low-energy CP phases, we also plot in Figure 13 the predictions for the BAU corresponding to the  $s$  values shown here. Here we have fixed  $M_N = 0.8$  (1.1) TeV and  $M_{Z'} = 4.9$  (5.0) TeV for strong NO (IO). These values of  $M_N$  and  $M_{Z'}$  have been chosen by taking cue from the red points in Figure 10 which

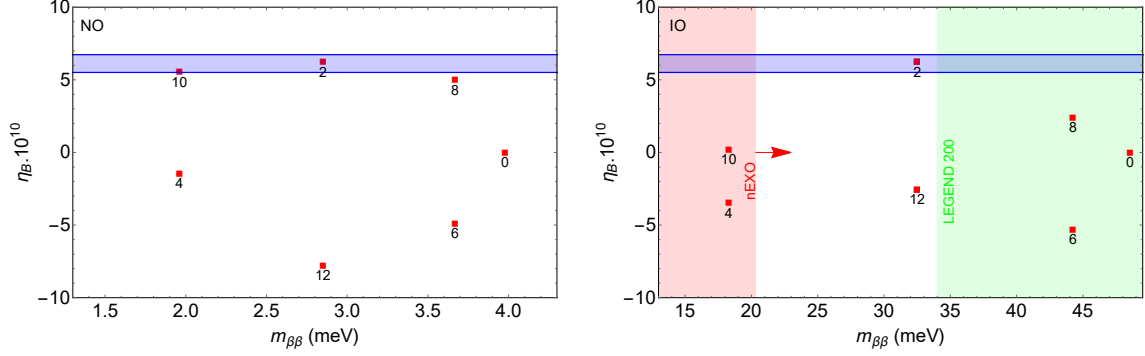


**Figure 14.** Correlation between the predicted BAU  $\eta_B$  and the effective neutrino mass  $m_{\beta\beta}$  for it Case 2 with  $n = 14$ ,  $k_1 = k_2 = 0$  and  $0 \leq t \leq n - 1$  (as shown by the numbered points). Only even  $t$  are allowed because of the condition  $u = 2s - t = 0$ . We have chosen the benchmark values  $M_N = 0.8$  (1.1) TeV and  $M_{Z'} = 4.3$  TeV for strong NO (IO) in the left (right) panel using the results from Figure 11. The blue-shaded horizontal bar corresponds to  $\eta_B$  within 10% of  $\eta_B^{\text{obs}}$ . The vertical shaded bands for the IO case indicate the smallest  $m_{\beta\beta}$  value (including the NME uncertainties) accessible to future  $0\nu\beta\beta$  experiments LEGEND-200 (green) and nEXO (red), as given in Eq. (6.7).

generate  $\eta_B$  values in the vicinity of  $\eta_B^{\text{obs}}$ , so that we are not off by orders of magnitude.<sup>12</sup> The horizontal blue-band corresponds to  $\eta_B$  values within 10% of the observed value. In fact, any point above this line is also allowed in our model, since we are calculating the maximum possible  $\eta_B$  and it is easy to lower its value by just going away from the resonance point. As can be seen in Figure 13, a few values of  $s$  like  $s = 2, 4$  (17) can successfully reproduce the observed BAU for strong NO (IO). Note that while some values of  $s$  like  $s = 17$  (4) in the NO (IO) can produce the correct magnitude of  $\eta_B$  but have the wrong sign and should be discarded. It should also be pointed out that since inclusion of  $Z'$  only contributes to the washout of the generated baryon asymmetry, increasing the value of  $M_{Z'}$  is akin to integrating out the  $Z'$  from the low-energy effective theory which leads to higher values of  $\eta_B$ . The  $0\nu\beta\beta$  predictions are insensitive to the choice of  $M_{Z'}$ .

## 6.2 Case 2

In this case both the Majorana phases  $\alpha_1$  and  $\alpha_2$  can in general have non-trivial values [cf. Eq. (3.32)]. Using the PMNS mixing matrix from Eq. (3.26), we get the following for strong NO and IO respectively:

$$m_{\beta\beta}^{\text{NO}} \approx \frac{1}{3} \left| \sqrt{\Delta m_{\text{sol}}^2} - 2(-1)^{k_1+k_2} e^{i\phi_v} \left( \cos\theta \sin\frac{\phi_u}{2} - i \sin\theta \cos\frac{\phi_u}{2} \right)^2 \sqrt{\Delta m_{\text{atm}}^2} \right|, \quad (6.10a)$$

$$m_{\beta\beta}^{\text{IO}} \approx \frac{1}{3} \left| 1 + (-1)^{k_1} e^{i\phi_v} (\cos\phi_u + \cos 2\theta - i \sin 2\theta \sin\phi_u) \right| \sqrt{|\Delta m_{\text{atm}}^2|}. \quad (6.10b)$$

For our choice of  $n = 14$  and  $u = 2s - t = 0$ , only even values of  $t$  between 0 and  $n - 1$  are allowed. Using the best-fit  $\theta_L \approx 2.96$ ,  $k_1 = k_2 = 0$ , and the best-fit values for the oscillation

<sup>12</sup>Although Figure 10 is for a fixed  $s$  value, we do not expect too much variation in  $\eta_B$  with respect to  $s$ , as confirmed in Figure 13.

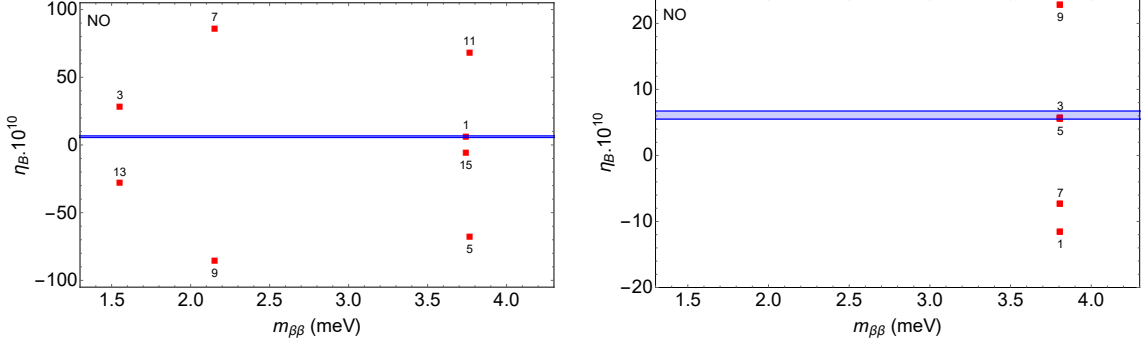


**Figure 15.** Correlation between the predicted BAU  $\eta_B$  and the effective neutrino mass  $m_{\beta\beta}$  for *Case 3a* (left) and *Case 3b.1* (right) both with NO and  $m$  odd,  $s$  odd. We have chosen  $n = 16$  (10),  $k_1 = k_2 = 0$ ,  $m = 1$  (5),  $M_N = 1.5$  (0.7) TeV and  $M_{Z'} = 5.0$  (4.4) TeV in the left (right) panel. In Case 3b.1, The blue-shaded horizontal bar corresponds to  $\eta_B$  within 10% of  $\eta_B^{\text{obs}}$ . The vertical shaded bands for the IO case indicate the smallest  $m_{\beta\beta}$  range (including the NME uncertainties) accessible to future  $0\nu\beta\beta$  experiments LEGEND-200 (green) and nEXO (red), as given in Eq. (6.7).

parameters, we get

$$2.0 \text{ meV} \lesssim m_{\beta\beta} \lesssim 4.0 \text{ meV (NO)}, \quad 18 \text{ meV} \lesssim m_{\beta\beta} \lesssim 49 \text{ meV (IO)}. \quad (6.11)$$

This is shown in Figure 14 by the red points, which correspond to different even values of  $t$  ranging from 0 to  $n - 1$ . The left (right) panel is for NO (IO). As in Case 1, for strong IO, most of the admitted values of  $m_{\beta\beta}$  can be tested with the proposed experiment LEGEND [176] and all of them can be explored with nEXO [175].

The corresponding values of  $\eta_B$  have been generated for  $M_{Z'} = 4.3$  TeV and for  $M_N = 0.8$  (1.1) TeV in the NO (IO) case. Similar to case 1, these values of  $M_N$  and  $M_{Z'}$  have been chosen from the red points in Figure 11, which are in the vicinity of  $\eta_B^{\text{obs}}$ . As can be seen in Figure 14,  $s = 2$  can successfully reproduce the observed BAU for both mass orderings.

### 6.3 Case 3

Following the leptogenesis analysis in Figure 12, we only consider the NO case here. The effective neutrino mass in terms of the high-energy CP phases is given by

$$(m_{\beta\beta}^{\text{NO}})_{3a} \approx \frac{1}{3} \left| \left( \sqrt{2} \sin \theta \cos \phi_m + e^{-3i\phi_s} \cos \theta \right)^2 \sqrt{\Delta m_{\text{sol}}^2} + 2(-1)^{k_1+k_2} \sin^2 \phi_m \sqrt{\Delta m_{\text{atm}}^2} \right|, \quad (6.12a)$$

$$(m_{\beta\beta}^{\text{NO}})_{3b.1} \approx \frac{1}{3} \left| \sin^2 \theta \sqrt{\Delta m_{\text{sol}}^2} + (-1)^{k_1} \cos^2 \theta \sqrt{\Delta m_{\text{atm}}^2} \right|. \quad (6.12b)$$

In case 3a for a given  $n$ , only certain values of  $m$  close to 0 or  $n$  reproduce the observed neutrino mixing angles with allowed ordering restricted to NO. Thus, we set  $n = 16$ ,  $m = 1$  with  $\theta_L$  computed separately for each value of  $s/n$ . In case 3b for a given  $n$ , values of  $m \sim n/2$  reproduce the observed neutrino mixing angles with allowed ordering restricted to NO. Thus, we set  $n = 10$ ,  $m = 5$  with  $\theta_L = 1.31$ . For Case 3a with NO and  $k_1 = k_2 = 0$ ,

we get

$$1.5 \text{ meV} \lesssim m_{\beta\beta} \lesssim 3.8 \text{ meV}, \quad (6.13)$$

whereas for Case 3b.1 with NO, we get a constant value of  $m_{\beta\beta} = 3.8 \text{ meV}$ , independent of  $s$  and  $k_1 = 0$ . This can be understood from Eq. (6.12b) which indeed is independent of the phase  $\phi_s = s/n$  (and thus of the chosen CP transformation). This is also shown in Figure 15, where the red points correspond to different odd  $s$  values between 0 and  $n - 1$  in both cases.

The corresponding values of  $\eta_B$  in Figure 15 have been generated for  $M_N = 2.8 \text{ TeV}$  and  $M_{Z'} = 5.8 \text{ TeV}$ . Similar to previous cases, these values of  $M_N$  and  $M_{Z'}$  have been chosen by analyzing the red points in Figure 12.

## 7 Conclusion

We have presented a low-scale type-I seesaw scenario with a flavor  $G_f$  and CP symmetry that are broken into non-trivial residual symmetries in the charged-lepton and neutrino sectors. We show that this class of models with nearly degenerate heavy right-handed neutrinos can naturally explain the observed baryon asymmetry of the universe through resonant leptogenesis mechanism. An important distinguishing feature of these models is the possibility of having a relatively long lifetime for one of the RHNs, which is attributed to enhanced residual symmetries. This allows the long-lived RHN to be accessible at the dedicated long-lived particle search facilities, while at the same time, the other two RHNs in the model can be probed via either prompt or displaced vertex signals at the LHC.

We have studied the correlation of the BAU predictions with the collider signals in a simple  $U(1)_{B-L}$  extension of the type-I seesaw. We find that while the LHC might not be able to probe the region allowed by successful leptogenesis, a future 100 TeV collider can easily access these regions, thereby providing a direct test of the leptogenesis mechanism in this framework. The collider prospects turn out to be better in case of normal mass ordering of light neutrinos.

We have also studied the correlation between the high- and low-energy CP phases in the model. This is exemplified by considering the classic low-energy lepton-number-violating process of neutrinoless double beta decay which crucially depends on the low-energy phases, and connecting it to BAU which depends on the high-energy CP phases. We find that the region allowing successful leptogenesis can be completely tested in future tonne-scale  $0\nu\beta\beta$  experiments provided the light neutrino mass ordering is inverted. Therefore, the collider and  $0\nu\beta\beta$  experiments will provide complementary probes of these flavor and CP symmetries and their roles in the generation of baryon asymmetry.

## Acknowledgments

We thank Marco Drewes for alerting us to their upcoming paper on a related subject. BD thanks Claudia Hagedorn and Emiliano Molinaro for many useful discussions and for collaboration during the early stages of this work, part of which was presented in Section

7.6 of Ref. [159]. BD also acknowledges the local hospitality at MIAPP, UMass Amherst and CP3 Odense, where parts of this work were done. The work of BD is supported in part by the US Department of Energy under Grant No. DE-SC0017987 and by a Fermilab Intensity Frontier Fellowship. This work was partly performed at the Aspen Center for Physics, which is supported by National Science Foundation grant PHY-1607611.

## A Group Theory of $\Delta(6n^2)$ and Representation Matrices

As discussed in Ref. [71], the discrete groups  $\Delta(3n^2)$ ,  $n \geq 2$  integer, can be described in terms of three generators  $a$ ,  $c$  and  $d$  fulfilling the relations

$$a^3 = e, \quad c^n = e, \quad d^n = e, \quad cd = dc, \quad aca^{-1} = c^{-1}d^{-1}, \quad ada^{-1} = c, \quad (\text{A.1})$$

with  $e$  being the identity element of the group. The discrete groups  $\Delta(6n^2)$ ,  $n \geq 2$  integer [72], are obtained by adding a fourth generator  $b$  to the set of  $a$ ,  $c$  and  $d$ . The relations involving  $b$  are

$$b^2 = e, \quad (ab)^2 = e, \quad bcb^{-1} = d^{-1}, \quad bdb^{-1} = c^{-1}. \quad (\text{A.2})$$

In the trivial representation  $\mathbf{1}$  all elements of the group are represented by the character 1. The explicit representation matrices  $g(\mathbf{3})$  for  $a$ ,  $b$ ,  $c$  and  $d$  can be chosen in the irreducible, faithful, complex three-dimensional representation  $\mathbf{3}$  as

$$a(\mathbf{3}) = \begin{pmatrix} 1 & 0 & 0 \\ 0 & \omega & 0 \\ 0 & 0 & \omega^2 \end{pmatrix}, \quad b(\mathbf{3}) = \begin{pmatrix} 1 & 0 & 0 \\ 0 & 0 & \omega^2 \\ 0 & \omega & 0 \end{pmatrix},$$

$$c(\mathbf{3}) = \frac{1}{3} \begin{pmatrix} 1 + 2 \cos \phi_n & 1 - \cos \phi_n - \sqrt{3} \sin \phi_n & 1 - \cos \phi_n + \sqrt{3} \sin \phi_n \\ 1 - \cos \phi_n + \sqrt{3} \sin \phi_n & 1 + 2 \cos \phi_n & 1 - \cos \phi_n - \sqrt{3} \sin \phi_n \\ 1 - \cos \phi_n - \sqrt{3} \sin \phi_n & 1 - \cos \phi_n + \sqrt{3} \sin \phi_n & 1 + 2 \cos \phi_n \end{pmatrix}, \quad (\text{A.3})$$

with  $\omega = e^{2\pi i/3}$  and  $\phi_n = 2\pi/n$ . The representation for  $d$  can be computed via  $d(\mathbf{3}) = a(\mathbf{3})^2 c(\mathbf{3}) a(\mathbf{3})$ .

The existence of an irreducible, in general unfaithful, real three-dimensional representation  $\mathbf{3}'$  requires that all its characters are real. This cannot be fulfilled in all groups  $\Delta(6n^2)$ , but only, if the index  $n$  is even. In this case the form of the representation matrices  $g(\mathbf{3}')$  is

$$a(\mathbf{3}') = a(\mathbf{3}), \quad b(\mathbf{3}') = b(\mathbf{3}), \quad c(\mathbf{3}') = \frac{1}{3} \begin{pmatrix} -1 & 2 & 2 \\ 2 & -1 & 2 \\ 2 & 2 & -1 \end{pmatrix} \quad (\text{A.4})$$

and  $d(\mathbf{3}') = a(\mathbf{3}')^2 c(\mathbf{3}') a(\mathbf{3}')$ . Note that the representation matrices  $g(\mathbf{3}')$  do not depend on the index  $n$  of the group and thus lead to the same representation for all groups  $\Delta(6n^2)$  with even  $n$ . Indeed, we can observe that the group generated by the representation matrices  $g(\mathbf{3}')$  has 24 elements and thus corresponds to the group  $\Delta(6 \cdot 2^2) = \Delta(24)$ . This group

is isomorphic to the permutation group  $S_4$ . This representation together with the one generated by the representation matrices  $a(\mathbf{3}')$ ,  $c(\mathbf{3}')$ ,  $d(\mathbf{3}')$  and  $-b(\mathbf{3}')$  (i.e. the representation matrix  $b(\mathbf{3}')$  acquires an overall sign [72]) are the only real three-dimensional representations in a generic group  $\Delta(6n^2)$  with even  $n$  and  $3 \nmid n$ . To see this we inspect the characters of the three-dimensional representations. Following Ref. [72] we see that the characters  $\chi(\mathbf{3}_{\text{gen}})$  of a generic irreducible three-dimensional representation  $\mathbf{3}_{\text{gen}}$  for a certain type of classes is given by  $\eta^{-\rho l}$  with  $\eta = e^{2\pi i/n}$ ,  $\rho = 0, \dots, n-1$  (labeling this type of class of the group  $\Delta(6n^2)$ ) and  $l = 1, \dots, n-1$  ( $l$  labels the different pairs of three-dimensional representations). We have to require that all  $\eta^{-\rho l}$  for a certain representation labeled by  $l$  are real. This is ensured, if  $\eta^{-l}$  is real for all powers  $\rho$  with  $\rho = 0, \dots, n-1$ , meaning  $\eta^{-l}$  should be real itself. Hence,  $2l/n$  must be an integer. With the constraint on  $l$ ,  $1 \leq l \leq n-1$ , we know that there is a single solution to  $2l/n$  being an integer, namely  $l = n/2$ , i. e. there is a single pair of irreducible three-dimensional representations that are real. In this case their characters are real for all classes, as can be explicitly checked with the help of the character table, shown in Ref. [72].

## B CP symmetries and form of CP transformations

The CP symmetries correspond to automorphisms of the flavor group  $\Delta(6n^2)$ , see discussion in Ref. [74]. In the present analysis we employ the ones, as used in Ref. [65]. These can be obtained as follows: consider the automorphism

$$a \rightarrow a, \quad c \rightarrow c^{-1}, \quad d \rightarrow d^{-1} \quad \text{and} \quad b \rightarrow b. \quad (\text{B.1})$$

The automorphism in Eq. (B.1) can be represented by  $X_0(\mathbf{1}) = 1$  in the trivial representation  $\mathbf{1}$  and by the matrix

$$X_0(\mathbf{3}) = X_0(\mathbf{3}') = \begin{pmatrix} 1 & 0 & 0 \\ 0 & 0 & 1 \\ 0 & 1 & 0 \end{pmatrix} \quad (\text{B.2})$$

in both three-dimensional representations  $\mathbf{3}$  and  $\mathbf{3}'$ . In Case 1, the CP transformation  $X(s)(\mathbf{3})$  has the explicit form  $a(\mathbf{3})b(\mathbf{3})c(\mathbf{3})d(\mathbf{3})^{2s} X_0$ . The form of the CP transformation  $X(s)(\mathbf{3}')$  in the representation  $\mathbf{3}'$  depends on whether  $s$  is even or odd, i. e.

$$X(s \text{ even})(\mathbf{3}') = \begin{pmatrix} 1 & 0 & 0 \\ 0 & 1 & 0 \\ 0 & 0 & 1 \end{pmatrix}, \quad (\text{B.3a})$$

$$X(s \text{ odd})(\mathbf{3}') = \frac{1}{3} \begin{pmatrix} -1 & 2 & 2 \\ 2 & -1 & 2 \\ 2 & 2 & -1 \end{pmatrix}. \quad (\text{B.3b})$$

In Case 2, the form of the CP transformation  $X(\mathbf{3})(s, t)$  in the representation  $\mathbf{3}$  can be chosen as  $c(\mathbf{3})^s d(\mathbf{3})^t X_0$ , and is more conveniently written in terms of the variables  $u = 2s - t$  and  $v = 3t$  with  $\phi_u = \pi u/n$  and  $\phi_v = \pi v/n$ . The form of the CP transformation  $X(s, t)(\mathbf{3}')$

depends on whether  $s$  and  $t$  are even or odd. The explicit form of  $X(s, t)(\mathbf{3}')$ , however, does neither contain  $s$  nor  $t$  as parameters.

$$X(s \text{ even}, t \text{ even})(\mathbf{3}') = \begin{pmatrix} 1 & 0 & 0 \\ 0 & 0 & 1 \\ 0 & 1 & 0 \end{pmatrix}, \quad (\text{B.4a})$$

$$X(s \text{ even}, t \text{ odd})(\mathbf{3}') = \frac{1}{3} \begin{pmatrix} -1 & 2\omega^2 & 2\omega \\ 2\omega^2 & 2\omega & -1 \\ 2\omega & -1 & 2\omega^2 \end{pmatrix}, \quad (\text{B.4b})$$

$$X(s \text{ odd}, t \text{ even})(\mathbf{3}') = \frac{1}{3} \begin{pmatrix} -1 & 2 & 2 \\ 2 & 2 & -1 \\ 2 & -1 & 2 \end{pmatrix}, \quad (\text{B.4c})$$

$$X(s \text{ odd}, t \text{ odd})(\mathbf{3}')(\mathbf{3}') = \frac{1}{3} \begin{pmatrix} -1 & 2\omega & 2\omega^2 \\ 2\omega & 2\omega^2 & -1 \\ 2\omega^2 & -1 & 2\omega \end{pmatrix}. \quad (\text{B.4d})$$

For Case 3a and Case 3b.1, the form of the CP transformation  $X(s, m)(\mathbf{3})$  is given as [74]

$$X(s)(\mathbf{3}) = \frac{1}{3} e^{-i\delta_s} \begin{pmatrix} 3 \cos 3\delta_s + i \sin 3\delta_s & -2i\omega \sin 3\delta_s & -2i\omega^2 \sin 3\delta_s \\ -2i\omega \sin 3\delta_s & \omega^2 (3 \cos 3\delta_s + i \sin 3\delta_s) & -2i \sin 3\delta_s \\ -2i\omega^2 \sin 3\delta_s & -2i \sin 3\delta_s & \omega (3 \cos 3\delta_s + i \sin 3\delta_s) \end{pmatrix} \quad (\text{B.5})$$

with  $\delta_s = \pi s/n$ . The form of the CP transformation  $X(s)(\mathbf{3}')$  only depends on whether  $s$  is even or odd. In particular,

$$X(s \text{ even})(\mathbf{3}') = \begin{pmatrix} 1 & 0 & 0 \\ 0 & \omega^2 & 0 \\ 0 & 0 & \omega \end{pmatrix}, \quad (\text{B.6a})$$

$$X(s \text{ odd})(\mathbf{3}') = \frac{1}{3} \begin{pmatrix} -1 & 2\omega & 2\omega^2 \\ 2\omega & -\omega^2 & 2 \\ 2\omega^2 & 2 & -\omega \end{pmatrix}. \quad (\text{B.6b})$$

## C Form of the Representation Matrices for Residual Symmetries

In the following, we list the form of the representation matrices in the representations  $\mathbf{3}$  and  $\mathbf{3}'$  for the different residual symmetries, used in Sections 2 and 3.

In all these cases, the residual flavor symmetry in the charged-lepton sector is generated by  $a$  which corresponds to the representation matrix  $a(\mathbf{3})$  given in Eq. (A.3). The residual flavor symmetry in the neutrino sector is generated by  $Z$ . In Case 1 and Case 2,  $Z$  is chosen as  $c^{n/2}$  which is in the representation  $\mathbf{3}$  of the form

$$Z(\mathbf{3}) = \frac{1}{3} \begin{pmatrix} -1 & 2 & 2 \\ 2 & -1 & 2 \\ 2 & 2 & -1 \end{pmatrix} \quad (\text{C.1})$$

independent of the index  $n$ , while the form of  $Z = c^{n/2}$  in  $\mathbf{3}'$  reads either

$$Z(\mathbf{3}') = \begin{pmatrix} 1 & 0 & 0 \\ 0 & 1 & 0 \\ 0 & 0 & 1 \end{pmatrix} \quad \text{for } n/2 \text{ even,} \quad (\text{C.2})$$

or

$$Z(\mathbf{3}') = \frac{1}{3} \begin{pmatrix} -1 & 2 & 2 \\ 2 & -1 & 2 \\ 2 & 2 & -1 \end{pmatrix} = Z(\mathbf{3}) \quad \text{for } n/2 \text{ odd.} \quad (\text{C.3})$$

In Case 3a and Case 3b.1,  $Z$  is chosen as  $bc^m d^m$  with  $m = 0, \dots, n-1$ . In the representation  $\mathbf{3}$  it is of the form [74]

$$Z(m)(\mathbf{3}) = \frac{1}{3} \begin{pmatrix} 1 + 2 \cos \gamma_m & \omega^2 (1 - \cos \gamma_m + \sqrt{3} \sin \gamma_m) & \omega (1 - \cos \gamma_m - \sqrt{3} \sin \gamma_m) \\ \omega (1 - \cos \gamma_m + \sqrt{3} \sin \gamma_m) & 1 - \cos \gamma_m - \sqrt{3} \sin \gamma_m & \omega^2 (1 + 2 \cos \gamma_m) \\ \omega^2 (1 - \cos \gamma_m - \sqrt{3} \sin \gamma_m) & \omega (1 + 2 \cos \gamma_m) & 1 - \cos \gamma_m + \sqrt{3} \sin \gamma_m \end{pmatrix} \quad (\text{C.4})$$

with  $\gamma_m = 2\pi m/n$ . For the special values,  $m = 0$ ,  $m = n$  and  $m = n/2$ , the form of  $Z(m)(\mathbf{3})$  simplifies and we find

$$Z(m=0)(\mathbf{3}) = Z(m=n)(\mathbf{3}) = \begin{pmatrix} 1 & 0 & 0 \\ 0 & 0 & \omega^2 \\ 0 & \omega & 0 \end{pmatrix}, \quad (\text{C.5a})$$

$$Z(m=n/2)(\mathbf{3}) = \frac{1}{3} \begin{pmatrix} -1 & 2\omega^2 & 2\omega \\ 2\omega & 2 & -\omega^2 \\ 2\omega^2 & -\omega & 2 \end{pmatrix}. \quad (\text{C.5b})$$

Similarly, we can analyze the form of the representation matrix  $Z(m)(\mathbf{3}')$ . The decisive criterion for this form is whether  $m$  is even or odd; otherwise there is no further dependence on the parameter  $m$  for  $Z(m)(\mathbf{3}')$ .

$$Z(m \text{ even})(\mathbf{3}') = \begin{pmatrix} 1 & 0 & 0 \\ 0 & 0 & \omega^2 \\ 0 & \omega & 0 \end{pmatrix}, \quad Z(m \text{ odd})(\mathbf{3}') = \frac{1}{3} \begin{pmatrix} -1 & 2\omega^2 & 2\omega \\ 2\omega & 2 & -\omega^2 \\ 2\omega^2 & -\omega & 2 \end{pmatrix}. \quad (\text{C.6})$$

We note that  $Z(m \text{ even})(\mathbf{3}')$  coincides with  $Z(m=0)(\mathbf{3}) = Z(m=n)(\mathbf{3})$ , and  $Z(m \text{ odd})(\mathbf{3}')$  coincides with  $Z(m=n/2)(\mathbf{3})$ .

## D Explicit Form of the Yukawa Couplings

### D.1 Case 1

The Yukawa parameters  $y_f$  in this case (irrespective of  $s$ ) are

$$y_1^2 = \frac{M_N}{2v^2} \left( m_1 - m_3 + \sqrt{m_1^2 + m_3^2 + 2m_1 m_3 \cos(4\theta_R)} \right) \sec(2\theta_R), \quad (\text{D.1a})$$

$$y_2^2 = \frac{M_N m_2}{v^2}, \quad (\text{D.1b})$$

$$y_3^2 = \frac{M_N}{2v^2} \left( -m_1 + m_3 + \sqrt{m_1^2 + m_3^2 + 2m_1 m_3 \cos(4\theta_R)} \right) \sec(2\theta_R). \quad (\text{D.1c})$$

## D.2 Case 2

$t$  even:

$$y_1^2 = \frac{M_N m_1}{v^2}, \quad (\text{D.2a})$$

$$y_2^2 = \frac{M_N m_2}{v^2}, \quad (\text{D.2b})$$

$$y_3^2 = \frac{M_N m_3}{v^2}. \quad (\text{D.2c})$$

$t$  odd:

$$y_1^2 = \frac{M_N}{2v^2} \left( -m_1 + m_3 + \sqrt{m_1^2 + m_3^2 - 2m_1 m_3 \cos(4\theta_R)} \right) \csc(2\theta_R), \quad (\text{D.3a})$$

$$y_2^2 = \frac{M_N m_2}{v^2}, \quad (\text{D.3b})$$

$$y_3^2 = \frac{M_N}{2v^2} \left( m_1 - m_3 + \sqrt{m_1^2 + m_3^2 - 2m_1 m_3 \cos(4\theta_R)} \right) \csc(2\theta_R). \quad (\text{D.3c})$$

## D.3 Case 3a

$m$  and  $s$ , both even or odd:

$$y_1^2 = \frac{M_N m_1}{v^2}, \quad (\text{D.4a})$$

$$y_2^2 = \frac{M_N m_2}{v^2}, \quad (\text{D.4b})$$

$$y_3^2 = \frac{M_N m_3}{v^2}. \quad (\text{D.4c})$$

$m$  even,  $s$  odd:

$$y_1^2 = \frac{M_N}{2v^2} \left( m_1 - m_2 + \sqrt{m_1^2 + m_2^2 + 2m_1 m_2 \cos(4\theta_R)} \right) \sec(2\theta_R), \quad (\text{D.5a})$$

$$y_2^2 = \frac{M_N}{2v^2} \left( -m_1 + m_2 + \sqrt{m_1^2 + m_2^2 + 2m_1 m_2 \cos(4\theta_R)} \right) \sec(2\theta_R), \quad (\text{D.5b})$$

$$y_3^2 = \frac{M_N m_3}{v^2}. \quad (\text{D.5c})$$

$m$  odd,  $s$  even:

$$y_1^2 = \frac{M_N m_1}{v^2}, \quad (\text{D.6a})$$

$$y_2^2 = \frac{M_N}{2v^2} \left( m_2 - m_3 + \sqrt{m_2^2 + m_3^2 + 2m_2 m_3 \cos(4\theta_R)} \right) \sec(2\theta_R), \quad (\text{D.6b})$$

$$y_3^2 = \frac{M_N}{2v^2} \left( -m_2 + m_3 + \sqrt{m_2^2 + m_3^2 + 2m_2 m_3 \cos(4\theta_R)} \right) \sec(2\theta_R). \quad (\text{D.6c})$$

#### D.4 Case 3b.1

$m$  and  $s$ , both even or odd:

$$y_1^2 = \frac{M_N m_2}{v^2}, \quad (\text{D.7a})$$

$$y_2^2 = \frac{M_N m_3}{v^2}, \quad (\text{D.7b})$$

$$y_3^2 = \frac{M_N m_1}{v^2}. \quad (\text{D.7c})$$

$m$  even,  $s$  odd:

$$y_1^2 = \frac{M_N}{2v^2} \left( -m_1 + m_2 + \sqrt{m_1^2 + m_2^2 + 2m_1 m_2 \cos(4\theta_R)} \right) \sec(2\theta_R), \quad (\text{D.8a})$$

$$y_2^2 = \frac{M_N m_3}{v^2}, \quad (\text{D.8b})$$

$$y_3^2 = \frac{M_N}{2v^2} \left( m_1 - m_2 + \sqrt{m_1^2 + m_2^2 + 2m_1 m_2 \cos(4\theta_R)} \right) \sec(2\theta_R), \quad (\text{D.8c})$$

$m$  odd,  $s$  even:

$$y_1^2 = \frac{M_N}{2v^2} \left( m_2 - m_3 + \sqrt{m_2^2 + m_3^2 + 2m_2 m_3 \cos(4\theta_R)} \right) \sec(2\theta_R), \quad (\text{D.9a})$$

$$y_2^2 = \frac{M_N}{2v^2} \left( -m_2 + m_3 + \sqrt{m_2^2 + m_3^2 + 2m_2 m_3 \cos(4\theta_R)} \right) \sec(2\theta_R), \quad (\text{D.9b})$$

$$y_3^2 = \frac{M_N m_1}{v^2}. \quad (\text{D.9c})$$

#### References

- [1] PLANCK collaboration, *Planck 2018 results. VI. Cosmological parameters*, *Astron. Astrophys.* **641** (2020) A6 [[1807.06209](#)].
- [2] A. D. Sakharov, *Violation of CP Invariance, C asymmetry, and baryon asymmetry of the universe*, *Pisma Zh. Eksp. Teor. Fiz.* **5** (1967) 32.
- [3] D. Bodeker and W. Buchmuller, *Baryogenesis from the weak scale to the grand unification scale*, *Rev. Mod. Phys.* **93** (2021) 035004 [[2009.07294](#)].
- [4] M. Fukugita and T. Yanagida, *Baryogenesis Without Grand Unification*, *Phys. Lett. B* **174** (1986) 45.
- [5] W. Buchmuller, R. D. Peccei and T. Yanagida, *Leptogenesis as the origin of matter*, *Ann. Rev. Nucl. Part. Sci.* **55** (2005) 311 [[hep-ph/0502169](#)].
- [6] S. Davidson, E. Nardi and Y. Nir, *Leptogenesis*, *Phys. Rept.* **466** (2008) 105 [[0802.2962](#)].
- [7] C. S. Fong, E. Nardi and A. Riotto, *Leptogenesis in the Universe*, *Adv. High Energy Phys.* **2012** (2012) 158303 [[1301.3062](#)].
- [8] V. A. Kuzmin, V. A. Rubakov and M. E. Shaposhnikov, *On the Anomalous Electroweak Baryon Number Nonconservation in the Early Universe*, *Phys. Lett. B* **155** (1985) 36.

- [9] P. Minkowski,  $\mu \rightarrow e\gamma$  at a Rate of One Out of  $10^9$  Muon Decays?, *Phys. Lett. B* **67** (1977) 421.
- [10] R. N. Mohapatra and G. Senjanovic, *Neutrino Mass and Spontaneous Parity Nonconservation*, *Phys. Rev. Lett.* **44** (1980) 912.
- [11] T. Yanagida, *Horizontal gauge symmetry and masses of neutrinos*, *Conf. Proc. C* **7902131** (1979) 95.
- [12] M. Gell-Mann, P. Ramond and R. Slansky, *Complex Spinors and Unified Theories*, *Conf. Proc. C* **790927** (1979) 315 [[1306.4669](#)].
- [13] S. Glashow, *The Future of Elementary Particle Physics*, *NATO Sci. Ser. B* **61** (1980) 687.
- [14] J. Schechter and J. W. F. Valle, *Neutrino Masses in  $SU(2) \times U(1)$  Theories*, *Phys. Rev. D* **22** (1980) 2227.
- [15] S. Davidson and A. Ibarra, *A Lower bound on the right-handed neutrino mass from leptogenesis*, *Phys. Lett. B* **535** (2002) 25 [[hep-ph/0202239](#)].
- [16] K. Moffat, S. Pascoli, S. T. Petcov, H. Schulz and J. Turner, *Three-flavored nonresonant leptogenesis at intermediate scales*, *Phys. Rev. D* **98** (2018) 015036 [[1804.05066](#)].
- [17] A. Pilaftsis and T. E. J. Underwood, *Resonant leptogenesis*, *Nucl. Phys. B* **692** (2004) 303 [[hep-ph/0309342](#)].
- [18] P. S. B. Dev, M. Garny, J. Klaric, P. Millington and D. Teresi, *Resonant enhancement in leptogenesis*, *Int. J. Mod. Phys. A* **33** (2018) 1842003 [[1711.02863](#)].
- [19] M. Flanz, E. A. Paschos and U. Sarkar, *Baryogenesis from a lepton asymmetric universe*, *Phys. Lett. B* **345** (1995) 248 [[hep-ph/9411366](#)].
- [20] L. Covi, E. Roulet and F. Vissani, *CP violating decays in leptogenesis scenarios*, *Phys. Lett. B* **384** (1996) 169 [[hep-ph/9605319](#)].
- [21] M. Flanz, E. A. Paschos, U. Sarkar and J. Weiss, *Baryogenesis through mixing of heavy Majorana neutrinos*, *Phys. Lett. B* **389** (1996) 693 [[hep-ph/9607310](#)].
- [22] A. Pilaftsis, *Resonant CP violation induced by particle mixing in transition amplitudes*, *Nucl. Phys. B* **504** (1997) 61 [[hep-ph/9702393](#)].
- [23] A. Pilaftsis, *CP violation and baryogenesis due to heavy Majorana neutrinos*, *Phys. Rev. D* **56** (1997) 5431 [[hep-ph/9707235](#)].
- [24] A. Pilaftsis and T. E. J. Underwood, *Electroweak-scale resonant leptogenesis*, *Phys. Rev. D* **72** (2005) 113001 [[hep-ph/0506107](#)].
- [25] F. F. Deppisch and A. Pilaftsis, *Lepton Flavour Violation and  $\theta(13)$  in Minimal Resonant Leptogenesis*, *Phys. Rev. D* **83** (2011) 076007 [[1012.1834](#)].
- [26] M. Drewes, B. Garbrecht, P. Hernandez, M. Kekic, J. Lopez-Pavon, J. Racker et al., *ARS Leptogenesis*, *Int. J. Mod. Phys. A* **33** (2018) 1842002 [[1711.02862](#)].
- [27] J.-M. Frere, T. Hambye and G. Vertongen, *Is leptogenesis falsifiable at LHC?*, *JHEP* **01** (2009) 051 [[0806.0841](#)].
- [28] S. Blanchet, Z. Chacko, S. S. Granor and R. N. Mohapatra, *Probing Resonant Leptogenesis at the LHC*, *Phys. Rev. D* **82** (2010) 076008 [[0904.2174](#)].
- [29] S. Blanchet, P. S. B. Dev and R. N. Mohapatra, *Leptogenesis with TeV Scale Inverse Seesaw in  $SO(10)$* , *Phys. Rev. D* **82** (2010) 115025 [[1010.1471](#)].

- [30] S. Iso, N. Okada and Y. Orikasa, *Resonant Leptogenesis in the Minimal B-L Extended Standard Model at TeV*, *Phys. Rev. D* **83** (2011) 093011 [[1011.4769](#)].
- [31] N. Okada, Y. Orikasa and T. Yamada, *Minimal Flavor Violation in the Minimal  $U(1)_{B-L}$  Model and Resonant Leptogenesis*, *Phys. Rev. D* **86** (2012) 076003 [[1207.1510](#)].
- [32] C. S. Fong, M. C. Gonzalez-Garcia, E. Nardi and E. Peinado, *New ways to TeV scale leptogenesis*, *JHEP* **08** (2013) 104 [[1305.6312](#)].
- [33] P. S. B. Dev, C.-H. Lee and R. N. Mohapatra, *Leptogenesis Constraints on the Mass of Right-handed Gauge Bosons*, *Phys. Rev. D* **90** (2014) 095012 [[1408.2820](#)].
- [34] P. S. B. Dev, C.-H. Lee and R. N. Mohapatra, *TeV Scale Lepton Number Violation and Baryogenesis*, *J. Phys. Conf. Ser.* **631** (2015) 012007 [[1503.04970](#)].
- [35] M. Dhuria, C. Hati, R. Rangarajan and U. Sarkar, *Falsifying leptogenesis for a TeV scale  $W_R^\pm$  at the LHC*, *Phys. Rev. D* **92** (2015) 031701 [[1503.07198](#)].
- [36] J. Heeck and D. Teresi, *Leptogenesis and neutral gauge bosons*, *Phys. Rev. D* **94** (2016) 095024 [[1609.03594](#)].
- [37] A. Caputo, P. Hernandez, J. Lopez-Pavon and J. Salvado, *The seesaw portal in testable models of neutrino masses*, *JHEP* **06** (2017) 112 [[1704.08721](#)].
- [38] C.-Q. Geng and H. Okada, *Neutrino masses, dark matter and leptogenesis with  $U(1)_{B-L}$  gauge symmetry*, *Phys. Dark Univ.* **20** (2018) 13 [[1710.09536](#)].
- [39] P. S. B. Dev, R. N. Mohapatra and Y. Zhang, *Leptogenesis constraints on  $B - L$  breaking Higgs boson in TeV scale seesaw models*, *JHEP* **03** (2018) 122 [[1711.07634](#)].
- [40] P.-H. Gu and R. N. Mohapatra, *Leptogenesis with TeV Scale  $W_R$* , *Phys. Rev. D* **97** (2018) 075014 [[1712.00420](#)].
- [41] P. S. B. Dev, R. N. Mohapatra and Y. Zhang, *CP Violating Effects in Heavy Neutrino Oscillations: Implications for Colliders and Leptogenesis*, *JHEP* **11** (2019) 137 [[1904.04787](#)].
- [42] D. Borah, A. Dasgupta and D. Mahanta, *TeV scale resonant leptogenesis with  $L_\mu$ - $L_\tau$  gauge symmetry in light of the muon  $g-2$* , *Phys. Rev. D* **104** (2021) 075006 [[2106.14410](#)].
- [43] W. Liu, K.-P. Xie and Z. Yi, *Testing leptogenesis at the LHC and future muon colliders: a  $Z'$  scenario*, [2109.15087](#).
- [44] E. J. Chun et al., *Probing Leptogenesis*, *Int. J. Mod. Phys. A* **33** (2018) 1842005 [[1711.02865](#)].
- [45] Z.-z. Xing, *Flavor structures of charged fermions and massive neutrinos*, *Phys. Rept.* **854** (2020) 1 [[1909.09610](#)].
- [46] J. A. Casas and A. Ibarra, *Oscillating neutrinos and  $\mu \rightarrow e, \gamma$* , *Nucl. Phys. B* **618** (2001) 171 [[hep-ph/0103065](#)].
- [47] P. S. B. Dev, P. Di Bari, B. Garbrecht, S. Lavignac, P. Millington and D. Teresi, *Flavor effects in leptogenesis*, *Int. J. Mod. Phys. A* **33** (2018) 1842001 [[1711.02861](#)].
- [48] G. C. Branco, T. Morozumi, B. M. Nobre and M. N. Rebelo, *A Bridge between CP violation at low-energies and leptogenesis*, *Nucl. Phys. B* **617** (2001) 475 [[hep-ph/0107164](#)].
- [49] M. N. Rebelo, *Leptogenesis without CP violation at low-energies*, *Phys. Rev. D* **67** (2003) 013008 [[hep-ph/0207236](#)].

- [50] S. Pascoli, S. T. Petcov and W. Rodejohann, *On the connection of leptogenesis with low-energy CP violation and LFV charged lepton decays*, *Phys. Rev. D* **68** (2003) 093007 [[hep-ph/0302054](#)].
- [51] Z.-z. Xing, *Casas-Ibarra Parametrization and Unflavored Leptogenesis*, *Chin. Phys. C* **34** (2010) 1 [[0902.2469](#)].
- [52] W. Rodejohann, *Non-Unitary Lepton Mixing Matrix, Leptogenesis and Low Energy CP Violation*, *EPL* **88** (2009) 51001 [[0903.4590](#)].
- [53] S. Antusch, S. Blanchet, M. Blennow and E. Fernandez-Martinez, *Non-unitary Leptonic Mixing and Leptogenesis*, *JHEP* **01** (2010) 017 [[0910.5957](#)].
- [54] G. J. Feldman, J. Hartnell and T. Kobayashi, *Long-baseline neutrino oscillation experiments*, *Adv. High Energy Phys.* **2013** (2013) 475749 [[1210.1778](#)].
- [55] M. J. Dolinski, A. W. P. Poon and W. Rodejohann, *Neutrinoless Double-Beta Decay: Status and Prospects*, *Ann. Rev. Nucl. Part. Sci.* **69** (2019) 219 [[1902.04097](#)].
- [56] S. Pascoli, S. T. Petcov and A. Riotto, *Connecting low energy leptonic CP-violation to leptogenesis*, *Phys. Rev. D* **75** (2007) 083511 [[hep-ph/0609125](#)].
- [57] G. C. Branco, R. Gonzalez Felipe and F. R. Joaquim, *A New bridge between leptonic CP violation and leptogenesis*, *Phys. Lett. B* **645** (2007) 432 [[hep-ph/0609297](#)].
- [58] S. Pascoli, S. T. Petcov and A. Riotto, *Leptogenesis and Low Energy CP Violation in Neutrino Physics*, *Nucl. Phys. B* **774** (2007) 1 [[hep-ph/0611338](#)].
- [59] A. Anisimov, S. Blanchet and P. Di Bari, *Viability of Dirac phase leptogenesis*, *JCAP* **04** (2008) 033 [[0707.3024](#)].
- [60] E. Molinaro and S. T. Petcov, *The Interplay Between the 'Low' and 'High' Energy CP-Violation in Leptogenesis*, *Eur. Phys. J. C* **61** (2009) 93 [[0803.4120](#)].
- [61] E. Molinaro and S. T. Petcov, *A Case of Subdominant/Suppressed 'High Energy' Contribution to the Baryon Asymmetry of the Universe in Flavoured Leptogenesis*, *Phys. Lett. B* **671** (2009) 60 [[0808.3534](#)].
- [62] K. Moffat, S. Pascoli, S. T. Petcov and J. Turner, *Leptogenesis from Low Energy CP Violation*, *JHEP* **03** (2019) 034 [[1809.08251](#)].
- [63] C. Hagedorn, R. N. Mohapatra, E. Molinaro, C. C. Nishi and S. T. Petcov, *CP Violation in the Lepton Sector and Implications for Leptogenesis*, *Int. J. Mod. Phys. A* **33** (2018) 1842006 [[1711.02866](#)].
- [64] P. Chen, G.-J. Ding and S. F. King, *Leptogenesis and residual CP symmetry*, *JHEP* **03** (2016) 206 [[1602.03873](#)].
- [65] C. Hagedorn and E. Molinaro, *Flavor and CP symmetries for leptogenesis and  $0 \nu \beta\beta$  decay*, *Nucl. Phys. B* **919** (2017) 404 [[1602.04206](#)].
- [66] C.-C. Li and G.-J. Ding, *Implications of residual CP symmetry for leptogenesis in a model with two right-handed neutrinos*, *Phys. Rev. D* **96** (2017) 075005 [[1701.08508](#)].
- [67] R. Samanta, R. Sinha and A. Ghosal, *Importance of generalized  $\mu\tau$  symmetry and its CP extension on neutrino mixing and leptogenesis*, *JHEP* **10** (2019) 057 [[1805.10031](#)].
- [68] F. Feruglio, C. Hagedorn and R. Ziegler, *Lepton Mixing Parameters from Discrete and CP Symmetries*, *JHEP* **07** (2013) 027 [[1211.5560](#)].

- [69] M. Holthausen, M. Lindner and M. A. Schmidt, *CP and Discrete Flavour Symmetries*, *JHEP* **04** (2013) 122 [[1211.6953](#)].
- [70] M.-C. Chen, M. Fallbacher, K. T. Mahanthappa, M. Ratz and A. Trautner, *CP Violation from Finite Groups*, *Nucl. Phys. B* **883** (2014) 267 [[1402.0507](#)].
- [71] C. Luhn, S. Nasri and P. Ramond, *The Flavor group  $\Delta(3n^{**2})$* , *J. Math. Phys.* **48** (2007) 073501 [[hep-th/0701188](#)].
- [72] J. A. Escobar and C. Luhn, *The Flavor Group  $\Delta(6n^{**2})$* , *J. Math. Phys.* **50** (2009) 013524 [[0809.0639](#)].
- [73] S. F. King and T. Neder, *Lepton mixing predictions including Majorana phases from  $\Delta(6n^2)$  flavour symmetry and generalised CP*, *Phys. Lett. B* **736** (2014) 308 [[1403.1758](#)].
- [74] C. Hagedorn, A. Meroni and E. Molinaro, *Lepton mixing from  $\Delta(3n^2)$  and  $\Delta(6n^2)$  and CP*, *Nucl. Phys. B* **891** (2015) 499 [[1408.7118](#)].
- [75] G.-J. Ding, S. F. King and T. Neder, *Generalised CP and  $\Delta(6n^2)$  family symmetry in semi-direct models of leptons*, *JHEP* **12** (2014) 007 [[1409.8005](#)].
- [76] G.-J. Ding and S. F. King, *Generalized CP and  $\Delta(3n^2)$  Family Symmetry for Semi-Direct Predictions of the PMNS Matrix*, *Phys. Rev. D* **93** (2016) 025013 [[1510.03188](#)].
- [77] J. Alimena et al., *Searching for long-lived particles beyond the Standard Model at the Large Hadron Collider*, *J. Phys. G* **47** (2020) 090501 [[1903.04497](#)].
- [78] D. Acosta et al., *Review of opportunities for new long-lived particle triggers in Run 3 of the Large Hadron Collider*, **2110.14675**.
- [79] F. F. Deppisch, P. S. B. Dev and A. Pilaftsis, *Neutrinos and Collider Physics*, *New J. Phys.* **17** (2015) 075019 [[1502.06541](#)].
- [80] Y. Cai, T. Han, T. Li and R. Ruiz, *Lepton Number Violation: Seesaw Models and Their Collider Tests*, *Front. in Phys.* **6** (2018) 40 [[1711.02180](#)].
- [81] I. Zurbano Fernandez et al., *High-Luminosity Large Hadron Collider (HL-LHC): Technical design report*, *CERN-2020-010* (2020) .
- [82] FCC collaboration, *FCC-hh: The Hadron Collider: Future Circular Collider Conceptual Design Report Volume 3*, *Eur. Phys. J. ST* **228** (2019) 755.
- [83] R. Gonzalez Felipe, F. R. Joaquim and B. M. Nobre, *Radiatively induced leptogenesis in a minimal seesaw model*, *Phys. Rev. D* **70** (2004) 085009 [[hep-ph/0311029](#)].
- [84] K. Turzynski, *Degenerate minimal seesaw and leptogenesis*, *Phys. Lett. B* **589** (2004) 135 [[hep-ph/0401219](#)].
- [85] G. C. Branco, R. Gonzalez Felipe, F. R. Joaquim and B. M. Nobre, *Enlarging the window for radiative leptogenesis*, *Phys. Lett. B* **633** (2006) 336 [[hep-ph/0507092](#)].
- [86] Y. H. Ahn, C. S. Kim, S. K. Kang and J. Lee,  *$\mu$ - $\tau$  Symmetry and Radiatively Generated Leptogenesis*, *Phys. Rev. D* **75** (2007) 013012 [[hep-ph/0610007](#)].
- [87] K. S. Babu, Y. Meng and Z. Tavartkiladze, *Common Origin for CP Violation in Cosmology and in Neutrino Oscillations*, **0812.4419**.
- [88] P. S. B. Dev, P. Millington, A. Pilaftsis and D. Teresi, *Corrigendum to "Flavour Covariant Transport Equations: an Application to Resonant Leptogenesis"*, *Nucl. Phys. B* **897** (2015) 749 [[1504.07640](#)].

- [89] Z.-h. Zhao, *Renormalization group evolution induced leptogenesis in the minimal seesaw model with the trimaximal mixing and mu-tau reflection symmetry*, *JHEP* **11** (2021) 170 [[2003.00654](#)].
- [90] PARTICLE DATA GROUP collaboration, *Review of Particle Physics*, *PTEP* **2020** (2020) 083C01.
- [91] I. Esteban, M. C. Gonzalez-Garcia, M. Maltoni, T. Schwetz and A. Zhou, *The fate of hints: updated global analysis of three-flavor neutrino oscillations*, *JHEP* **09** (2020) 178 [[2007.14792](#)].
- [92] P. F. Harrison, D. H. Perkins and W. G. Scott, *Tri-bimaximal mixing and the neutrino oscillation data*, *Phys. Lett. B* **530** (2002) 167 [[hep-ph/0202074](#)].
- [93] S. F. King and C. Luhn, *Neutrino Mass and Mixing with Discrete Symmetry*, *Rept. Prog. Phys.* **76** (2013) 056201 [[1301.1340](#)].
- [94] F. Feruglio, C. Hagedorn and R. Ziegler, *A realistic pattern of lepton mixing and masses from  $S_4$  and CP*, *Eur. Phys. J. C* **74** (2014) 2753 [[1303.7178](#)].
- [95] W. Buchmuller, P. Di Bari and M. Plumacher, *Leptogenesis for pedestrians*, *Annals Phys.* **315** (2005) 305 [[hep-ph/0401240](#)].
- [96] P. S. B. Dev, P. Millington, A. Pilaftsis and D. Teresi, *Flavour Covariant Transport Equations: an Application to Resonant Leptogenesis*, *Nucl. Phys. B* **886** (2014) 569 [[1404.1003](#)].
- [97] P. S. B. Dev, P. Millington, A. Pilaftsis and D. Teresi, *Kadanoff–Baym approach to flavour mixing and oscillations in resonant leptogenesis*, *Nucl. Phys. B* **891** (2015) 128 [[1410.6434](#)].
- [98] A. Kartavtsev, P. Millington and H. Vogel, *Lepton asymmetry from mixing and oscillations*, *JHEP* **06** (2016) 066 [[1601.03086](#)].
- [99] J. Klarić, M. Shaposhnikov and I. Timiryasov, *Reconciling resonant leptogenesis and baryogenesis via neutrino oscillations*, *Phys. Rev. D* **104** (2021) 055010 [[2103.16545](#)].
- [100] G. C. Branco, L. Lavoura and M. N. Rebelo, *Majorana Neutrinos and CP Violation in the Leptonic Sector*, *Phys. Lett. B* **180** (1986) 264.
- [101] G. C. Branco, M. N. Rebelo and J. I. Silva-Marcos, *Leptogenesis, Yukawa textures and weak basis invariants*, *Phys. Lett. B* **633** (2006) 345 [[hep-ph/0510412](#)].
- [102] E. E. Jenkins and A. V. Manohar, *Algebraic Structure of Lepton and Quark Flavor Invariants and CP Violation*, *JHEP* **10** (2009) 094 [[0907.4763](#)].
- [103] F. F. Deppisch, J. Harz and M. Hirsch, *Falsifying High-Scale Leptogenesis at the LHC*, *Phys. Rev. Lett.* **112** (2014) 221601 [[1312.4447](#)].
- [104] F. F. Deppisch, J. Harz, M. Hirsch, W.-C. Huang and H. Päs, *Falsifying High-Scale Baryogenesis with Neutrinoless Double Beta Decay and Lepton Flavor Violation*, *Phys. Rev. D* **92** (2015) 036005 [[1503.04825](#)].
- [105] F. F. Deppisch, L. Graf, J. Harz and W.-C. Huang, *Neutrinoless Double Beta Decay and the Baryon Asymmetry of the Universe*, *Phys. Rev. D* **98** (2018) 055029 [[1711.10432](#)].
- [106] A. Pilaftsis, *Radiatively induced neutrino masses and large Higgs neutrino couplings in the standard model with Majorana fields*, *Z. Phys. C* **55** (1992) 275 [[hep-ph/9901206](#)].
- [107] D. Tommasini, G. Barenboim, J. Bernabeu and C. Jarlskog, *Nondecoupling of heavy neutrinos and lepton flavor violation*, *Nucl. Phys. B* **444** (1995) 451 [[hep-ph/9503228](#)].

- [108] J. Gluza, *On teraelectronvolt Majorana neutrinos*, *Acta Phys. Polon. B* **33** (2002) 1735 [[hep-ph/0201002](#)].
- [109] J. Kersten and A. Y. Smirnov, *Right-Handed Neutrinos at CERN LHC and the Mechanism of Neutrino Mass Generation*, *Phys. Rev. D* **76** (2007) 073005 [[0705.3221](#)].
- [110] Z.-z. Xing, *Naturalness and Testability of TeV Seesaw Mechanisms*, *Prog. Theor. Phys. Suppl.* **180** (2009) 112 [[0905.3903](#)].
- [111] M. B. Gavela, T. Hambye, D. Hernandez and P. Hernandez, *Minimal Flavour Seesaw Models*, *JHEP* **09** (2009) 038 [[0906.1461](#)].
- [112] X.-G. He, S. Oh, J. Tandean and C.-C. Wen, *Large Mixing of Light and Heavy Neutrinos in Seesaw Models and the LHC*, *Phys. Rev. D* **80** (2009) 073012 [[0907.1607](#)].
- [113] R. Adhikari and A. Raychaudhuri, *Light neutrinos from massless texture and below TeV seesaw scale*, *Phys. Rev. D* **84** (2011) 033002 [[1004.5111](#)].
- [114] A. Ibarra, E. Molinaro and S. T. Petcov, *TeV Scale See-Saw Mechanisms of Neutrino Mass Generation, the Majorana Nature of the Heavy Singlet Neutrinos and  $(\beta\beta)_{0\nu}$ -Decay*, *JHEP* **09** (2010) 108 [[1007.2378](#)].
- [115] A. Ibarra, E. Molinaro and S. T. Petcov, *Low Energy Signatures of the TeV Scale See-Saw Mechanism*, *Phys. Rev. D* **84** (2011) 013005 [[1103.6217](#)].
- [116] M. Mitra, G. Senjanovic and F. Vissani, *Neutrinoless Double Beta Decay and Heavy Sterile Neutrinos*, *Nucl. Phys. B* **856** (2012) 26 [[1108.0004](#)].
- [117] C.-H. Lee, P. S. B. Dev and R. N. Mohapatra, *Natural TeV-scale left-right seesaw mechanism for neutrinos and experimental tests*, *Phys. Rev. D* **88** (2013) 093010 [[1309.0774](#)].
- [118] A. E. Cárcamo Hernández, M. González and N. A. Neill, *Low scale type I seesaw model for lepton masses and mixings*, *Phys. Rev. D* **101** (2020) 035005 [[1906.00978](#)].
- [119] J. Lopez-Pavon, E. Molinaro and S. T. Petcov, *Radiative Corrections to Light Neutrino Masses in Low Scale Type I Seesaw Scenarios and Neutrinoless Double Beta Decay*, *JHEP* **11** (2015) 030 [[1506.05296](#)].
- [120] E. Fernandez-Martinez, J. Hernandez-Garcia, J. Lopez-Pavon and M. Lucente, *Loop level constraints on Seesaw neutrino mixing*, *JHEP* **10** (2015) 130 [[1508.03051](#)].
- [121] E. Fernandez-Martinez, J. Hernandez-Garcia and J. Lopez-Pavon, *Global constraints on heavy neutrino mixing*, *JHEP* **08** (2016) 033 [[1605.08774](#)].
- [122] A. Das and N. Okada, *Bounds on heavy Majorana neutrinos in type-I seesaw and implications for collider searches*, *Phys. Lett. B* **774** (2017) 32 [[1702.04668](#)].
- [123] P. D. Bolton, F. F. Deppisch and P. S. B. Dev, *Neutrinoless double beta decay versus other probes of heavy sterile neutrinos*, *JHEP* **03** (2020) 170 [[1912.03058](#)].
- [124] W.-Y. Keung and G. Senjanovic, *Majorana Neutrinos and the Production of the Right-handed Charged Gauge Boson*, *Phys. Rev. Lett.* **50** (1983) 1427.
- [125] A. Datta, M. Guchait and A. Pilaftsis, *Probing lepton number violation via majorana neutrinos at hadron supercolliders*, *Phys. Rev. D* **50** (1994) 3195 [[hep-ph/9311257](#)].
- [126] T. Han and B. Zhang, *Signatures for Majorana neutrinos at hadron colliders*, *Phys. Rev. Lett.* **97** (2006) 171804 [[hep-ph/0604064](#)].

- [127] F. del Aguila, J. A. Aguilar-Saavedra and R. Pittau, *Heavy neutrino signals at large hadron colliders*, *JHEP* **10** (2007) 047 [[hep-ph/0703261](#)].
- [128] A. Atre, T. Han, S. Pascoli and B. Zhang, *The Search for Heavy Majorana Neutrinos*, *JHEP* **05** (2009) 030 [[0901.3589](#)].
- [129] P. S. B. Dev, A. Pilaftsis and U.-k. Yang, *New Production Mechanism for Heavy Neutrinos at the LHC*, *Phys. Rev. Lett.* **112** (2014) 081801 [[1308.2209](#)].
- [130] D. Alva, T. Han and R. Ruiz, *Heavy Majorana neutrinos from  $W\gamma$  fusion at hadron colliders*, *JHEP* **02** (2015) 072 [[1411.7305](#)].
- [131] A. Das and N. Okada, *Improved bounds on the heavy neutrino productions at the LHC*, *Phys. Rev. D* **93** (2016) 033003 [[1510.04790](#)].
- [132] CMS collaboration, *Search for heavy Majorana neutrinos in same-sign dilepton channels in proton-proton collisions at  $\sqrt{s} = 13$  TeV*, *JHEP* **01** (2019) 122 [[1806.10905](#)].
- [133] ATLAS collaboration, *Search for heavy neutral leptons in decays of  $W$  bosons produced in 13 TeV  $pp$  collisions using prompt and displaced signatures with the ATLAS detector*, *JHEP* **10** (2019) 265 [[1905.09787](#)].
- [134] A. Davidson,  *$B - L$  as the fourth color within an  $SU(2)_L \times U(1)_R \times U(1)$  model*, *Phys. Rev. D* **20** (1979) 776.
- [135] R. E. Marshak and R. N. Mohapatra, *Quark - Lepton Symmetry and  $B-L$  as the  $U(1)$  Generator of the Electroweak Symmetry Group*, *Phys. Lett. B* **91** (1980) 222.
- [136] W. Buchmuller, C. Greub and P. Minkowski, *Neutrino masses, neutral vector bosons and the scale of  $B-L$  breaking*, *Phys. Lett. B* **267** (1991) 395.
- [137] L. Basso, A. Belyaev, S. Moretti and C. H. Shepherd-Themistocleous, *Phenomenology of the minimal  $B-L$  extension of the Standard model:  $Z'$  and neutrinos*, *Phys. Rev. D* **80** (2009) 055030 [[0812.4313](#)].
- [138] P. Fileviez Perez, T. Han and T. Li, *Testability of Type I Seesaw at the CERN LHC: Revealing the Existence of the  $B-L$  Symmetry*, *Phys. Rev. D* **80** (2009) 073015 [[0907.4186](#)].
- [139] Z. Kang, P. Ko and J. Li, *New Avenues to Heavy Right-handed Neutrinos with Pair Production at Hadronic Colliders*, *Phys. Rev. D* **93** (2016) 075037 [[1512.08373](#)].
- [140] P. Cox, C. Han and T. T. Yanagida, *LHC Search for Right-handed Neutrinos in  $Z'$  Models*, *JHEP* **01** (2018) 037 [[1707.04532](#)].
- [141] C. Han, T. Li and C.-Y. Yao, *Searching for heavy neutrino in terms of tau lepton at future hadron collider*, *Phys. Rev. D* **104** (2021) 015036 [[2103.03548](#)].
- [142] ALEPH, DELPHI, L3, OPAL, LEP ELECTROWEAK collaboration, *Electroweak Measurements in Electron-Positron Collisions at  $W$ -Boson-Pair Energies at LEP*, *Phys. Rept.* **532** (2013) 119 [[1302.3415](#)].
- [143] ATLAS collaboration, *Search for high-mass dilepton resonances using 139  $\text{fb}^{-1}$  of  $pp$  collision data collected at  $\sqrt{s} = 13$  TeV with the ATLAS detector*, *Phys. Lett. B* **796** (2019) 68 [[1903.06248](#)].
- [144] CMS collaboration, *Search for a narrow resonance in high-mass dilepton final states in proton-proton collisions using 140  $\text{fb}^{-1}$  of data at  $\sqrt{s} = 13$  TeV*, *CMS-PAS-EXO-19-019* (2019) .

- [145] A. Das, P. S. B. Dev, Y. Hosotani and S. Mandal, *Probing the minimal  $U(1)_X$  model at future electron-positron colliders via the fermion pair-production channel*, [2104.10902](#).
- [146] T. Appelquist, B. A. Dobrescu and A. R. Hopper, *Nonexotic Neutral Gauge Bosons*, *Phys. Rev. D* **68** (2003) 035012 [[hep-ph/0212073](#)].
- [147] A. Das, N. Okada and D. Raut, *Enhanced pair production of heavy Majorana neutrinos at the LHC*, *Phys. Rev. D* **97** (2018) 115023 [[1710.03377](#)].
- [148] A. E. Faraggi and M. Masip, *Leptophobic Z-prime from superstring derived models*, *Phys. Lett. B* **388** (1996) 524 [[hep-ph/9604302](#)].
- [149] D. Gomez Dumm, *Leptophobic character of the Z-prime in an  $SU(3)(C) \times SU(3)(L) \times U(1)(X)$  model*, *Phys. Lett. B* **411** (1997) 313 [[hep-ph/9709245](#)].
- [150] M. Malinsky, J. C. Romao and J. W. F. Valle, *Novel supersymmetric  $SO(10)$  seesaw mechanism*, *Phys. Rev. Lett.* **95** (2005) 161801 [[hep-ph/0506296](#)].
- [151] M. R. Buckley, D. Hooper and J. L. Rosner, *A Leptophobic  $Z'$  And Dark Matter From Grand Unification*, *Phys. Lett. B* **703** (2011) 343 [[1106.3583](#)].
- [152] F. F. Deppisch, N. Desai and J. W. F. Valle, *Is charged lepton flavor violation a high energy phenomenon?*, *Phys. Rev. D* **89** (2014) 051302 [[1308.6789](#)].
- [153] CMS collaboration, *Search for narrow and broad dijet resonances in proton-proton collisions at  $\sqrt{s} = 13$  TeV and constraints on dark matter mediators and other new particles*, *JHEP* **08** (2018) 130 [[1806.00843](#)].
- [154] ATLAS collaboration, *Search for New Phenomena in Dijet Events using  $139 \text{ fb}^{-1}$  of pp collisions at  $\sqrt{s} = 13 \text{ TeV}$  collected with the ATLAS Detector*, ATLAS-CONF-2019-007 (2019) .
- [155] A. Alloul, N. D. Christensen, C. Degrande, C. Duhr and B. Fuks, *FeynRules 2.0 - A complete toolbox for tree-level phenomenology*, *Comput. Phys. Commun.* **185** (2014) 2250 [[1310.1921](#)].
- [156] S. Amrith, J. M. Butterworth, F. F. Deppisch, W. Liu, A. Varma and D. Yallup, *LHC Constraints on a  $B - L$  Gauge Model using Contur*, *JHEP* **05** (2019) 154 [[1811.11452](#)].
- [157] J. Alwall, R. Frederix, S. Frixione, V. Hirschi, F. Maltoni, O. Mattelaer et al., *The automated computation of tree-level and next-to-leading order differential cross sections, and their matching to parton shower simulations*, *JHEP* **07** (2014) 079 [[1405.0301](#)].
- [158] FASER collaboration, *FASER's physics reach for long-lived particles*, *Phys. Rev. D* **99** (2019) 095011 [[1811.12522](#)].
- [159] D. Curtin et al., *Long-Lived Particles at the Energy Frontier: The MATHUSLA Physics Case*, *Rept. Prog. Phys.* **82** (2019) 116201 [[1806.07396](#)].
- [160] A. Das, P. S. B. Dev and N. Okada, *Long-lived TeV-scale right-handed neutrino production at the LHC in gauged  $U(1)_X$  model*, *Phys. Lett. B* **799** (2019) 135052 [[1906.04132](#)].
- [161] C.-W. Chiang, G. Cottin, A. Das and S. Mandal, *Displaced heavy neutrinos from  $Z'$  decays at the LHC*, *JHEP* **12** (2019) 070 [[1908.09838](#)].
- [162] S. Bray, J. S. Lee and A. Pilaftsis, *Resonant CP violation due to heavy neutrinos at the LHC*, *Nucl. Phys. B* **786** (2007) 95 [[hep-ph/0702294](#)].
- [163] J. Schechter and J. W. F. Valle, *Neutrinoless Double beta Decay in  $SU(2) \times U(1)$  Theories*, *Phys. Rev. D* **25** (1982) 2951.

- [164] J. Kotila and F. Iachello, *Phase space factors for double- $\beta$  decay*, *Phys. Rev. C* **85** (2012) 034316 [[1209.5722](#)].
- [165] A. Neacsu and M. Horoi, *An effective method to accurately calculate the phase space factors for  $\beta^-\beta^-$  decay*, *Adv. High Energy Phys.* **2016** (2016) 7486712 [[1510.00882](#)].
- [166] D.-L. Fang, A. Faessler and F. Simkovic,  *$0\nu\beta\beta$  -decay nuclear matrix element for light and heavy neutrino mass mechanisms from deformed quasiparticle random-phase approximation calculations for  $^{76}\text{Ge}$ ,  $^{82}\text{Se}$ ,  $^{130}\text{Te}$ ,  $^{136}\text{Xe}$ , and  $^{150}\text{Nd}$  with isospin restoration*, *Phys. Rev. C* **97** (2018) 045503 [[1803.09195](#)].
- [167] H. Ejiri, *Neutrino-Mass Sensitivity and Nuclear Matrix Element for Neutrinoless Double Beta Decay*, *Universe* **6** (2020) 225.
- [168] G. Racah, *On the symmetry of particle and antiparticle*, *Nuovo Cim.* **14** (1937) 322.
- [169] W. H. Furry, *On transition probabilities in double beta-disintegration*, *Phys. Rev.* **56** (1939) 1184.
- [170] KAMLAND-ZEN collaboration, *Search for Majorana Neutrinos near the Inverted Mass Hierarchy Region with KamLAND-Zen*, *Phys. Rev. Lett.* **117** (2016) 082503 [[1605.02889](#)].
- [171] EXO-200 collaboration, *Search for Neutrinoless Double- $\beta$  Decay with the Complete EXO-200 Dataset*, *Phys. Rev. Lett.* **123** (2019) 161802 [[1906.02723](#)].
- [172] GERDA collaboration, *Final Results of GERDA on the Search for Neutrinoless Double- $\beta$  Decay*, *Phys. Rev. Lett.* **125** (2020) 252502 [[2009.06079](#)].
- [173] CUORE collaboration, *High sensitivity neutrinoless double-beta decay search with one tonne-year of CUORE data*, [2104.06906](#).
- [174] NEMO-3 collaboration, *Detailed studies of  $^{100}\text{Mo}$  two-neutrino double beta decay in NEMO-3*, *Eur. Phys. J. C* **79** (2019) 440 [[1903.08084](#)].
- [175] nEXO collaboration, *nEXO: neutrinoless double beta decay search beyond  $10^{28}$  year half-life sensitivity*, *J. Phys. G* **49** (2022) 015104 [[2106.16243](#)].
- [176] LEGEND collaboration, *The Large Enriched Germanium Experiment for Neutrinoless  $\beta\beta$  Decay: LEGEND-1000 Preconceptual Design Report*, [2107.11462](#).
- [177] A. Avasthi et al., *Kilotonne-scale xenon detectors for neutrinoless double beta decay and other new physics searches*, [2110.01537](#).